University of Southampton

FACULTY OF ENGINEERING, SCIENCE AND MATHEMATICS

INSTITUTE OF SOUND AND VIBRATION RESEARCH

FUNDAMENTAL INVESTIGATION INTO THE DIRECTIVITY FUNCTION OF MULTI-MODE SOUND FIELDS FROM DUCTS

Author: Samuel Sinayoko

Supervisors: Dr P F Joseph
Dr A McAlpine

A dissertation submitted in partial fulfilment
of the requirements for the degree of MSc by
instructional course

April 2008

Abstract

Multi-mode sound radiation from hard-walled semi-infinite ducts with uniform subsonic flow is investigated theoretically. An analytic expression, valid in the high frequency limit, is derived for the multi-mode directivity function in the forward arc of the duct for a general family of mode distribution function. The multi-mode directivity depends on the amplitude of each mode, and on the single mode directivity functions. The amplitude of each mode is expressed as a function of cut-off ratio for a uniform distribution of incoherent monopoles, a uniform distribution of incoherent axial dipoles and for equal power per mode. The single mode directivity functions are obtained analytically by applying a Lorentz Transformation to the zero flow solution. The analytic formula for the multi-mode directivity with flow is derived by assuming total transmission of power at the open-end of the duct. The high frequency formula is compared to exact numerical solutions from the Wiener Hopf technique and for a flanged duct. The agreement is shown to be excellent.

A mon grand père

Acknowledgements

I would like to express my gratitude to the Ecole Nationale des Ponts et Chaussees (ENPC), which allowed me to spend my final year at the University of Southampton and supported me from the beginning. In particular, many thanks to Professor Ehrlacher, Director of the Mechanical Engineering Department, and to Thomas Archarick, responsible for final year students studying abroad. Thanks to the "Fondation Georges Besse" and "Region Ile de France", which helped me financially during this year and without whom this experience would not have been possible. A heart felt thank you to my family, who gave me taste for learning in the first place, and continued to support me for so many years, and to Margaret, who first agreed to follow me to Southampton, and then endured the long hours spent working on this thesis.

I must acknowledge the great work done by the staff of the MSc in Sound and Vibration Studies, at the Institute of Sound and Vibration Research, where I spent a very enriching year. Thanks in particular to Professor Thomson for the great organisation of the program, and of course to Sue Brindle, who is always so helpful and efficient. My sincere thanks to Drs Phil Joseph and Alan Mac Alpine, my two supervisors during this MSc project, for their constant commitment, guidance and encouragements throughout this year. I reckon that not all students are offered such a great support, and I very much appreciated working with them from the beginning. A special thank you to Phil Joseph, which shook my hand every time we met, like a true Frenchman. I must also thank Dr Gwenael Gabard for his providing us his code, which validated the results from this thesis, and for answering my many questions on the Lorentz Transformation.

Contents

I Literature review **3**

1.1 Single mode theory in the absence of flow 4
1.1.1 Mode shapes 4
1.1.2 Single mode directivity for a flanged duct 4
1.1.3 Effect of the open end of the duct 4
1.1.4 Single mode directivity for an unflanged duct 5
1.2 Multi-Mode directivity in the absence of flow 5
1.2.1 Modal amplitude models 5
1.2.2 Rice's method 6
1.2.3 Exact resolution of the multi-mode directivity 6
1.3 Multi-Mode directivity in the presence of flow 7
1.3.1 Single mode directivity 7
1.3.2 Amplitude models 8

II Theory of sound transmission and radiation in ducts without flow **10**

2 Pressure field in a cylindrical waveguide **11**

2.1 Wave equation 11
2.2 Solution of the wave equation 12
2.3 Boundary conditions 14
2.4 Eigenfunctions 15
2.4.1 Definition 15
2.4.2 Normalization 16
2.5 Modal decomposition of the pressure field 18
2.5.1 General expression 18
2.5.2 Cut-on modes 18
2.5.3 Physical interpretation 20
2.5.4 Geometrical interpretation 21

3 Radiated pressure in the far field **22**

3.1 Derivation of $|H_{mn}(ka, \theta)|^2$ 23

3.1.1 Flanged duct . . . 23
3.1.2 Unflanged duct . . . 27
3.1.3 Validation of the flanged transfer functions . . . 28
3.2 Weighting models . . . 29
3.2.1 Uniform distribution of incoherent monopoles . . . 30
3.2.2 Uniform distribution of incoherent axial dipoles . . . 31
3.2.3 Equal power per mode . . . 32
3.2.4 General expression of the modal amplitude without flow . . . 34
3.3 High frequency approximation . . . 34
3.3.1 Introduction . . . 34
3.3.2 Far field power in direction $\boldsymbol{\theta}$ . . . 34
3.3.3 Relation between far field power and in-duct power . . . 35
3.3.4 In duct power transmitted in direction θ . . . 36
3.3.5 Multi-Mode far field directivity without flow . . . 38
3.4 Directivity factor . . . 38
3.4.1 Directivity factor in terms of a modal summation . . . 39
3.4.2 Continuous analytical estimation of the directivity factor in the high frequency limit . . . 39

4 Validation of the model **40**
4.1 Theoretical analysis of the error on the directivity factor . . . 40
4.2 Sufficient condition on the modal transmission coefficients . . . 41
4.3 Analysis of the modal transmission coefficients . . . 41
4.3.1 Variation with frequency . . . 41
4.3.2 Maximum angle of validity . . . 42
4.4 Conclusion . . . 43

5 Results **44**

III Multi-mode directivity with flow **46**

6 The Lorentz Transformation **47**
6.1 Convected wave equation . . . 47
6.2 Solution of the homogeneous convected wave equation . . . 47
6.3 Solution of the homogeneous convected Helmholtz equation . . . 48
6.3.1 Cartesian coordinates . . . 48
6.3.2 Polar coordinates . . . 49
6.3.3 Spherical coordinates . . . 49
6.4 Issues regarding the application of the Lorentz Transformation . . . 50
6.4.1 The frequency factor . . . 50

6.4.2 Singular solutions 50
6.4.3 Lorentz Transformation and momentum equation 51

7 Pressure field in a cylindrical waveguide **54**
7.1 Solution of the convected Helmholtz equation with the Lorentz Transformation 54
7.2 Boundary conditions 55
7.3 General expression for the in-duct pressure 55
7.4 Cut-on modes 56
7.5 Direction of propagation of a single mode with flow 56
7.5.1 Preliminary results from ray theory 56
7.5.2 Application of ray theory to a single mode with flow 58

8 Pressure radiated to the far field **61**
8.1 Derivation of $|H_{mn}(ka, \theta)|$ 61
8.1.1 Solution using the Lorentz Transformation 61
8.1.2 Solution using the Wiener-Hopf Technique 68
8.1.3 Validation of the Lorentz Transformation 69
8.1.4 Validation of the flanged duct transfer functions 69
8.1.5 Variation of the modal directivity with Mach number 71
8.2 Mode weighting models 73
8.2.1 Green's function in a rigid wall infinite cylinder with flow 73
8.2.2 Generalization of the Kirchhoff-Helmholtz equation with flow . . . 75
8.2.3 Uniform distribution of incoherent monopoles 76
8.2.4 Uniform distribution of incoherent axial dipoles 78
8.2.5 Equal power per mode 79
8.2.6 General expression of the modal amplitude 81
8.3 High frequency approximation for the multi-mode far field directivity . . . 83
8.3.1 Introduction 83
8.3.2 Far field intensity with flow 83
8.3.3 Far field power with flow radiated in direction θ 85
8.3.4 Relation between far field power and in-duct power 86
8.3.5 In duct power transmitted in direction θ 87
8.3.6 Multi-Mode far field directivity 90
8.4 Directivity factor 92
8.4.1 Modal expression of the directivity factor with flow 92
8.4.2 Analytic estimation of the directivity factor with flow in the high frequency limit 93

9 Validation **94**
9.1 Variation with frequency 94
9.2 Maximum angle of validity 94
9.3 Sound power variation with Mach number 95

10 Results **98**

Bibliography **107**

List of Figures

2.1 Cylindrical polar coordinates system 12
2.2 Boundary conditions 14
2.3 Modes shapes 17
2.4 Cut-on modes diagram 19
2.5 Number of cut-on modes in a cylindrical duct as a function of frequency . . 20
2.6 Direction of propagation of mode (m, n). 21

3.1 Spherical coordinates system 22
3.2 Flanged duct model 24
3.3 Angle of maximum radiation for a well cut-on mode and a nearly cut-off mode $ka = 10$ 27
3.4 In duct to far field transfer function at 0 degree 27
3.5 Variation of modal transfer function with frequency 28
3.6 Comparison of the modal transfer functions from a flanged model and from the Wiener Hopf Technique 29
3.7 Propagation of acoustic power inside and outside the duct 35

4.1 Modal transmission coefficient as a function of cut-off ratio for zero flow at low and high frequencies. 42
4.2 Pourcentage of modes such that $\tau_{mn} < 0.8$. 42
4.3 Sketch of the variation of τ_{mn} as a function of α^0_{mn}. 43

5.1 Directivity factor of the pressure field radiating from a semi-infinite cylindrical duct without flow, for $ka = 50$ and for three different model of sound sources 45

6.1 Lorentz Transformation in cylindrical coordinates when $\sigma = \beta$ 49
6.2 Lorentz Transformation in spherical coordinates when $\sigma = \beta$ 51
6.3 Effect of the Lorentz Transformation on the relation between pressure and velocity potential 52
6.4 Correct application of the Lorentz Transformation 53

7.1 Cut-on modes at frequency ka=20 for various values of the absolute value of the Mach number $|M|$ 57
7.2 Propagation of a ray in direction θ with respect to the z-axis 57
7.3 Direction of propagation of mode (m, n) inside a cylindrical duct with flow. 60

8.1 For an exhaust problem ($M > 0$) the sheer layer creates a discontinuity of the velocity potential but the pressure field is regular. 62
8.2 Plot of $S(\theta)$ for $0 \leq \theta \leq \pi$ and $-0.9 \leq M \leq 0.9$. 62
8.3 For an inlet problem ($M < 0$) the pressure is singular at the open end of the duct but the velocity potential is regular. 63
8.4 Direction of the main lobe of radiation in the far field for mode (m, n) with flow. 68
8.5 Comparison of the modal transfer functions with flow from the zero flow solution given by the Wiener Hopf Technique followed by a Lorentz Transformation, and the direct solution with flow from the Wiener Hopf Technique 70
8.6 Comparison of the modal transfer functions obtained by using a flanged duct model together with a Lorentz Transformation, or the exact direct Wiener Hopf Technique 71
8.7 Variation of the modal transfer function with Mach number for mode $(8, 1)$ which is well cut-on at zero Mach number (top), and mode $(7, 4)$ which is almost cut-off at zero Mach number (bottom) 72
8.8 Direction of the main radiation lobe θ_{mn} as a function of the zero flow cut-off ratio for Mach numbers of 0, 0.3, 0.6 and 0.9 73
8.9 Logarithmic plots of the weighting model $F_{\mu,\nu,\gamma}$ as a function of cut-off ratio α_{mn} and Mach number M for various source models 82
8.10 $F(\theta)$ as a function of θ and M, for θ between 0 and π and M between -0.9 and 0.9. 85
8.11 Relation between power transmitted along the duct between angles θ and $\theta + d\theta$, denoted by $dW(\theta)$, and power radiated to the far field between angles θ and $\theta + d\theta$, denoted by $dW_f(\theta)$ 86
8.12 Modal power function $L_{\mu,\nu,\gamma}$ plotted as a function of Mach number M and cut-off ratio α_{mn}. The cut-off ratio varies between 0 and 1 and the Mach number between -0.9 and 0.9. 88
8.13 Function T plotted as a function of θ and M. T represents a directivity factor in the multi-mode broadband directivity factor. 91
8.14 Function $G_{\mu,\nu,\gamma}$ plotted as a function of θ and M. It represents the weighting coeficient for modes whose cut-off ratio is close to $\alpha(\theta)$. 92

9.1 Variation of the transmission coefficients as a function of cut-off ratio for $ka = 20$ and $ka = 50$. The Mach number is constant 95

9.2 Percentage of modes such that $\tau_{mn} < 0.8$. 96
9.3 In duct power with flow normalized by the zero flow in-duct power, as a function of Mach number, for the source distributions of incoherent distribution of monopoles, incoherent distribution of axial dipoles, and equal power per mode. 97

10.1 $M < 0$, Uniform distribution of incoherent monopoles 99
10.2 $M > 0$, Uniform distribution of incoherent monopoles 100
10.3 $M < 0$, Uniform distribution of incoherent dipoles 101
10.4 $M > 0$, Uniform distribution of incoherent dipoles 102
10.5 $M < 0$, Equal power per mode model 103
10.6 $M > 0$, Equal power per mode model 104

Introduction

The development of aero engines for commercial flights in the 1950s is the main reason why duct acoustics has become a major research subject. The noise generated by these engines was so intense that it jeopardised the development of this technology. It became important to understand the mechanisms responsible for the generation, transmission and radiation of sound from an aero-engine. In that respect, the noise field directivity from the exhaust or inlet of a cylindrical duct is of great interest. It shows in which directions the sound radiates when it radiates from the engine. It is usually defined in terms of the acoustic intensity, which is proportionnal to the mean square pressure. To predict this directivity it is necessary to estimate the impact of the noise radiated towards the ground. The directivity can also be used to study the sound radiated from exhaust mufflers or large exhaust stacks.

It is useful to describe the behaviour of a duct in terms of its acoustic modes. Analytical results already exist to calculate the directivity when only one particular mode propagates along the duct. This is important to understand the sound generated by the engine at very specific frequencies. However, the rotation of the blades also generates a broadband excitation. In that case, several acoustic modes are excited and propagate simultaneously along the duct: the total pressure is then given by the superposition of theses modes. Little research has been done so far to study the multi-mode directivity of a duct. The most recent was carried out by Joseph and Morfey in 1999 [1]. The authors derived a simple analytic formula for the multi-mode directivity function from a semi-infinite cylindrical duct without flow, which is valid in the high frequency limit in the forward arc of the duct. Such formula are interesting because they allow the avoidance of the calculation of all the modal components which is complex and computationally expensive. The objective of this thesis is to extend the results found by Joseph and Morfey to the case where flow is present in and outside the duct. To avoid further complications induced by the presence of a shear layer in the case of an exhaust duct, the mean flow velocity will be assumed to be the same in and outside the duct.

This thesis is divided into three parts. First, a literature review presents the concepts which are necessary to tackle this problem. It also demonstrates the relatively small amount of work which has been carried out on multi-mode directivities from ducts. Second, the zero flow theory is presented in great detail, in order to illustrate the methods used by Joseph and Morfey to obtain their multi-mode directivity function for the zero flow prob-

lem. In particular, all the derivation are reproduced, or carried out in a different manner, to identify the steps which are likely to be affected by the presence of flow. In part three, the duct is immersed in a mean flow and the zero flow derivation is generalised, to take into account the presence of flow. This constitutes the essential result of this thesis.

Thus, this thesis is self contained and presents a number of classical results in the field of duct acoustics, before extending them to the case when a mean flow is present. A number of new results have been derived in this thesis. Analytic solution have been obtained for the multi-mode directivity of sound radiation from ducts in the presence of flow that fit the exact computation extremely well.

Part I

Literature review

This review will first introduce classical concepts and results which are used in duct acoustics. These are for example the mode shapes and cut-off ratio, as well as the single mode directivity function. This will lead to the few articles tackling multi-mode directivity in the absence of flow, which will be analysed in more details. The aim will be to highlight the methods which could be useful for this project. It will also give an opportunity to find the gaps in previous studies. Finally, the research on the acoustic behaviour of ducts in the presence of flow will be reviewed to understand what has to be done to estimate the multi-mode directivity in that case.

1.1 Single mode theory in the absence of flow

1.1.1 Mode shapes

The pressure inside a duct can be expressed as a linear combination of its modes of vibration. Each mode is associated with a natural frequency and a mode shape. The mode shape shows how the duct responds when it is excited at this natural frequency. The first mode is a plane wave while higher order modes have the form of Bessel functions of the first kind, as has been shown for example by Morse [2]. It is important to understand that a duct does not in general allow all the modes to propagate. It behaves like a waveguide which filters higher frequencies. Thus for a given harmonic excitation, a finite number of so called cut-on modes will propagate along the duct. In particular, at very low frequency, only plane waves can propagate. However, the rotation speed in an aero engine is in general large enough to enable several hundreds of modes to be cut-on.

1.1.2 Single mode directivity for a flanged duct

The importance of these higher order modes for compressor noise has been first understood by Tyler and Sofrin in 1962 [3]. They took into account all the cut-on modes in the expression of the pressure in the duct. They could then derive the velocity field at the open end of the duct. This enabled to approximate the modal directivity function in the far field by using Rayleigh's integral. This method is only an approximation because it requires to suppose that the duct ends up in an infinite baffle. This theory was found to compare very well with experimental results except for angles close to the infinite baffle, or behind it.

1.1.3 Effect of the open end of the duct

It is also important to notice a second approximation in the results of Tyler and Sofrin. The authors assumed that the open end of the duct does not generate any reflections. This means that the energy transported along the duct is entirely radiated away. The validity of this assumption has been confirmed by Morfey which has derived the transmission coefficient at the open end of the duct [4, 5]. He found that apart from the modes which are

close to the cut-off frequency, the transmission coefficient is very close to one. Thus, the modal directivity derived by Tyler and Sofrin is valid for most of the cut-on modes. In our frequency of interest, where hundreds of modes propagate along the duct, it can therefore be used to derive the broadband directivity. The effect will be to slightly overestimate this broadband directivity, especially close to the flange where the modes which are close to cut-off radiate most of the sound. Since the flanged approximation is mostly used to derive the directivity away from the infinite baffle, it will be used in this project without taking into account the transmission coefficients derived by Morfey.

1.1.4 Single mode directivity for an unflanged duct

In 1947, Levine and Schwinger obtained an exact solution of the radiation from an unflanged duct in the case where only the first mode (a plane wave) propagates along the duct [6]. They computed the reflection coefficient at the end of the duct, as well as the radiated power outside the duct, by using the Wiener-Hopf technique. In 1969, Weinstein generalized these results to higher order modes [7]. These solutions were exact everywhere which was not the case of the flanged method whose solution was only valid in the far field. However, the results were given in terms of surface integrals, whose physical interpretation were not straightforward. It is not until 1974, when the results were written in a different form by Homicz and Lordi [8], that they became widely used. In particular, these authors explained how to derive very easily the position of the main lobe, as well as the number and position of the side lobes. Most importantly, they showed that their results could be extended by very simple transforms to include mean flow.

1.2 Multi-Mode directivity in the absence of flow

1.2.1 Modal amplitude models

Each cut-on mode can propagate along the duct and eventually hit the open end and radiate away, thus contributing to the multi-mode directivity. The weight of each mode in the global directivity is governed by a series of complex coefficients which take into account the respective amplitude and phase of each mode. However, there is no simple mean of determining the value of these coefficients. It is therefore necessary to make some assumptions about their phase and magnitude. In general, the modes are supposed to be incoherent therefore the phase of each modal amplitude can be seen as a uniform random variable between 0 and 2π. Concerning the magnitude of each mode, several models have been developed. The most simple one assumes that all the modes have the same amplitude, another one that the power is equally shared among the modes. In 1976, Saule [9] used these two models to derive the multi-mode directivity in the far field by using the flanged duct model. He compared his results with experimental measurements of broadband noise

radiated from the intake of different ducts. However, his method was not practical because it required to compute the amplitude and directivity of all the cut-on modes.

1.2.2 Rice's method

In 1978, Rice found a way to simplify the derivation of the far field multi-mode directivity by using the cutoff ratio. For a given mode, the cutoff ratio is a dimensionless coefficient which can be defined for each mode as a function of frequency. It shows how far a mode is from its cutoff frequency. Rice expressed the single mode directivity as a function of the cutoff ratio by using the flanged duct model. He then developed an approximate method to estimate analytically the multi-mode directivity. His method was based on the fact that each mode radiates mainly at a particular angle which depends on the cutoff ratio. The contribution of this mode is negligible at other angles in comparison with other modes. For a given angle, Rice also managed to estimate the range of cutoff ratios contributing to the directivity around this angle. He then integrated their contributions to the multi-mode directivity by using his previous expression of the cutoff ratio density function [10]. In the case of an equal power per mode model, Rice found that the far field directivity was simply proportional to a cosine function. He also showed that this results compared very well with experimental measurements. The importance of this work is that it can be generalized to other models as long as the amplitude coefficients can be expressed as functions of the cutoff ratio. One of the main objective of this project will be to adapt Rice's method to the case where flow is present.

1.2.3 Exact resolution of the multi-mode directivity

Joseph and Morfey have extended the work of Rice in 1999 [1]. First of all, they used the exact expression of the single mode directivity instead of the approximate one. They also showed that three different models of sources all lead to modal amplitudes which could be expressed as powers of the cutoff ratio α. Thus, if the power is shared equally between all modes, the amplitude coefficients are proportionnal to the inverse of α. If the acoustic sources are formed by a distribution of monopoles uniformly distributed in a section of the duct, then modal amplitudes are proportionnal to α^{-2}. Thirdly, in the case of a distribution of axial dipoles, these amplitudes are proportionnal to α^{0}. The authors thus obtained three different directivity patterns corresponding to each of these models. Above all, they derived high frequency approximations by using the cutoff ratio probability density by analogy with Rice. Thus, they obtained very simple analytic formulas and showed that their precision was excellent for angles up to 70° from the outlet axis. These results give a chance to obtain simple analytical expressions of the multi-mode directivity when flow is present, by using exact solutions taking into account the shear layer and by examining their behaviour at high frequency.

Another important result found by Joseph and Morfey is that the directivity gives a very simple means of measuring the power radiated from a duct. The power can be estimated from the multi-mode directivity model with only one measurement of the intensity at any angle. This gives a very simple method of measuring the radiated power which is however highly dependant on the validity of the model. Surprisingly, the authors found that at 55° from the outlet axis, the directivity was practically independent of the three physical models they had presented. This means that measuring the intensity at this precise angle is in general a good way of estimating the power radiated from a duct. This project should give the opportunity to discover how this critical angle is modified in the presence of flow.

1.3 Multi-Mode directivity in the presence of flow

The determination of the multi-mode directivity when flow is added in and outside the duct requires two things. First, the single mode directivity pattern must be derived. As explained earlier, this can be done very easily at the intake of the duct but the single mode directivity at the outlet requires further results. Secondly, the classical models governing the amplitude of each mode must be generalized to take into account the effect of the flow inside the duct. Once these two tasks have been carried out, the methods described previously should lead to numerical and possibly analytical expressions of the directivity in the presence of flow.

1.3.1 Single mode directivity

Because of the shear layer at the exhaust of the duct, the radiation of sound is much more complex here than in the zero-flow case. Several physical phenomena occur such as the the diffraction of sound at the trailing edge of the duct, which triggers an instability in the shear layer. This instability is one of the reason why the problem has been so difficult to solve. In 1977, Munt solved it rigorously by considering the diffraction of sound at the open end of a semi-infinite duct containing a cylindrical jet moving at a certain speed, the whole being immersed in a fluid moving axially at different velocity [11]. He modelled the separation between the two fluids by a vortex layer and solved the problem by using the Wiener-Hopf technique. He calculated the far field pressure and the match between his results and experimental measurements was excellent. He later extended his solution in 1990 and found the near field expression of the pressure field [12].

A less general solution where the flow speed is the same in an outside the duct was given by Rienstra in 1984 [13]. However, this study addressed the important issue of the presence of a centre body extending beyond the exhaust of the duct. This centre body is a more realistic model of the modern bypass turbofans than that of a cylindrical duct. Rienstra's work has recently been extended by Gabard and Astley to take into account the difference of speed between the inner and outer flow [14]. In addition to providing the exact solution for the single mode directivity, Gabard and Astley also gave an example of

multi-mode directivity for equal power per mode. However, they did not try to extract any simple analytical expression for the multi-mode directivity in the far field, which will be the main objective of this project.

1.3.2 Amplitude models

The modelling of the modal amplitudes is necessary to estimate the contribution of each mode to the total directivity. The amplitude coefficients with flow, for ideal distributions of sources such as a uniform distribution of monopoles, a uniform distribution of axial dipoles, and an equal power per mode model, have been studied by Joseph *et al.* in [15].

Conclusion

The derivation of the multi-mode directivity from ducts can be divided into two parts. On the one hand, the single mode directivity pattern must be derived. On the other hand, physical models must be created to determine the weight of each mode in the broadband directivity.

Two principal methods have been developed to estimate the single mode directivity. The first one assumes that the duct is flanged and gives approximate results in the far field by using Rayleigh's integral at the open end of the duct. This method is attractive because of its simplicity and has therefore been used by Rice to study the multi-mode radiation pattern with zero-flow. It could be generalized to take into account the presence of flow. This would be a good way to estimate the radiation from the duct intake. However, it would not be valid at the duct exhaust because of more complex phenomena involving vortex shedding in the shear layer. The second method of calculating the single mode directivity relies on the Wiener-Hopf technique and gives exact results everywhere. The no-flow solution, presented by Homicz and Lordi, has been used by Joseph and Morfey to derive the multi-mode directivity. As for the approximate method, simple transforms can be used to derive new expressions for the sound radiated from the intake of a duct immersed in a mean flow, but more complex results are required for the exhaust directivity. To avoid this problem for an exhaust duct, we will assume that the flow is uniform around the duct: the velocity will be the same inside and outside the duct. The most general exact solution of the single mode radiation pattern from the outlet of a duct with flow have been derived by Gabard and Astley. It will be applied to the case when the flow speed is identical inside and outside the duct, to validate our results.

The issue of the respective weight of each mode has been thoroughly studied by Joseph and Morfey who extended Rice's idea of expressing the modal amplitude in terms of the cutoff ratio. They presented different models based either on uniform distributions of sources inside the duct, or on the distribution of power between the modes. These models have already been extended to the situation where flow is moving at a constant speed inside

the duct.

This literature review has shown that little work has been carried out so far on multi-mode directivity in general, and multi-mode directivity with flow in particular. This thesis is an opportunity to address these important issues on multi-mode directivity functions from ducts.

Part II

Theory of sound transmission and radiation in ducts without flow

Chapter 2

Pressure field in a cylindrical waveguide

The pressure field transmitted along the duct must satisfy the wave equation and the boundary conditions.

2.1 Wave equation

When no source is present inside the waveguide, the pressure field must satisfy the homogeneous wave equation

$$\nabla^2 p^0(\boldsymbol{x}, t) = \frac{1}{c_0^2} \frac{\partial^2 p^0(\boldsymbol{x}, t)}{\partial t^2}, \tag{2.1.1}$$

where c_0 is the speed of sound, p^0 the pressure and $\boldsymbol{x}$ the position in the cylinder. The superscript 0 is used to denote the zero flow solution.

The pressure field is assumed to be harmonic in time

$$p^0(\boldsymbol{x}, t) = \Re\left\{p^0(\boldsymbol{x}, \omega) e^{j\omega t}\right\},$$

where ω is the angular frequency and $p^0(\boldsymbol{x})$ the complex pressure. Note that, for simplicity, the same notation has been used to designate the real pressure $p(\boldsymbol{x}, t)$ and the complex pressure $p^0(\boldsymbol{x})$. It can be shown that, if the pressure field is harmonic, the wave equation is equivalent to the homogeneous Helmholtz equation

$$\boxed{\nabla^2 p^0(\boldsymbol{x}) + k^2 p^0(\boldsymbol{x}) = 0,} \tag{2.1.2}$$

where $k = \omega / c_0$ is the wavenumber.

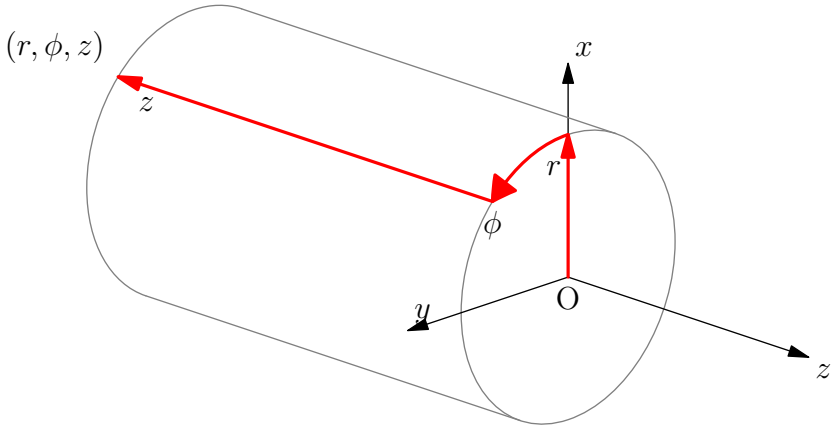

Figure 2.1 – Cylindrical polar coordinates system

2.2 Solution of the wave equation

The solution of the Helmholtz equation can be found by using the method of the seperation of variables. Let the complex pressure $p^0(\boldsymbol{x})$ be of the form

$$p^0(\boldsymbol{x}) = R(r)\Phi(\phi)Z(z), \tag{2.2.1}$$

where (r, ϕ, z) are cylindrical polar coordinates (see figure 2.1). The homogeneous Helmholtz equation gives

$$\frac{1}{r}\frac{\partial}{\partial r}\left(r\frac{\partial p^0}{\partial r}\right) + \frac{1}{r^2}\frac{\partial^2 p^0}{\partial \phi^2} + \frac{\partial^2 p^0}{\partial z^2} + k^2 p^0 = 0,$$

Substituting equation (2.2.1) into the above expression,

$$\frac{1}{r}\left[rR''(r) + R'(r)\right]\Phi(\phi)Z(z) + \frac{1}{r^2}R(r)\Theta''(\phi)Z(z) + R(r)\Theta(\phi)Z''(z) + k^2R(r)\Theta(\phi)Z(z) = 0.$$

Dividing the last equation by $R(r)\Theta(\phi)Z(z)$ gives

$$\underbrace{\left(R''(r) + \frac{1}{r}R'(r)\right)\frac{1}{R(r)} + \frac{1}{r^2}\frac{\Theta''(\phi)}{\Theta(\phi)} + k^2}_{\text{function } F(r,\phi) \text{ of } r \text{ and } \phi \text{ only}} + \underbrace{\frac{Z''(z)}{Z(z)}}_{\text{function } G(z) \text{ of z only}} = 0.$$

There is a complex constant, say k_z, such that:

$$G(z) = -k_z^2; \tag{2.2.2}$$
$$F(r, \phi) = k_z^2. \tag{2.2.3}$$

Equation (2.2.2) is equivalent to

$$Z''(z) + k_z^2 Z(z) = 0,$$

The solution of the ordinary differential equation can be expressed as

$$Z(z) = Ae^{\pm k_z z}, \tag{2.2.4}$$

where A is an arbitrary constant. Equation (2.2.3) is equivalent to

$$\underbrace{\left(R''(r) + \frac{1}{r}R'(r)\right)\frac{r^2}{R(r)} + r^2(k^2 - k_z^2)}_{\text{function } F_1(r) \text{ of } r \text{ only}} + \underbrace{\frac{\Theta''(\phi)}{\Theta(\phi)}}_{\text{function } F_2(\phi) \text{ of } \phi \text{ only}} = 0.$$

There is a constant, say K, such that:

$$F_1(r) = +K; \tag{2.2.5}$$

$$F_2(\phi) = -K. \tag{2.2.6}$$

Equation (2.2.6) is equivalent to

$$\Theta''(\phi) + K\Theta(\phi) = 0 \quad \Rightarrow \Theta(\phi) = Be^{\pm j\sqrt{K}\phi}, \tag{2.2.7}$$

where B is an arbitrary constant. Since Θ must be 2π-periodic, because of the use of a cylindrical duct, then $\sqrt{K}$ must be an integer, say m, and equation (2.2.5) then gives

$$R''(r) + \frac{1}{r}R'(r) + \left(k^2 - k_z^2 - \frac{m^2}{r^2}\right)R(r) = 0$$

which is know as Bessel's equation. The solutions of this ordinary differential equation are of the form

$$R(r) = CJ_m(\kappa r) + DY_m(\kappa r),$$

where J_m and Y_m are respectively the Bessel functions of the first and second kind, C and D are arbitrary constants, and κ_m is related to k and k_z by the dispersion relation

$$\kappa^2 = k^2 - k_z^2. \tag{2.2.8}$$

Since $Y_m(r)$ goes to infinity when r tends to 0, which corresponds to the centre of the duct, D must be equal to zero and

$$R(r) = CJ_m(\kappa r). \tag{2.2.9}$$

Combining equations (2.2.4), (2.2.7) and (2.2.9) into equation (2.2.1) shows that for a given constant k_z, the solutions of the wave equation are of the form

$$p_m^0(r, \phi, z) = A_m^0 J_m(\kappa r)e^{\pm jm\phi}e^{\pm jk_z z}, \quad m \in \mathbb{Z}, \tag{2.2.10}$$

where A_m^0 is a constant. Equation (2.2.10) gives a first indication of the type of acoustic waves which can travel along the duct. Each value of k_z and each value of m correspond to a particular wave solution. The wave travels in the positive or negative direction along the axis of the duct ($e^{\pm jk_z z}$ term), and rotates in the positive or negative direction around the same axis ($e^{\pm jm\phi}$ term). If only the waves travelling in the positive z-direction are retained, thereby neglecting the reflections from the open end of the duct,

$$p_m^0(r,\phi,z) = A_m^0 J_m(\kappa r) e^{\pm jm\phi} e^{-jk_z z}, \quad m \in \mathbb{Z}.$$

A priori, for a given integer $m \in \mathbb{Z}^*$ the two following waves should be retained:

$$p_m^0(r,\phi,z) = A_m^0 J_m(\kappa r) e^{-jm\phi} e^{-jk_z z}, \quad m \in \mathbb{Z} \tag{2.2.11}$$

$$p_m^0(r,\phi,z) = A_m^0 J_m(\kappa r) e^{+jm\phi} e^{-jk_z z}, \quad m \in \mathbb{Z} \tag{2.2.12}$$

However, letting $n = -m$ in equation (2.2.12),

$$A_m^0 J_m(\kappa r) e^{+jm\phi} e^{-jk_z z} = A_{-n}^0 J_{-n}(\kappa r) e^{-jn\phi} e^{-jk_z z} = A_n' J_n(\kappa r) e^{-jn\phi} e^{-jk_z z},$$

where $A_n' = (-1)^n A_{-n}^0$ from the following property of Bessel functions

$$J_{-m}(z) = (-1)^m J_m(z), \quad \forall\, (m,x) \in \mathbb{Z} \times \mathbb{C}. \tag{2.2.13}$$

This shows that equation (2.2.12) reduces to equation (2.2.11). In this proof, it has been assumed that κ and k_z did not depend on the sign of m which will be verified in the following sections. Hence without any loss of generality, the solution of the wave equation is a sum of terms of the form

$$\boxed{p_m^0(r,\phi,z) = A_m^0 J_m(\kappa_m r) e^{-jm\phi} e^{-jk_z z}, \quad m \in \mathbb{Z}.} \tag{2.2.14}$$

2.3 Boundary conditions

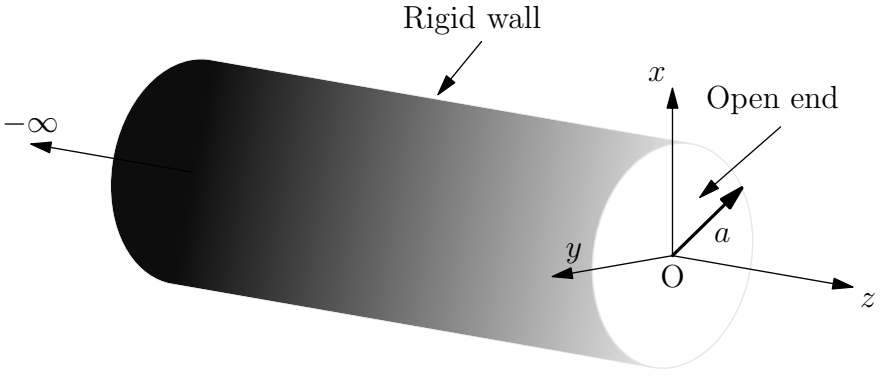

Figure 2.2 – Boundary conditions. Semi-infinite rigid-walled cylindrical duct of radius a.

In addition to being a solution of the wave equation, p_m^0 must also satisfy the boundary conditions. The walls are assumed to be rigid, as illustrated in figure 2.2, therefore the normal velocity is zero. Let $\boldsymbol{u}^0(\boldsymbol{x})$ be the complex velocity, $\boldsymbol{n}$ the vector normal to the surface of the duct, and a the radius of the duct. The boundary condition is given by

$$u_n^0(a,\phi,z) = \boldsymbol{u}^0(a,\phi,z)\cdot\boldsymbol{n} = 0, \quad \forall(\phi,z). \tag{2.3.1}$$

The conservation of momentum implies that

$$\rho_0 \frac{\partial u_n^0(\boldsymbol{x},t)}{\partial t} = -\boldsymbol{\nabla} p_m^0 \cdot \boldsymbol{n},$$
$$\rho_0 j\omega u_n^0(a,\phi,z) = -\frac{\partial p_m^0}{\partial r}(a,\phi,z).$$

Hence, from equations (2.3.1) and (2.2.14)

$$\frac{\partial p_m^0}{\partial r}(a,\phi,z) = 0 \quad \forall(\phi,z),$$
$$J_m'(\kappa a) = 0,$$

where J_m' denotes the derivative of J_m. Therefore, κa must be a root of J_m'. Let j_{mn} denote the nth root of J_m' where $n \geq 1$, then define

$$\boxed{\kappa_{mn}^0 = \frac{j_{mn}}{a}.} \tag{2.3.2}$$

The azimuthal wavenumber κ must equal to κ_{mn}^0 for some value of (m,n). Note that from equation (2.2.13), κ_{mn}^0 and j_{mn} are independent of the sign of m.

2.4 Eigenfunctions

2.4.1 Definition

From equations (2.2.14) and (2.3.2), for any integers $m \in \mathbb{Z}$ and $n \in \mathbb{N}^*$, the function p_{mn}^0 defined by

$$p_{mn}^0(r,\phi,z) = A_{mn}^0 \psi_{mn}(r,\phi) e^{-jk_{z,mn}z}, \tag{2.4.1}$$

where A_{mn}^0 is a constant and

$$\psi_{mn}(r,\phi) = J_m(\kappa_{mn}^0 r) e^{-jm\phi}, \tag{2.4.2}$$

satisfies the wave equation and the boundary conditions. The functions ψ_{mn} are called the eigenfunctions of the duct. They each satisfy the boundary conditions as well as the

following equation

$$\nabla_{\perp}^2 \psi_{mn}(r,\phi) + (\kappa_{mn}^0)^2 \psi_{mn}(r,\phi) = 0, \tag{2.4.3}$$

where

$$\nabla_{\perp}^2 = \frac{1}{r}\frac{\partial}{\partial r}\left(r\frac{\partial}{\partial r}\right) + \frac{1}{r^2}\frac{\partial^2}{\partial \phi^2}.$$

and where κ_{mn}^0 has been defined by equation (2.3.2). The term κ_{mn}^0 is an eigenvalue of the duct.

2.4.2 Normalization

An important property of the eigenfunctions is that they are orthogonal, i.e.,

$$\forall m, n \in \mathbb{Z} \text{ and } n, n' \in \mathbb{N}^*, \begin{cases} \displaystyle\int_{\mathcal{A}} \psi_{mn}(r,\phi)\psi^*_{m'n'}(r,\phi)\ d\mathcal{A} = 0 & \text{if} \quad m \neq m' \text{ or } n \neq n' \\ \displaystyle\int_{\mathcal{A}} \psi_{mn}(r,\phi)\psi^*_{m'n'}(r,\phi)\ d\mathcal{A} \neq 0 & \text{if} \quad m = m' \text{ and } n = n' \end{cases}$$

However, the eigenfunctions defined by equation (2.4.2) are not unique. They can be multiplied by any non-zero constant and still satisfy the required equations. To obtain a unique set of eigenfunctions, one can normalize them as follows. Let

$$\Psi_{mn} = \frac{\psi_{mn}}{N_{mn}}, \tag{2.4.4}$$

where N_{mn} is defined such that

$$\int_{\mathcal{A}} |\Psi_{mn}(r,\phi)|^2\ d\mathcal{A} = \mathcal{A}, \tag{2.4.5}$$

where $\mathcal{A} = \pi a^2$, therefore

$$\Leftrightarrow\ \frac{1}{N_{mn}^2}\int_{\mathcal{A}} |\psi_{mn}(r,\phi)|^2\ d\mathcal{A} = \mathcal{A}. \tag{2.4.6}$$

Solving for N_{mn},

$$\Leftrightarrow\ N_{mn} = \sqrt{\frac{1}{\mathcal{A}}\int_{\mathcal{A}} |\psi_{mn}^2(r,\phi)|\ d\mathcal{A}},$$

Combining this result with equation (2.4.2) gives

$$N_{mn} = \sqrt{\frac{2}{a^2}\int_0^a J_m(\kappa_{mn}^0 r)^2 r\ dr}.$$

This integral can be calculated either numerically, or by using the relation $J'_m(\kappa^0_{mn}a) = 0$ and the following properties of the Bessel functions:

$$\int J_m^2(z)z\, dz = \frac{z^2}{2}\left(J_m^2(z) - J_{m-1}(z)J_{m+1}(z)\right), \qquad \forall\, m \in \mathbb{Z};$$

$$J'_m(z) = \frac{1}{2}\left(J_{m-1}(z) - J_{m+1}(z)\right), \qquad \forall\, m \in \mathbb{Z};$$

$$J_{m-1}(z) + J_{m+1}(z) = \frac{2m}{z}J_m(z), \qquad \forall\, m \in \mathbb{Z} \quad (\text{ if } z \neq 0).$$

It can therefore be shown that

$$\boxed{N_{01} = 1 \quad \text{and} \quad \forall\,(m,n) \neq (0,1),\ N_{mn} = \sqrt{J_m(j_{mn})^2\left[1 - \left(\frac{m}{j_{mn}}\right)^2\right]}.}$$

Note that for any root j_{mn} of J'_m, $m/j_{mn} < 1$ so that N_{mn} is always real and positive. In addition, N_{mn} is independent of the sign of m.

Examples of shape functions are presented in figure 2.3, for various modes. Given a mode (m, n), the corresponding mode shape Ψ_{mn} has m axes of symmetry and is divided into n parts in the radial direction. Thus, figure 2.2(c) shows that Ψ_{23} has 2 axes of symmetry and is divided into 3 in the radial direction.

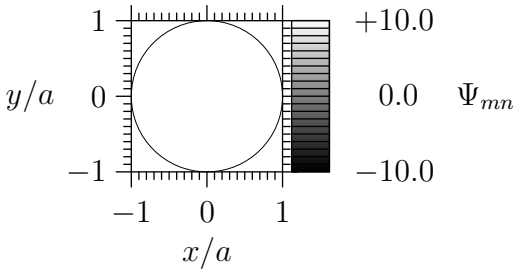

(a) Mode (0,1), plane wave

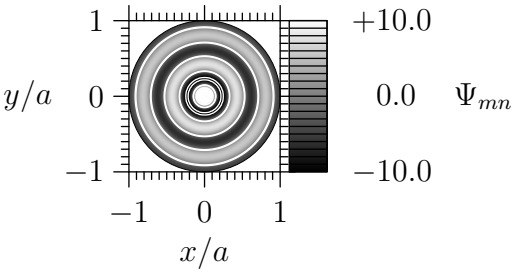

(b) Mode (0,6), 0 axis of antisymmetry, 6 radial divisions.

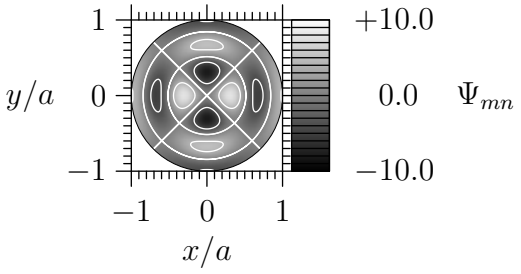

(c) Mode (2,3): 2 axes of antisymmetry, 3 radial divisions.

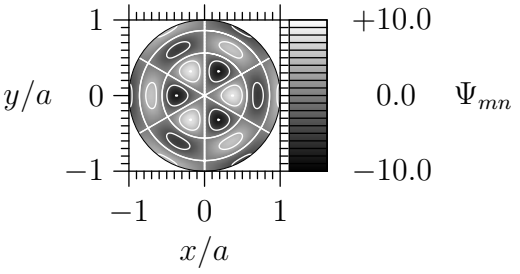

(d) Mode (3,3): 3 axes of antisymmetry, 3 axes of antisymmetry.

Figure 2.3 – Contour plots of different mode shapes Ψ_{mn} of a cylindrical duct (real part) . The contour lines are drawn in white. Straight lines and circles are contours for which the mode shape goes to 0. The straight lines are axes of antisymmetry ; Ψ_{mn} has m axes of antisymmetry. The circles divide the cross section into n parts in the radial direction ; Ψ_{mn} has $n - 1$ such circles.

The modal pressure p_{mn} can be redefined in terms of the normalized shape functions. The definition given in equation (2.4.1) is replaced by

$$\boxed{p^0_{mn}(r,\phi,z) = A^0_{mn}\Psi_{mn}(r,\phi)e^{-jk_{z,mn}z}}, \tag{2.4.7}$$

where the modal weighting A^0_{mn} is now uniquely defined.

2.5 Modal decomposition of the pressure field

2.5.1 General expression

From equations (2.4.1), (2.4.2) and (2.4.4), the solutions of the wave equation travelling in the positive-z direction and satisfying the boundary conditions are given by

$$p^0(r,\phi,z) = \sum_{m=-\infty}^{+\infty}\sum_{n=1}^{+\infty} A^0_{mn}\Psi_{mn}(r,\phi)e^{-jk_z z}, \tag{2.5.1}$$

where

$$\Psi_{mn}(r,\phi) = \frac{J_m(\kappa^0_{mn}r)}{N_{mn}}e^{-jm\phi}. \tag{2.5.2}$$

The coefficients A^0_{mn} are modal amplitudes. Estimating the pressure field from this equation is difficult, because it requires an infinite number of terms. However, only a finite number of terms actually contribute to the pressure field. These are called the cut-on modes.

2.5.2 Cut-on modes

From equations (2.2.8) and (2.3.2), k_z can be expressed as a function of k, i.e.

$$k_z = \sqrt{k^2 - (\kappa^0_{mn})^2}, \tag{2.5.3}$$

$$\Leftrightarrow \boxed{k_z = \alpha^0_{mn}k \quad \text{where} \quad \alpha^0_{mn} = \sqrt{1 - \left(\frac{j_{mn}}{ka}\right)^2}}. \tag{2.5.4}$$

Here, α^0_{mn} is called the cut-off ratio. It does not depend on the sign of m. It will be shown to be important in the derivation of the far field pressure radiated from the duct. The term α^0_{mn} can either be real or imaginary, depending on the value of $\xi_{mn} = j_{mn}/ka$, i.e.

$$\begin{cases} \xi_{mn} < 1 \Rightarrow j_{mn} < ka \Rightarrow \alpha^0_{mn} \in \mathbb{R} & \text{the mode } (m,\, n) \text{ is cut-on;} \\ \xi_{mn} > 1 \Rightarrow j_{mn} > ka \Rightarrow \alpha^0_{mn} \in \mathbb{C}\backslash\mathbb{R} & \text{the mode } (m,\, n) \text{ is cut-off.} \end{cases} \tag{2.5.5}$$

The mode is said to be cut-off when α_{mn}^0 is imaginary because in that case, for a wave propagating in the positive z-direction, expressing k_z as $j|k_z|$ leads to

$$e^{jk_z z} = e^{-|k_z|z},$$

which shows that the wave decays exponentially with z. Thus, the cut-off modes are somehow filtered out by the duct. The modal coefficient ξ_{mn} is called cut-on ratio. The relation between cut-off and cut-on ratios is

$$(\alpha_{mn}^0)^2 + \xi_{mn}^2 = 1.$$

The cut-on modes are presented in figure 2.4 for various frequencies ka. The x-axis gives the value of m and the y-axis the value of n. Each square represents a cut-on mode, for a particular frequency. Thus, the purple squares illustrate the cut-on modes for $ka = 10$. The modes which become cut-on by increasing the frequency up to $ka = 20$ are then plotted in green. Similarly, the additionnal cut-on modes for $ka = 30$, 40, and 50 are respectively plotted in blue, red and black.

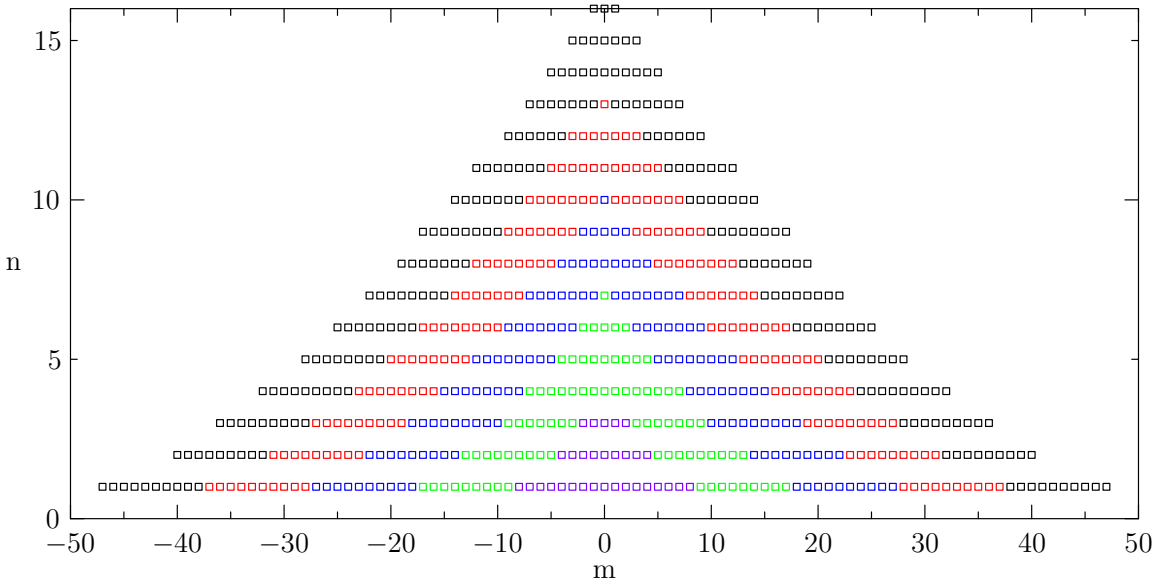

Figure 2.4 – Cut-on modes of a cylindrical duct for five different frequencies ka ; the frequency varies among the following values : 10 (purple), 20 (green), 30 (blue), 40 (rend), 50 (black).

Figure 2.5 is a plot of the number of cut-on modes with frequency. The exact number is represented by red triangles. It is in very good agreement with the asymptotic approximation, derived, for example, by Rice [16],

$$N_1(ka) = ka/2 + (ka/2)^2.$$

In the frequency range of interest, for example for $ka = 50$, the number of cut-on modes is higher than 600. This large number gives an indication of the amount of computational

cost of the pressure field calculation for a multi-mode sound transmission inside the duct.

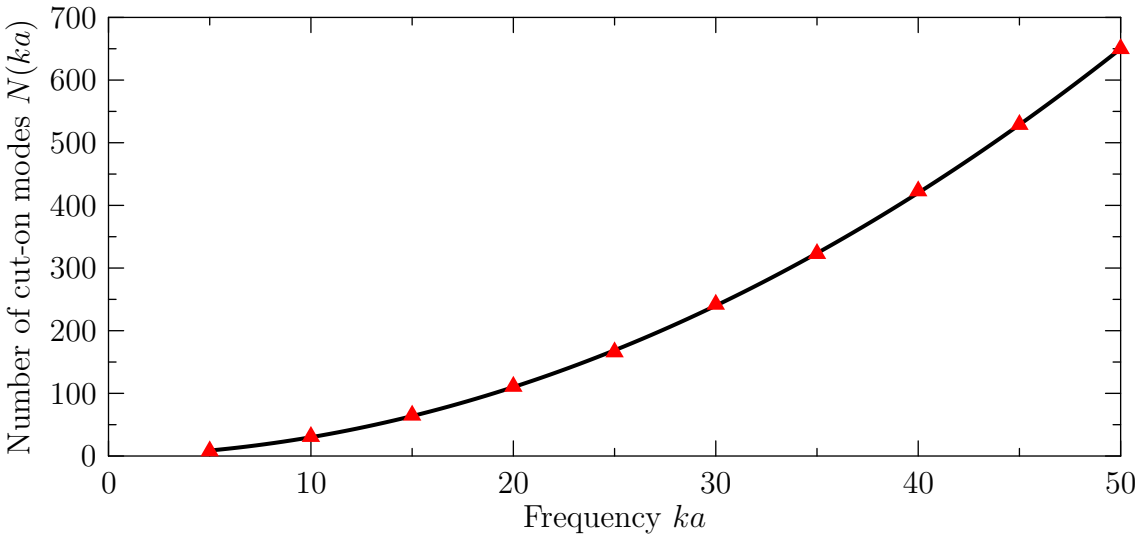

Figure 2.5 – Number of cut-on modes in a cylindrical duct as a function of frequency. The exact value $N(ka)$ is represented by the red triangles ; the black line is a high frequency approximation whose equation is defined by $N_1(ka) = ka/2 + (ka/2)^2$.

2.5.3 Physical interpretation

From equations (2.5.1) and (2.5.4), the general expression of the pressure field travelling in the positive z-direction inside the duct is

$$\boxed{p^0(r,\phi,z) = \sum_{m=-\infty}^{+\infty} \sum_{n=1}^{+\infty} A^0_{mn} \Psi_{mn}(r,\phi) e^{-j\alpha^0_{mn} kz}}. \tag{2.5.6}$$

It can be seen from equation (2.5.5) that any particular mode (m, n) becomes cut-on if the frequency is large enough. Similarly, at a particular frequency of excitation, only the modes such that $\xi_{mn} < 1$ will be cut-on. This means that the duct behaves like a low pass filter such that only a finite number of modes can propagate at any given frequency. This allows the infinite sum in equation (2.5.1) to be truncated,

$$\boxed{p^0(r,\phi,z) = \sum_{(m,n)\in\mathcal{O}} A^0_{mn} \Psi_{mn}(r,\phi) e^{-j\alpha^0_{mn} kz},} \tag{2.5.7}$$

where $\mathcal{O}$ is the set of cut-on modes,

$$\mathcal{O} = \Big\{ (m,n) \in \mathbb{Z} \times \mathbb{N}^* \quad | \quad \xi_{mn} < 1 \Big\}.$$

Note that because of the normalization of the eigenfunctions, the modal amplitudes A^0_{mn} are uniquely defined in that decomposition. They have the dimension of pressure.

2.5.4 Geometrical interpretation

The cut-on and cut-off ratio can be related to the direction of propagation of a particular mode inside the duct. If θ denotes the angle between the direction of propagation and the duct axis, then

$$k_{z,mn} = k\cos\theta,$$
$$\kappa_{mn}^0 = k\sin\theta,$$

therefore from equation (2.5.4),

$$\alpha_{mn}^0 = \cos\theta, \tag{2.5.8}$$
$$\xi_{mn}^0 = \sin\theta. \tag{2.5.9}$$

This results are illustrated in figure 2.6.

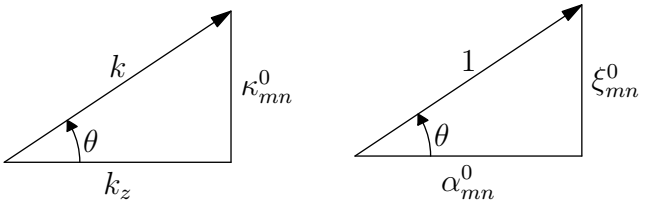

(a) In terms of κ_{mn}^0 **(b)** In terms of α_{mn}^0

Figure 2.6 – Direction of propagation of mode (m, n).

Chapter 3

Radiated pressure in the far field

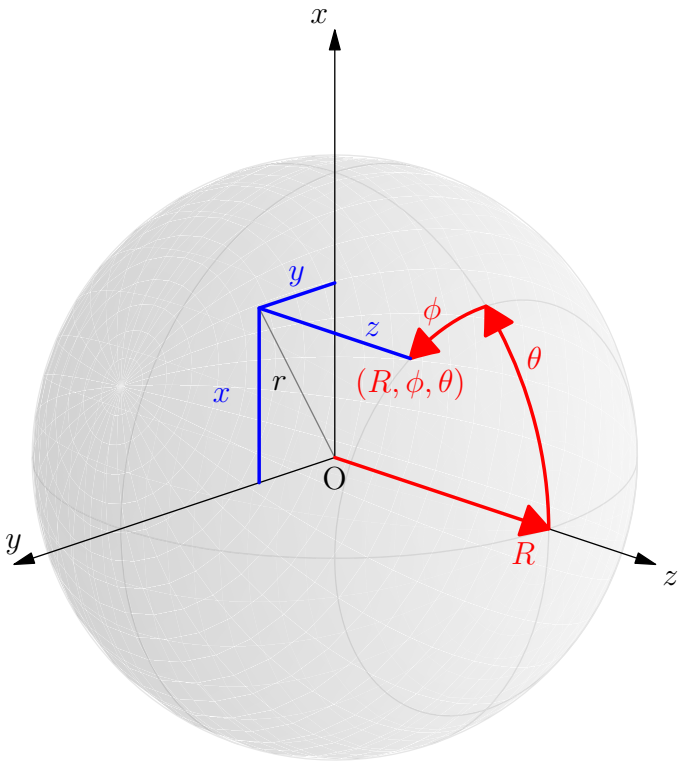

Figure 3.1 – Spherical coordinates system

The radiated pressure in the far field can be expressed in terms of the cut-on modal pressures

$$p_f(R,\theta,\phi,k) = \sum_{(m,n)\in\mathcal{O}} p_{mn,f}(R,\theta,\phi,k), \tag{3.0.1}$$

where, as illustrated in figure 3.1, R is the distance from the centre of the open end of the duct to the observation point, θ the zenith angle, ϕ the azimuth angle and ka the non dimensional frequency. The modes are assumed to be incoherent (their phase varies randomly). The objective is to estimate the mean square far field pressure $\frac{1}{2}E\{|p_f|^2\}$. Since the modes

are incoherent,

$$E\{p^*_{mn,f}(R,\theta,\phi)p_{m'n',f}(R,\theta,\phi)\} = 0 \quad \forall\,(m,n) \neq (m',n').$$

The mean square far field pressure is therefore given by

$$\overline{p^2_f(R,\theta,\phi,k)} = \frac{1}{2}E\{|p^2_f(R,\theta,\phi,k)|\} = \frac{1}{2}\sum_{(m,n)\in\mathcal{O}} E\{|p^2_{mn,f}(R,\theta,\phi,k)|\}.$$

The modal pressure $p_{mn,f}$ can be expressed in terms of the dimensionless in-duct to far-field transfer function $H_{mn}(ka,\theta)$, defined by Joseph and Morfey [1],

$$p_{mn,f}(R,\theta,\phi,k) = \frac{a}{R}A^0_{mn}H_{mn}(ka,\theta)e^{-jm\phi}e^{-jkR}. \tag{3.0.2}$$

Thus,

$$\boxed{E\{|p_{mn,f}(R,\theta,ka)|^2\} = \left(\frac{a}{R}\right)^2 |H_{mn}(ka,\theta)|^2 E\{|A^0_{mn}|^2\}}. \tag{3.0.3}$$

Thus, the sound field is axi-symmetric. Equation (3.0.3) shows that two quantities must be calculated in order to estimate the mean square modal pressure in the far field. First, $|H_{mn}(ka,\theta)|^2$ must be derived for each cut-on mode. Second, an estimation of the modal amplitudes $E\{|A^0_{mn}|^2\}$must be obtained.

The modal amplitudes depend on the type of sources which generate the sound. The distribution of sources in the duct can be modelled in different ways. The models developed by Joseph *et al.* [4, 1] will be presented in section 3.2.

3.1 Derivation of $|H_{mn}(ka,\theta)|^2$

In this dissertation, H_{mn} is obtained in two different ways. If one assume that the duct terminates in an infinite baffle, H_{mn} can be derived analytically from Rayleigh's integral. The other method gives the exact solution for an unflanged duct and is based on the Wiener-Hopf technique. However, it gives only a numerical solution.

3.1.1 Flanged duct

Computation by Rayleigh Integral

The flanged duct model is illustrated in figure 3.2. The pressure radiated from the open end of a flanged duct is given by Rayleigh's Integral

$$p^0(\boldsymbol{r}) = \frac{jk}{2\pi}\rho_0 c_0 \int_{\mathcal{A}} u^0_z(\boldsymbol{r_s})\frac{e^{-jk|\boldsymbol{r}-\boldsymbol{r_s}|}}{|\boldsymbol{r}-\boldsymbol{r_s}|}\,d\mathcal{A}, \tag{3.1.1}$$

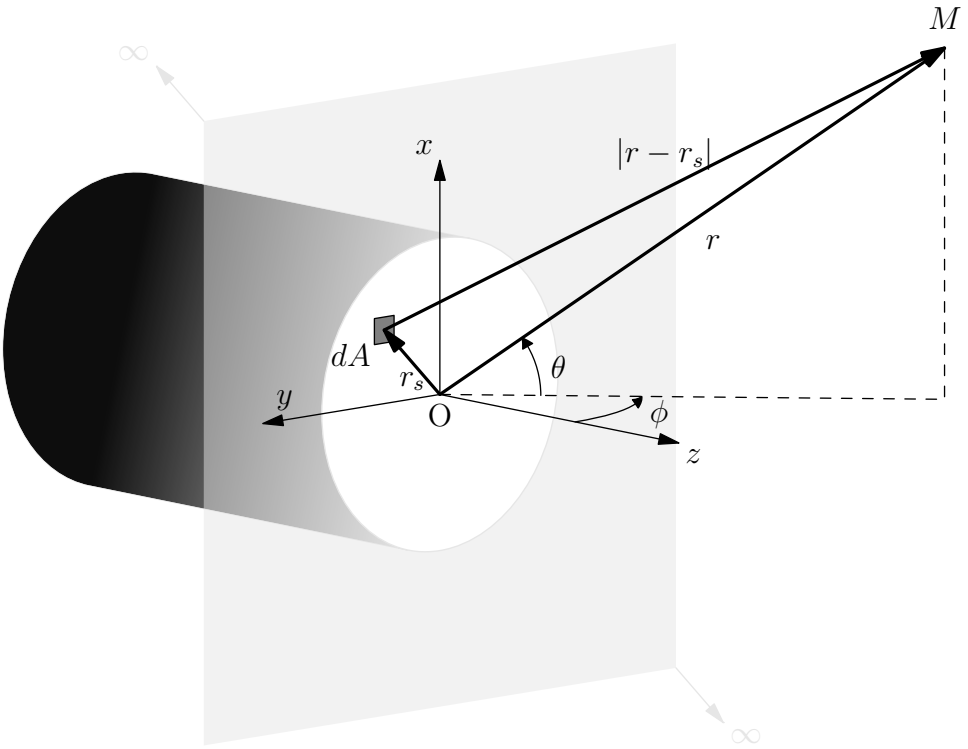

Figure 3.2 – Flanged duct approximation: an infinite flange is added at the open end of the duct. This enables to obtain an approximation of the in-duct to far field transfer function in the forward arc.

where $\boldsymbol{r} = (R, \phi, \theta)$ is the position in the far field in spherical coordinates, and $\boldsymbol{r_s} = (R_s, \phi_s, \pi/2)$ the position of an infinitesimal piston source situated at the open end of the duct. The particle velocity $u_z^0(\boldsymbol{r_s})$ transmitted along the duct can be derived from the momentum equation

$$\rho_0 j\omega u_z^0(\boldsymbol{r_s}) = -\frac{\partial p}{\partial z}\Big|_{z=0} = j \sum_{(m,n)\in\mathcal{O}} A_{mn}^0 \alpha_{mn}^0 k \Psi_{mn}(R_s, \phi_s) \alpha_{mn}^0 k e^{-j\alpha_{mn}^0 kz}\Big|_{z=0}, \quad (3.1.2)$$

$$u_z^0(\boldsymbol{r_s}) = \frac{1}{\rho_0 c_0} \sum_{(m,n)\in\mathcal{O}} A_{mn}^0 \alpha_{mn}^0 \Psi_{mn}(R_s, \phi_s). \quad (3.1.3)$$

In the far-field, $R_s \ll R$, so that

$$|\boldsymbol{r} - \boldsymbol{r_s}| = R\left(1 - 2\frac{R_s}{R}\sin(\theta)\cos(\phi - \phi_s) + \left(\frac{R_s}{R}\right)^2\right)^{1/2},$$

$$|\boldsymbol{r} - \boldsymbol{r_s}| \approx R - R_s \sin(\theta)\cos(\phi - \phi_s),$$

$$\frac{1}{|\boldsymbol{r} - \boldsymbol{r_s}|} \approx \frac{1}{R}.$$

Combining the expressions of u_z^0 and $|\boldsymbol{r} - \boldsymbol{r_s}|$ into equation (3.1.1) gives

$$p^0(\boldsymbol{r}) \approx \sum_{(m,n)\in\mathcal{O}} A_{mn}^0 \frac{jk}{2\pi} \frac{\alpha_{mn}^0}{R} e^{-jkR} \times \int_0^a \int_0^{2\pi} e^{jkR_s \sin(\theta)\cos(\phi-\phi_s)} \Psi_{mn}(R_s, \phi_s) R_s \, \mathrm{d}\phi_s \, \mathrm{d}R_s.$$

From the definition of Ψ_{mn} given in equation (2.4.4) and the definition of far field modal pressure $p_{mn,f}$,

$$p_{mn,f} = A_{mn}^0 \frac{jk}{2\pi} \alpha_{mn}^0 \frac{e^{-jkR}}{R} \times \int_0^a \Big[\int_0^{2\pi} e^{jkR_s \sin(\theta)\cos(\phi-\phi_s)} e^{-jm\phi_s} \, d\phi_s \Big] \frac{J_m(\kappa_{mn}^0 R_s)}{N_{mn}} R_s \, dR_s. \tag{3.1.4}$$

The two integrals can be calculated by using the following properties of Bessel functions

$$\int_0^{2\pi} e^{jm(\phi-\phi_s)} e^{jz\cos(\phi-\phi_s)} \, d\phi_s = 2\phi j^m J_m(z);$$
$$\int_0^a J_m(\alpha r) J_m(\beta r) r \, dr = \frac{a}{\alpha^2 - \beta^2} \times \left[\beta J_m(\alpha a) J_m'(\beta a) - \alpha J_m(\beta a) J_m'(\alpha a)\right], \text{if } \alpha \neq \beta.$$

Using these two properties successively gives

$$p_{mn,f} = \frac{a}{R} A_{mn}^0 e^{-jm\phi} e^{-jkR} j^{m+1} \frac{\alpha_{mn}^0}{N_{mn}} J_m(j_{mn}) \frac{k^2 \sin\theta}{(\kappa_{mn}^0)^2 - k^2(\sin\theta)^2} J_m'(ka\sin\theta). \tag{3.1.5}$$

From the definition of the in-duct to far-field transfer function given by equation (3.0.2), H_{mn} can be expressed as follows in the case of a flanged duct

$$\boxed{H_{mn}(ka,\theta) = j^{m+1} \frac{\alpha_{mn}^0}{N_{mn}} J_m(j_{mn}) \frac{(ka)^2 \sin\theta}{j_{mn}^2 - (ka)^2(\sin\theta)^2} J_m'(ka\sin\theta).} \tag{3.1.6}$$

Angle of maximum radiation

According to equation (3.1.6), the denominator of the transfer function goes to zero when

$$ka\sin\theta \neq j_{mn}, \tag{3.1.7}$$

which gives the angle of maximum radiation, which will be denoted by θ_{mn}^0. According to equation (2.3.2), the above equation is equivalent to the condition

$$k\sin\theta_{mn} = \kappa_{mn}. \tag{3.1.8}$$

Thus, following figure 2.6, θ_{mn} corresponds to the angle of propagation of mode (m,n) inside the duct. Interpreting the wave as a ray, it is straightforward to see that a mode propagating in direction θ inside the duct tends to radiate in that same direction after reaching the open-end of the duct. Thus, the angle of maximum radiation is simply related to the

cut-off ratio by

$$\boxed{\cos\theta_{mn} = \alpha^0_{mn}.} \tag{3.1.9}$$

The maximum value of H_{mn} can be obtained by studying the limit of $h(X)$ as $X \to j_{mn}$, where

$$h(X) = \frac{1}{\sin\theta}\frac{X^2}{j_{mn}^2 - X^2}J'_m(X).$$

Note that

$$H_{mn}(ka,\theta) = j^{m+1}\frac{\alpha^0_{mn}}{N_{mn}}J_m(j_{mn})h(ka\sin\theta).$$

Since $J'_m(j_{mn}) = 0$ and since J'_m is differentiable at j_{mn},

$$h(X) = -\frac{1}{\sin\theta}\frac{X^2}{X + j_{mn}}\frac{J'_m(X) - J'_m(j_{mn})}{X - j_{mn}} \to -\frac{1}{\sin\theta}\frac{j_{mn}}{2}J''_m(j_{mn}) \quad \text{as } X \to j_{mn}.$$

Thus,

$$\boxed{H_{mn}(ka,\theta)\Big|_{ka\sin\theta = j_{mn}} = -j^{m+1}\frac{\alpha^0_{mn}}{N_{mn}}\frac{j_{mn}}{2\sin\theta}J_m(j_{mn})J''_m(j_{mn}).} \tag{3.1.10}$$

To simplify the computation of $J''_m(j_{mn})$ one can use the following formulae

$$J''_m(j_{mn}) = \left(\left(\frac{m}{j_{mn}}\right)^2 - 1\right)J_m(j_{mn}) \qquad \text{if } (m,n) \neq (0,1);$$

$$J''_0(j_{01}) = -J'_1(j_{01}) \qquad \text{if } (m,n) = (0,1).$$

BEHAVIOUR OF THE TRANSFER FUNCTIONS

Variation with cut-off ratio Figure 3.3 shows the variation of $|H_{mn}|^2$ with θ for a well cut-on and a nearly cut-off mode for $ka = 10$. The angle of maximum radiation is plotted in grey. It can be seen that modes which have their cut-off ratio close to 1 tend to radiate mostly around the axis of the duct, and are well cut-on, whereas those which have their cut-off ratio close to 0 tend to radiate towards $90°$ and are nearly cut-off.

Zero pressure for $\theta = 0$ From equation (3.1.6), the directivity function goes to zero when $\theta = 0$ except when $j_{mn} = 0$ which occurs only for the plane wave mode $(1,0)$. Thus, the plane wave mode is the only one which radiates in the direction of the duct-axis. This is illustrated in figure 3.5.

Variation with frequency Given a mode (m,n), we study the variation of the functions $|H_{mn}(ka,\theta)|^2$ as ka increases. As illustrated in figure 3.5, the main radiation lobe tend towards $\theta = 0$. This is due to the fact that the mode becomes more cut-on as ka increases. Besides, the number of side lobes increases also for the same reason.

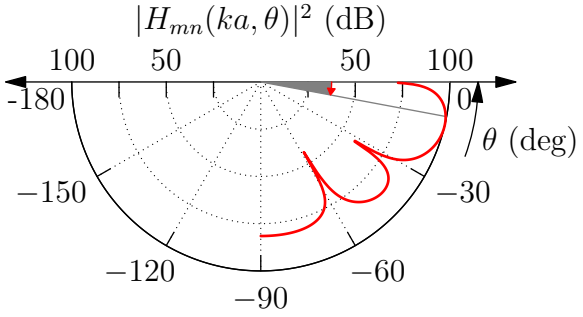

(a) mode (m, n)=(1,1), ka=10, α^0_{mn} =0.98

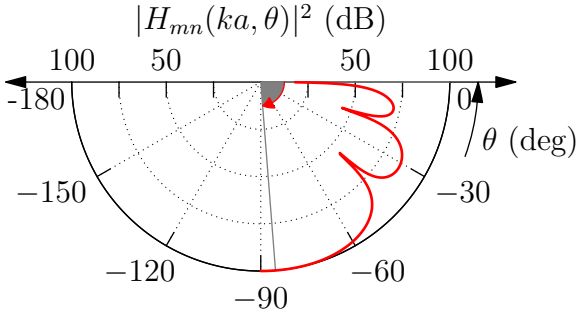

(b) mode (m, n)=(2,3), ka=10, α^0_{mn} =0.08

Figure 3.3 – Angle of maximum radiation (in grey) from a cylindrical duct for a well cut-on mode (a) and a nearly cut-off mode (b), at $ka = 10$. The well cut-on modes radiate mostly around the z-axis ; the modes close to cut-off radiate mostly at 90 degrees.

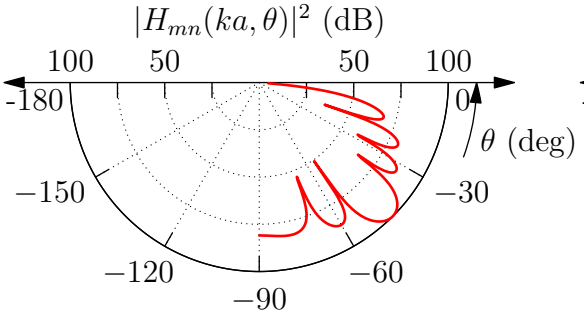

(a) Higher order mode,(m,n)=(8,4), ka=30.

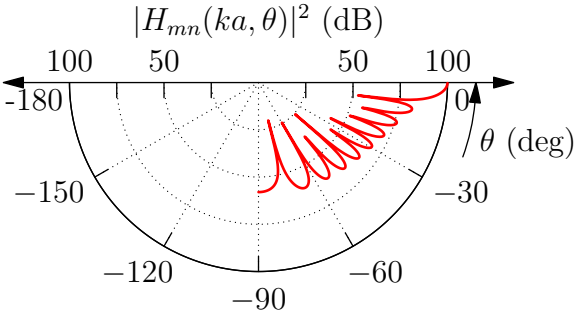

(b) Plane wave mode, (m,n)=(0,1), ka=30.

Figure 3.4 – For all frequencies, the in duct to far field transfer function is zero at 0 degree for all higher order modes $(m, n) \neq (0, 1)$ (a). The plane wave mode is the only one for which the transfer function is non-zero at 0 degree (b).

3.1.2 Unflanged duct

The exact modal in-duct to far field transfer function for an unflanged duct has been presented by Homicz and Lordi [8]. Its magnitude is given by

$$|H_{mn}(ka,\theta)| = N_{mn}a \left| \frac{J_m(\kappa^0_{mn}a)\alpha^0_{mn}}{\alpha^0_{mn} - \cos\theta} \right| \times \sqrt{\frac{(\kappa^0_{mn}a)^2 - m^2}{\pi(\kappa^0_{mn})^2} \sin[\Omega_m(ka\sin\theta)]}$$

$$\times \sqrt{\prod_{\substack{s=1 \\ s\neq n}}^{n_0} \frac{\alpha^0_{ms} + \alpha^0_{mn}}{\alpha^0_{ms} - \alpha^0_{mn}} \prod_{q=1}^{n_0} \frac{\alpha^0_{mq} - \cos\theta}{\alpha^0_{mq} + \cos\theta}} \exp[T_m(\alpha^0_{mn}, ka) - T_m(\cos\theta, ka)] \quad (3.1.11)$$

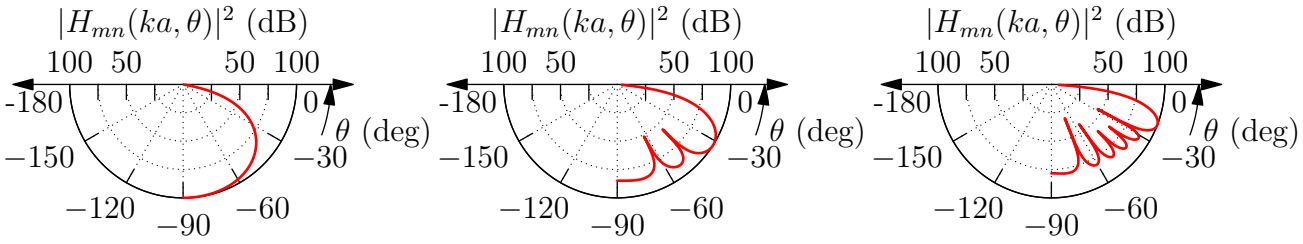

(a) mode (m,n)=(8,1), ka=10, α^0_{mn}=0.26

(b) mode (m,n)=(8,1), ka=20, α^0_{mn}=0.88

(c) mode (m,n)=(8,1), ka=30, α^0_{mn}=0.95

Figure 3.5 – Variation of the in duct to far field transfer function for mode (8,1) at ka equals 10,20 and 30.

where Ω_m and T_m are defined by

$$\Omega_m(\nu) = \tan^{-1}\frac{Y'_m(\nu)}{J'_m(\nu)} + \frac{\pi}{2} \qquad \text{if } m = 0,$$

$$\Omega_m(\nu) = \tan^{-1}\frac{Y'_m(\nu)}{J'_m(\nu)} - \frac{\pi}{2} \qquad \text{if } m < 0,$$

$$T_m(\eta, ka) = \frac{1}{2\pi}\int_{-1}^{1}\frac{\Omega(ka\sqrt{1-\xi^2})}{\xi-\eta}\,d\xi.$$

The term Y'_m is the derivative of the mth Bessel function of the second kind, and Ω represents the phase of the Hankel function derivative. It must be continuous and therefore must be unwrapped. Note that when $\nu = \kappa^0_{mn}a$, Ω is given by

$$\Omega_m(\kappa^0_{mn}a) = n\pi$$

Note that, from equation (3.1.11), the amplitude of the transfer function $|H_{mn}|$ is maximum when

$$\alpha^0_{mn} = \cos\theta,$$

which is the same relation than the one derived for a flanged duct, i.e. equation (3.1.9.

3.1.3 Validation of the flanged transfer functions

The exact Wiener-Hopf solution of equation (3.1.11) is compared to the flanged duct transfer function of equation (3.1.6). The results are presented in figure 3.6. The agreement between the two is excellent for well cut-on modes 3.6(b). For modes which are close to cut-off, the agreement is very good but the secondary lobes are slightly underestimated by the flanged duct model. Thus, the main lobe is This validates the flanged duct approximation for the in-duct to far field transfer function in the zero-flow case.

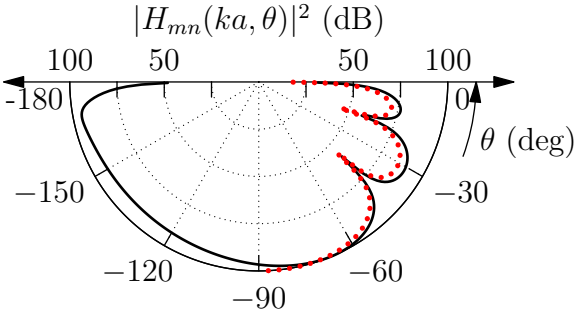

(a) ka=10, (m,n)=(2,3), mode nearly cut-off

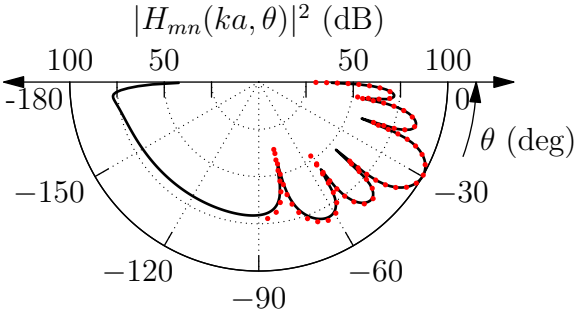

(b) ka=20, (m,n)=(2,3), mode well cut-on

Figure 3.6 – Comparison of the modal transfer functions from a flanged model (red dots curve) and from the Wiener Hopf Technique (black curve), for (m,n)=(2,3). The mode is amost cut-off at ka=10, and well cut-on at ka=20 (the cut-off ratio is respectively equal to 0.08 and 0.98).

3.2 Weighting models

The modal amplitudes A^0_{mn} depend on the sound sources present in the duct. Let $Q_{vol}(\boldsymbol{x})$ be a volume distribution of sources. The sound field generated in the duct by this distribution of sources must satisfy the following equation

$$\nabla^2 p^0(\boldsymbol{x}) + k^2 p^0(\boldsymbol{x}) = -Q_{vol}(\boldsymbol{x})$$

Let $G(\boldsymbol{x}|\boldsymbol{y})$ be a Green's function of the duct satisfying the rigid wall boundary condition. It represents the sound field at $\boldsymbol{x}$ generated by a point source situated at $\boldsymbol{y}$. For any given point $\boldsymbol{x}$, let $\boldsymbol{x_s}$ be the projection of $\boldsymbol{x}$ in the plane $z = 0$, and x_3 the z-coordinate of $\boldsymbol{x}$. Using the formula derived by Goldstein[17], or using the flow Green's function derived in section 8.2.1 with zero Mach number, $G(\boldsymbol{x}|\boldsymbol{y})$ can be expressed as

$$G(\boldsymbol{x}|\boldsymbol{y}) = \sum_{m,n} -\frac{j}{2\mathcal{A}\alpha^0_{mn}k}\Psi^*_{mn}(\boldsymbol{y_s})\Psi_{mn}(\boldsymbol{x_s})e^{-j\alpha^0_{mn}rk|x_3-y_3|}. \tag{3.2.1}$$

The sound field $p^0(\boldsymbol{x})$ in the duct can be calculated from the distribution of sources $Q_{vol}(\boldsymbol{y})$ and the Green's function $G(\boldsymbol{x}|\boldsymbol{y})$,i.e.

$$\boxed{p^0(\boldsymbol{x}) = \int_V Q_{vol}(\boldsymbol{y})G(\boldsymbol{x}|\boldsymbol{y})\ d^3\boldsymbol{y}}. \tag{3.2.2}$$

For simple volume source distributions, it is possible to derive $E\{|A^0_{mn}|^2\}$ as a function of the cut-on ratio α^0_{mn}. Alternatively, one can make some assumptions regarding the distribution of sound power between all modes. Castres and Joseph [18] have recently shown that assuming an equal partition of energy between all cut-on modes was a good model for broadband sound from a ducted fan. The expression of $E\{|A^0_{mn}|^2\}$ will therefore be derived for this "equal power per mode" model.

3.2.1 Uniform distribution of incoherent monopoles

Let $Q_{vol}(\boldsymbol{y})$ be a uniform distribution of incoherent monopoles located in the plane $z = z_0$. $Q_{vol}(\boldsymbol{y})$ is of the form

$$Q_{vol}(\boldsymbol{y}) = \rho_0 j\omega q_s(\boldsymbol{y_s})\delta(y_3 - z_0), \tag{3.2.3}$$

where $q_s(\boldsymbol{y_s})$ is a volume velocity source per unit surface. From equations (3.2.2) and (3.2.3)

$$p^0(\boldsymbol{x}) = \int_V \rho_0 j\omega q_s(\boldsymbol{y_s})\delta(y_3 - z_0)G(\boldsymbol{x}|\boldsymbol{y})\ d^3\boldsymbol{y}. \tag{3.2.4}$$

Substituting $d^3\boldsymbol{y}$ by $d^2\boldsymbol{y_s}\,dy_3$ in (3.2.4) and using equation (3.2.1) gives

$$p^0(\boldsymbol{x}) = \rho_0 j\omega \sum_{(m,n)\in\mathcal{O}} \frac{-j}{2\mathcal{A}\alpha^0_{mn}k} \times \int_{\mathcal{A}}\int_{-\infty}^{0} q_s(\boldsymbol{y_s})\delta(y_3 - z_0)\Psi^*_{mn}(\boldsymbol{y_s})\Psi_{mn}(\boldsymbol{x_s})e^{-j\alpha^0_{mn}k|y_3-x_3|}\ \mathrm{d}y_3\,\mathrm{d}\boldsymbol{y_s}$$

$$p^0(\boldsymbol{x}) = \rho_0 j\omega \sum_{m,n} \frac{-j}{2\mathcal{A}\alpha^0_{mn}k} \int_{\mathcal{A}} q_s(\boldsymbol{y_s})\Psi^*_{mn}(\boldsymbol{y_s})\Psi_{mn}(\boldsymbol{x_s})e^{-j\alpha^0_{mn}k|z_0-x_3|}\ d^2\boldsymbol{y_s}$$

For $x_3 \geq z_0$,

$$p^0(\boldsymbol{x}) = \rho_0 j\omega e^{j\alpha^0_{mn}z_0} \sum_{m,n} \left(\frac{-j}{2\mathcal{A}\alpha^0_{mn}k} \int_{\mathcal{A}} q_s(\boldsymbol{y_s})\Psi^*_{mn}(\boldsymbol{y_s})\ d^2\boldsymbol{y_s} \right) \Psi_{mn}(\boldsymbol{x_s})e^{-j\alpha^0_{mn}kx_3}$$

Thus, from equation (2.5.7)

$$A^0_{mn} = \frac{\rho_0 c_0}{2\mathcal{A}\alpha^0_{mn}} e^{j\alpha^0_{mn}kz_0} \int_{\mathcal{A}} q_s(\boldsymbol{y_s})\Psi^*_{mn}(\boldsymbol{y_s})\ d^2\boldsymbol{y_s}$$

$$|A^0_{mn}|^2 = A^0_{mn}A^0_{mn}* = \frac{\rho_0^2 c_0^2}{4\mathcal{A}^2(\alpha^0_{mn})^2} \int_{\mathcal{A}'}\int_{\mathcal{A}} q_s(\boldsymbol{y_s})\Psi^*_{mn}(\boldsymbol{y_s})q^*_s(\boldsymbol{y'_s})\Psi_{mn}(\boldsymbol{y'_s})\ \mathrm{d}^2\boldsymbol{y_s}\,\mathrm{d}^2\boldsymbol{y'_s}$$

$$E\{|A^0_{mn}|^2\} = \frac{\rho_0^2 c_0^2}{4\mathcal{A}^2(\alpha^0_{mn})^2} \int_{\mathcal{A}'}\int_{\mathcal{A}} \Psi^*_{mn}(\boldsymbol{y_s})\Psi_{mn}(\boldsymbol{y'_s})E\{q_s(\boldsymbol{y_s})q^*_s(\boldsymbol{y'_s})\}\ \mathrm{d}^2\boldsymbol{y_s}\,\mathrm{d}^2\boldsymbol{y'_s}$$

If the monopoles are incoherent,

$$E\{q_s(\boldsymbol{y_s})q_s^*(\boldsymbol{y'_s})\} = 2\overline{Q_s^2}\mathcal{A}\delta(\boldsymbol{y_s} - \boldsymbol{y'_s})$$

where $\overline{Q_s^2}$ is source strength which represents the mean square volume velocity of the monopoles per unit surface, and where $\mathcal{A}$ is the cross-sectional area of the duct. Thus,

$$E\{|A_{mn}^0|^2\} = \frac{\rho_0^2 c_0^2}{2(\alpha_{mn}^0)^2}\frac{\overline{Q_s^2}}{\mathcal{A}}\int_{\mathcal{A}} |\Psi_{mn}(\boldsymbol{y'_s})|^2 \; d^2\boldsymbol{y'_s}$$

$$\boxed{E\{|A_{mn}^0|^2\} = \frac{\rho_0^2 c_0^2}{2}\overline{Q_s^2}(\alpha_{mn}^0)^{-2}.} \tag{3.2.5}$$

3.2.2 Uniform distribution of incoherent axial dipoles

Let $Q_{vol}(\boldsymbol{y})$ be a uniform distribution of incoherent axial dipoles located in the plane $z = z_0$. The source $Q_{vol}(\boldsymbol{y})$ is of the form

$$Q_{vol}(\boldsymbol{y}) = -\boldsymbol{\nabla_y} \cdot \boldsymbol{f_{vol}}(\boldsymbol{y}), \tag{3.2.6}$$

where

$$\boldsymbol{f_{vol}}(\boldsymbol{y}) = f_s(\boldsymbol{y})\delta(y_3 - z_0)\boldsymbol{e_z}. \tag{3.2.7}$$

In the above expression, $f_s(\boldsymbol{y_s})$ is a force per unit surface and $\boldsymbol{e_z}$ is the unit vector in the z-direction. From equations (3.2.2) and (3.2.6)

$$p^0(\boldsymbol{x}) = \int_V \Big(\boldsymbol{\nabla_y} \cdot \boldsymbol{f_{vol}}(\boldsymbol{y})\Big)G(\boldsymbol{x}|\boldsymbol{y}) \; d^3\boldsymbol{y}$$
$$p^0(\boldsymbol{x}) = \int_V \boldsymbol{\nabla_y} \cdot \Big[\boldsymbol{f_{vol}}(\boldsymbol{y})G(\boldsymbol{x}|\boldsymbol{y})\Big] \; d^3\boldsymbol{y} - \int_V \boldsymbol{\nabla_y}G(\boldsymbol{x}|\boldsymbol{y}) \cdot \boldsymbol{f_{vol}}(\boldsymbol{y}) \; d^3\boldsymbol{y}$$

The first integral can be calculated by using Green's theorem. Let ∂V be the boundary of volume V. Since the sources are bounded, if V is large enough,

$$\boldsymbol{f_{vol}}(\boldsymbol{y}) = 0 \quad \forall\, \boldsymbol{y} \in \partial V$$

$$\int_V \boldsymbol{\nabla_y} \cdot \Big[\boldsymbol{f_{vol}}(\boldsymbol{y})G(\boldsymbol{x}|\boldsymbol{y})\Big] \; d^3\boldsymbol{y} = \int_{\partial V} \boldsymbol{f_{vol}}(\boldsymbol{y})G(\boldsymbol{x}|\boldsymbol{y}) \cdot \boldsymbol{n} \; d\boldsymbol{y} = 0$$

Thus,

$$p^0(\boldsymbol{x}) = -\int_V \boldsymbol{\nabla_y}G(\boldsymbol{x}|\boldsymbol{y}) \cdot \boldsymbol{f_{vol}}(\boldsymbol{y}) \; d^3\boldsymbol{y} \tag{3.2.8}$$

Combining equations (3.2.7) and (3.2.8) gives

$$p^0(\boldsymbol{x}) = -\int_V \boldsymbol{\nabla}_{\boldsymbol{y}} G(\boldsymbol{x}|\boldsymbol{y}) \cdot f_s(\boldsymbol{y})\delta(y_3 - z_0)\boldsymbol{e_z}\ d^3\boldsymbol{y}$$

$$p^0(\boldsymbol{x}) = -\int_{\partial V}\int_{-\infty}^{0} \frac{\partial G(\boldsymbol{x}|\boldsymbol{y})}{\partial y_3} f_s(\boldsymbol{y})\delta(y_3 - z_0)\ \mathrm{d}y_3\, \mathrm{d}^2\boldsymbol{y_s}$$

$$p^0(\boldsymbol{x}) = -\int_{\partial V} \frac{\partial G(\boldsymbol{x}|\boldsymbol{y})}{\partial y_3}\Big|_{y_3=z_0} f_s(\boldsymbol{y_s})\ d\boldsymbol{y_s} \tag{3.2.9}$$

From (3.2.1), if $x_3 \geq z_0$

$$p^0(\boldsymbol{x}) = \sum_{m,n}\int_{\mathcal{A}} \frac{1}{2\mathcal{A}}\Psi^*_{mn}(\boldsymbol{y_s})\Psi_{mn}(\boldsymbol{x_s})e^{-j\alpha^0_{mn}k(x_3-z_0)} f_s(\boldsymbol{y_s})\ d^2\boldsymbol{y_s}$$

$$p^0(\boldsymbol{x}) = \sum_{m,n} \frac{1}{2\mathcal{A}}\Psi_{mn}(\boldsymbol{x_s})e^{-j\alpha^0_{mn}k(x_3-z_0)} \int_{\mathcal{A}} \Psi^*_{mn}(\boldsymbol{y_s}) f_s(\boldsymbol{y_s})\ d^2\boldsymbol{y_s}$$

From (2.5.7)

$$A^0_{mn} = \frac{1}{2\mathcal{A}} e^{j\alpha^0_{mn}kz_0} \int_{\mathcal{A}} \Psi^*_{mn}(\boldsymbol{y_s}) f_s(\boldsymbol{y_s})\ d^2\boldsymbol{y_s} \tag{3.2.10}$$

Thus,

$$E\{|A^0_{mn}|^2\} = \frac{1}{4\mathcal{A}^2}\int_{\mathcal{A}}\int_{\mathcal{A}'} \Psi^*_{mn}(\boldsymbol{y_s})\Psi_{mn}(\boldsymbol{y'_s})E\{\boldsymbol{f_s}(\boldsymbol{y_s})\boldsymbol{f_s}^*(\boldsymbol{y'_s})\}\ \mathrm{d}^2\boldsymbol{y'_s}\,\mathrm{d}^2\boldsymbol{y_s}$$

If the dipoles are uniform and incoherent,

$$E\{\boldsymbol{f_s}(\boldsymbol{y_s})\boldsymbol{f_s}^*(\boldsymbol{y'_s})\} = 2\overline{F_s^2}\mathcal{A}\delta(\boldsymbol{y_s} - \boldsymbol{y'_s})$$

where $\overline{F_s^2}$ is the mean square force per unit surface created by the dipole distribution.

$$E\{|A^0_{mn}|^2\} = \frac{\overline{F_s^2}}{2\mathcal{A}}\int_{\mathcal{A}} |\Psi_{mn}(\boldsymbol{y_s})|^2\ d^2\boldsymbol{y_s}$$

$$\boxed{E\{|A^0_{mn}|^2\} = \frac{\overline{F_s^2}}{2}.} \tag{3.2.11}$$

3.2.3 Equal power per mode

The sound power of the wave transmitted along the duct is

$$W^0 = \int_{\mathcal{A}} \boldsymbol{I}(\boldsymbol{y}) \cdot \boldsymbol{e_z}\ d^2\boldsymbol{y}, \tag{3.2.12}$$

where $I(\boldsymbol{y})$ is the time averaged intensity of the wave given by

$$\boldsymbol{I} = \frac{1}{2}\text{Re}\left\{p^0(\boldsymbol{y})^*\boldsymbol{u}^0(\boldsymbol{y})\right\}. \tag{3.2.13}$$

From equations (3.2.12) and (3.2.13),

$$W^0 = \frac{1}{2}\text{Re}\left\{\int_{\mathcal{A}} p^0(\boldsymbol{y})^* u_z^0(\boldsymbol{y})\ d^2\boldsymbol{y}\right\}. \tag{3.2.14}$$

Using the momentum equation and the modal decomposition of the sound field from equations (3.1.2) and (2.5.7), it can be shown that

$$u_z^0(\boldsymbol{y}) = \sum_{m,n} \frac{\alpha_{mn}^0}{\rho_0 c_0} p_{mn}(\boldsymbol{y}) \tag{3.2.15}$$

Thus, from (3.2.14),

$$W^0 = \frac{1}{2}\text{Re}\left\{\int_{\mathcal{A}} \sum_{\substack{m,n\\q,l}} \alpha_{ql} p_{mn}(\boldsymbol{y})^* p_{ql}(\boldsymbol{y})\ d^2\boldsymbol{y}\right\}.$$

Substituting equations (2.5.7) and (3.2.15) into the above expression,

$$W^0 = \frac{1}{2}\text{Re}\left\{\sum_{\substack{m,n\\q,l}} A_{mn}^0 * A_{ql} \frac{\alpha_{ql}}{\rho_0 c_0} \int_{\mathcal{A}} \Psi_{mn}^*(\boldsymbol{y})\Psi_{ql}(\boldsymbol{y}) e^{-j(\alpha_{mn}^0 - \alpha_{ql})kz}\ d^2\boldsymbol{y}\right\}.$$

By definition of the shape functions, this equation can be simplified as

$$W^0 = \frac{1}{2}\text{Re}\left\{\sum_{m,n} |A_{mn}^0|^2 \frac{\alpha_{mn}^0}{\rho_0 c_0}\mathcal{A}\right\},$$

$$W^0 = \sum_{(m,n)\in\mathcal{O}} \frac{\mathcal{A}}{2\rho_0 c_0} |A_{mn}^0|^2 \alpha_{mn}^0.$$

Thus,

$$E\{W^0\} = \sum_{(m,n)\in\mathcal{O}} \frac{\mathcal{A}}{2\rho_0 c_0} E\{|A_{mn}^0|^2\}\alpha_{mn}^0.$$

The expected value of the modal power is therefore given by

$$\boxed{E\{W_{mn}^0\} = \frac{\mathcal{A}}{2\rho_0 c_0} E\{|A_{mn}^0|^2\}\alpha_{mn}^0}. \tag{3.2.16}$$

If the power is equally shared between all the cut-on modes,

$$E\{W^0_{mn}\} = W_0, \tag{3.2.17}$$

where W_0 is the power transmitted by each mode. Combining equations (3.2.16) and (3.2.17) gives

$$\boxed{E\{|A^0_{mn}|^2\} = 2\rho_0 c_0 \frac{W_0}{\mathcal{A}} (\alpha^0_{mn})^{-1}}. \tag{3.2.18}$$

$W_0/\mathcal{A}$ is the averaged intensity transported by each cut-on mode.

3.2.4 General expression of the modal amplitude without flow

The expectancy of the modal amplitude for each of the three models studied above can be written in a compact form. From equations (3.2.5), (3.2.11) and (3.2.18),

$$\boxed{E\{|A^0_{mn}|^2\} = P_q^2 (\alpha^0_{mn})^{-q},} \tag{3.2.19}$$

where q is an integer equal to 0, 1 or 2, and P_q a source strength which depends on the source model, i.e.

	Monopole	Dipole	Equal Power
P_q	$\rho_0 c_0 (\overline{Q_s^2}/2)^{1/2}$	$(\overline{F_s^2}/2)^{1/2}$	$(2\rho_0 c_0 W_0/\mathcal{A})^{1/2}$
q	2	0	1

3.3 High frequency approximation

3.3.1 Introduction

The aim of this section is to derive a simple analytic formula for the multi-mode directivity function with flow for the general source distributions presented in the above section. The proof relies in observing that the power radiated from the duct in a particular direction is approximately equal to that travelling along the duct in that same direction. Since for a given source, the power travelling in the duct in any direction can be obtained easily, this allows the estimation of the far field power in any direction. Moreover, the far field power radiated in a particular direction is related to the pressure directivity through the radial intensity. Thus, these energy considerations offer one method for estimating, analytically, the pressure directivity in the far field.

3.3.2 Far field power in direction θ

Consider the sound power $dW_f(\theta)$ radiated to the far field between angles θ and $\theta + d\theta$. By definition of the time average acoustic intensity, the mean power radiated to the far field

through surface $\mathcal{S}$, denoted by $E\{dW_f(\theta)\}$, is given by

$$dW_f(\theta) = \int_{\mathcal{S}} I_R(R', \phi', \theta') \; d^2\boldsymbol{y_s}, \tag{3.3.1}$$

where $\mathcal{S}$ is the surface defined in the spherical coordinate system (R', ϕ', θ') by

$$\begin{cases} R' = R, \\ 0 \leq \phi' \leq 2\pi, \\ \theta \leq \theta' \leq \theta + d\theta. \end{cases}$$

Thus,

$$dW_f(\theta) = \int_0^{2\pi} \int_{\theta}^{\theta+d\theta} I_R(R, \phi, \theta) R^2 \sin\theta' \; \mathrm{d}\theta' \, \mathrm{d}\phi', \tag{3.3.2}$$

In the far field, the sound wave propagates as a plane wave therefore $p_f/u_R = \rho_0 c_0$ and

$$I_R(\boldsymbol{y}) = \frac{1}{2}\mathrm{Re}\left\{p_f(R,\theta)^* u_R(R,\theta)\right\} = \frac{|p_f(R,\theta)|^2}{2\rho_0 c_0}. \tag{3.3.3}$$

Combining equations (3.3.2) and (3.3.3), the expected value of the far field power radiated between angles θ and $\theta + d\theta$ can be expressed as

$$\boxed{E\{dW_f(\theta)\} = \frac{\pi R^2}{\rho_0 c_0} E\{|p_f|^2\} \sin\theta d\theta.} \tag{3.3.4}$$

3.3.3 Relation between far field power and in-duct power

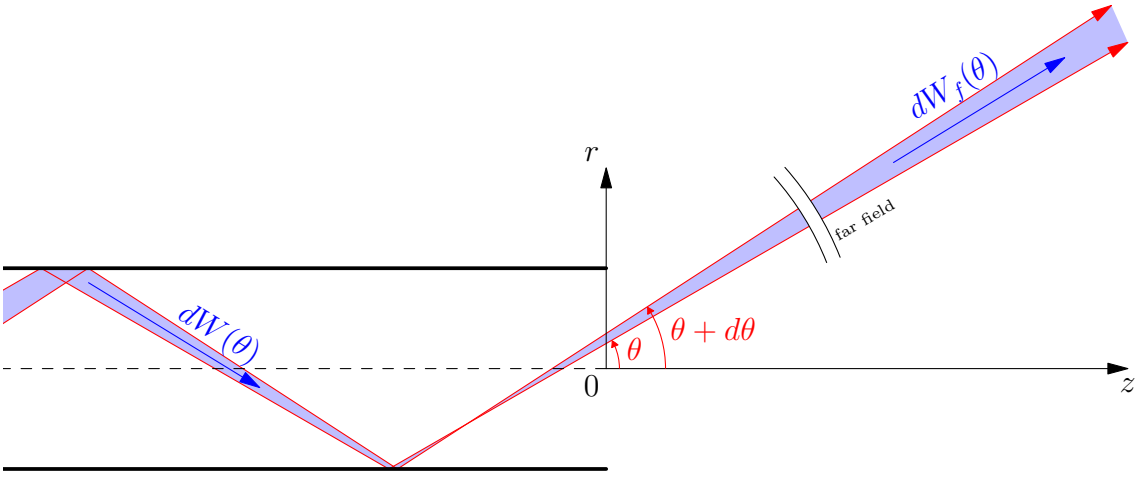

Figure 3.7 – Relation between power transmitted along the duct between angles θ and $\theta + d\theta$, denoted by $dW(\theta)$, and power radiated to the far field between angles θ and $\theta + d\theta$, denoted by $dW_f(\theta)$. If the open-end of the duct is acoustically transparent, $dW(\theta) = dW_f(\theta)$.

Interpreting the acoustic waves in terms of rays, $dW_f(\theta)$ is given by the sum of the powers carried along by the rays travelling between angles θ and $\theta + d\theta$. Assuming that no energy is lost at the open-end of the duct, the power transported by one ray into the far field is equal to the power transported by that same ray inside the duct. This is illustrated in figure 8.11. Thus, $dW_f(\theta)$ is equal to the power transported inside the duct by rays travelling between angles θ and $\theta + d\theta$, which is denoted by $dW(\theta)$, i.e

$$\boxed{dW_f(\theta) = dW(\theta)} \tag{3.3.5}$$

3.3.4 In duct power transmitted in direction θ

Interpreting the modes in terms of rays, the in-duct power transmitted along the duct between θ and $\theta + d\theta$ is the sum of the modal power transmitted by each mode travelling in a direction comprised between θ and $\theta + d\theta$. From figure 2.6, the direction of propagation θ_{mn} of mode (m, n) is given by equation

$$\cos\theta_{mn} = \alpha^0_{mn},$$

therefore by definition of $dW(\theta)$,

$$dW(\theta) = \sum_{(m,n)\in\mathcal{O}_\theta} W_{mn}, \tag{3.3.6}$$

where

$$\mathcal{O}_\theta = \{(m, n) \in \mathcal{O} \text{ such that } \theta \leq \theta_{mn} \leq \theta + d\theta\}. \tag{3.3.7}$$

From equations (3.2.5), (3.2.11) and (3.2.18), the mean square modal amplitude can be expressed as a power of the cut-on ratio

$$E\big\{|A^0_{mn}|^2\big\} = P_q^2(\alpha^0_{mn})^{-q}$$

where P_q^2 and q are constants which depend on the source model. From equations (3.2.16) and (8.3.15), the expected value of the modal powers is given by

$$E\big\{W_{mn}\big\} = \frac{\mathcal{A}}{2\rho_0 c_0} P_q^2 \sum_{(m,n)\in\mathcal{O}_\theta} (\alpha^0_{mn})^{1-q}. \tag{3.3.8}$$

Thus,

$$E\big\{dW(\theta)\big\} = \frac{\mathcal{A}}{2\rho_0 c_0} P_q^2 \sum_{(m,n)\in\mathcal{O}_\theta} (\alpha^0_{mn})^{1-q}. \tag{3.3.9}$$

For all $(m, n) \in \mathcal{O}_\theta$, $\theta_{mn} \approx \theta$ because $d\theta \ll \theta$, therefore

$$\alpha^0_{mn} = \cos\theta_{mn} \approx \cos\theta. \tag{3.3.10}$$

Substituting this result into equation (3.3.9), the in-duct power travelling in direction θ can be expressed as

$$E\{dW(\theta)\} = \frac{\mathcal{A}}{2\rho_0 c_0} P_q^2 \text{Card}\Big(\mathcal{O}_\theta\Big) \cos^{1-q}\theta, \tag{3.3.11}$$

where $\text{Card}\Big(\mathcal{O}_\theta\Big)$ is the number of modes in $\mathcal{O}_\theta$.

Derivation of $\mathcal{O}_\theta$ To estimate $\text{Card}\Big(\mathcal{O}_\theta\Big)$, we introduce the function $N(\theta)$ defined as the number of modes (m,n) such that $\theta_{mn} \leq \theta$, i.e.

$$N(\theta) = \text{Card}\Big(\ \{(m,n) \in \mathcal{O} \quad \text{such that} \quad \theta_{mn} \leq \theta\}\ \Big) \tag{3.3.12}$$

By definition of $N(\theta)$,

$$\text{Card}\Big(\mathcal{O}_\theta\Big) = N(\theta + d\theta) - N(\theta). \tag{3.3.13}$$

Since $d\theta \ll \theta$, the above expression can be expressed in terms of the derivative of $N(\theta)$, denoted by $N'(\theta)$,

$$\text{Card}\Big(\mathcal{O}_\theta\Big) = N'(\theta)d\theta \tag{3.3.14}$$

In the above expression, $N'(\theta)$ can be interpreted as a modal density.

The function $N(\theta)$ can be estimated as follows. First observe that

$$0 \leq \theta_{mn} \leq \theta \leq \frac{\pi}{2} \quad \Leftrightarrow \quad k\sin\theta_{mn} \leq k\sin\theta. \tag{3.3.15}$$

From figure 2.6,

$$k\sin\theta_{mn} \leq k\sin\theta \Leftrightarrow \kappa_{mn} \leq \kappa(\theta), \tag{3.3.16}$$

where

$$\kappa(\theta) = k\sin\theta. \tag{3.3.17}$$

Secondly, let $M(\kappa)$ denote the number of cut-on modes (m,n) such that $\kappa_{mn} \leq \kappa$, i.e

$$M(\kappa) = \text{Card}\Big(\ \{(m,n) \in \mathcal{O} \quad \text{such that} \quad \kappa_{mn} \leq \kappa\}\ \Big). \tag{3.3.18}$$

Equations (3.3.15) and (3.3.17) show that

$$N(\theta) = M(\kappa(\theta)). \tag{3.3.19}$$

Good analytical approximations for $M(\kappa)$ are given by Roe [19] and Rice [16],

$$M(\kappa) = \frac{(\kappa a)^2}{4} + \frac{\kappa a}{2} \approx \frac{(\kappa a)^2}{4}, \tag{3.3.20}$$

where the second order term is neglected in the second equality, which is a good approxi-

mation when $\kappa a \gg 1$ (well cut-on modes). Thus, $N(\theta)$ can be approximated by

$$N(\theta) = \frac{(\kappa(\theta)a)^2}{4} = \frac{(ka)^2}{4}\sin^2\theta. \tag{3.3.21}$$

Taking the derivative of the above expression gives

$$N'(\theta) = \frac{(ka)^2}{2}\sin\theta\cos\theta. \tag{3.3.22}$$

Thus, substituting equation (3.3.22) into equation (3.3.14), the number of cut-on modes which radiate between angle θ and $\theta + d\theta$ is given by

$$\text{Card}\Big(\mathcal{O}_\theta\Big) = \frac{(ka)^2}{2}\sin\theta\cos\theta d\theta. \tag{3.3.23}$$

In duct power in direction θ The in-duct power transmitted between propagation angles θ and $\theta + d\theta$ is obtained by combining equations (3.3.23) and (3.3.11), which gives

$$\boxed{E\big\{dW(\theta)\big\} = \frac{\mathcal{A}(ka)^2}{4\rho_0 c_0}P_q^2\sin\theta\cos^{2-q}\theta d\theta.} \tag{3.3.24}$$

3.3.5 Multi-Mode far field directivity without flow

Substituting the in-duct power, from equation (3.3.24), and the far field power, given by equation (3.3.4), into equation (3.3.5), gives

$$\frac{\pi R^2}{\rho_0 c_0}E\big\{|p_f|^2\big\}\sin\theta d\theta = \frac{(ka)^2\mathcal{A}}{4\rho_0 c_0}P_q^2\sin\theta\cos^{2-q}\theta d\theta. \tag{3.3.25}$$

Solving the above equation for $E\big\{|p_f|^2\big\}$, and substituting $\mathcal{A}$ by πa^2 gives

$$\boxed{E\big\{|p_f(R,\phi,\theta)|^2\big\} = \left(\frac{a}{R}\right)^2\frac{(ka)^2}{4}P_q^2\cos^{2-q}(\theta).} \tag{3.3.26}$$

This result is consistent with the one derived by Joseph and Morfey[1].

3.4 Directivity factor

The directivity factor can be expressed in non-dimensional form as

$$Q(ka,\theta) = \frac{2\pi R^2}{\rho_0 c_0 E\big\{W\big\}}E\big\{|p_f(R,\phi,\theta,\omega)|^2\big\}. \tag{3.4.1}$$

Note that for a spherical source, $Q(ka,\theta) = 1$. The mean square pressure $\frac{1}{2}E\big\{p_f^2(R,\phi,\theta,\omega)\big\}$ can be computed by using a discrete modal summation, or by applying a continuous ana-

lytic formula that is valid in the high frequency limit. The power W can be expressed as a discrete sum of modal powers, or as the integral of a continuous function.

3.4.1 Directivity factor in terms of a modal summation

One expression for $E\{p_f^2(R,\phi,\theta,\omega)\}$ is obtained by combining equations (3.0.3) and (3.2.19), to give

$$E\{p_f^2(R,\phi,\theta,\omega)\} = \left(\frac{a}{R}\right)^2 P_q^2 \sum_{(m,n)\in\mathcal{O}} |H_{mn}(ka,\theta)|^2 (\alpha_{mn}^0)^{-q}. \tag{3.4.2}$$

The expected value of the source power, $E\{W\}$, can be expressed by summing the modal powers, given by equation (3.3.8), over all cut-on modes:

$$E\{W\} = \frac{\pi a^2}{2\rho_0 c_0} P_q^2 \sum_{(m,n)\in\mathcal{O}} (\alpha_{mn}^0)^{1-q}. \tag{3.4.3}$$

The directivity factor is then obtained by substituting equations (3.4.2) and (3.4.3) into equation (3.4.1), to give

$$\boxed{Q(ka,\theta) = \frac{4\sum_{(m,n)\in\mathcal{O}} |H_{mn}(ka,\theta)|^2 (\alpha_{mn}^0)^{-q}}{\sum_{(m,n)\in\mathcal{O}} (\alpha_{mn}^0)^{1-q}}.} \tag{3.4.4}$$

3.4.2 Continuous analytical estimation of the directivity factor in the high frequency limit

In the forward arc ($\theta \leq \pi/2$), the directivity factor can be estimated directly by using the analytical expressions derived in this chapter. Thus, the mean square pressure can be expressed from equation (3.3.26) as

$$E\{|p_f(R,\phi,\theta)|^2\} = \left(\frac{a}{R}\right)^2 \frac{(ka)^2}{4} P_q^2 \cos^{2-q}(\theta) \tag{3.4.5}$$

The expected value of the source power can be obtained by summing the elementary contributions $E\{dW(\theta)\}$ between 0 and $\pi/2$. Thus, from equation (3.3.24),

$$E\{W\} = \int_0^{\pi/2} E\{dW(\theta)\} = \frac{\pi a^2}{\rho_0 c_0} \frac{(ka)^2}{4} \int_0^{\pi/2} P\ d_q^2 \sin\theta \cos^{2-q}(\theta)\theta = \frac{\pi a^2}{\rho_0 c_0} \frac{(ka)^2}{4(3-q)} P_q^2. \tag{3.4.6}$$

Substituting equations (3.4.5) and (3.4.6) into equation (3.4.1) gives

$$\boxed{Q(ka,\theta) = 2(3-q)\cos^{2-q}(\theta).} \tag{3.4.7}$$

Chapter 4

Validation of the model

The proof leading to the expression for the multi-mode far-field directivity relies essentially on one assumption, which is that the open end of the duct does not generate any reflected wave travelling back into the duct. Thus it is assumed that the power radiated to the far field is equal to the power transmitted along the duct. It is claimed that this assumption is a good approximation at high frequency. The aim of this section is to assess the validity of this assumption.

4.1 Theoretical analysis of the error on the directivity factor

The relation between in-duct power W, far field mean square pressure $|p_f|^2$, and directivity factor Q_τ is of the form

$$Q_\tau = \frac{2\pi R^2}{\rho_0 c_0} \frac{|p_f|^2}{W}. \tag{4.1.1}$$

The in-duct power W is related to the far field power by

$$W_f = \tau W, \tag{4.1.2}$$

where τ denotes the power transmission coefficient. Thus,

$$Q_\tau = \frac{2\pi R^2}{\rho_0 c_0} \tau \frac{|p_f|^2}{W_f}. \tag{4.1.3}$$

In the previous chapter, we assume that $\tau = 1$, which results in estimating the directivity factor as,

$$Q_1 = \frac{2\pi R^2}{\rho_0 c_0} \frac{|p_f|^2}{W_f}. \tag{4.1.4}$$

Thus, the exact directivity factor Q_τ is related to the estimated directivity factor Q_1 by

$$\frac{Q_\tau}{Q_1} = \tau. \tag{4.1.5}$$

Note that, in the above expression, τ is angle dependent. The approximate directivity factor Q_1 is an estimation of Q_τ accurate to 1 dB if and only if

$$|10\log Q_\tau - 10\log Q_1| \leq 1 \quad \Leftrightarrow \quad -10\log\tau \leq 1 \quad \Leftrightarrow \quad \tau \geq 10^{-1/10} \tag{4.1.6}$$

The numerical evaluation of the above expression gives

$$\boxed{|10\log Q_\tau - 10\log Q_1| \leq 1 \quad \Leftrightarrow \quad 0.8 \leq \tau.} \tag{4.1.7}$$

4.2 Sufficient condition on the modal transmission coefficients

In particular, a sufficient condition to satisfy equation (4.1.7) is that

$$\boxed{0.8 \leq \tau_{mn}}, \tag{4.2.1}$$

for all cut-on modes, where τ_{mn} is the modal transmission coefficient defined as

$$\tau_{mn} = \frac{W_{f,mn}}{W_f}. \tag{4.2.2}$$

From equations (3.3.4), (3.0.3) and (3.2.16),

$$\tau_{mn} = \frac{2\int_0^\pi |H^0_{mn}(ka,\theta)|^2 E\{|A^0_{mn}|^2\}\sin\theta \; d\theta}{E\{|A^0_{mn}|^2\}\alpha_{mn}}. \tag{4.2.3}$$

The weighting coefficients cancel out and,

$$\boxed{\tau_{mn} = \frac{2\int_0^\pi |H^0_{mn}(ka,\theta)|^2 \sin\theta \; d\theta}{\alpha_{mn}}.} \tag{4.2.4}$$

4.3 Analysis of the modal transmission coefficients

4.3.1 Variation with frequency

Figure 4.1 shows the value of the transmission coefficient for all cut-on modes and for $ka = 20$ and 50, as a function of the cut-off ratio. It appears that the modal transmission coefficient tend to one as frequency increases. This is consistent with the theory developed by Morfey [5]. To be more precise, we study the percentage of modes which are such that $\tau_{mn} < 0.8$. Figure 4.1 shows that, as expected, this error coefficient tends to 0 as ka increases.

$$\text{Error } = \frac{\text{number of modes } (m,n) \text{ such that } \tau_{mn} < 0.8}{\text{Total number of modes}}. \tag{4.3.1}$$

The variation of the error as ka increases is plotted in figure

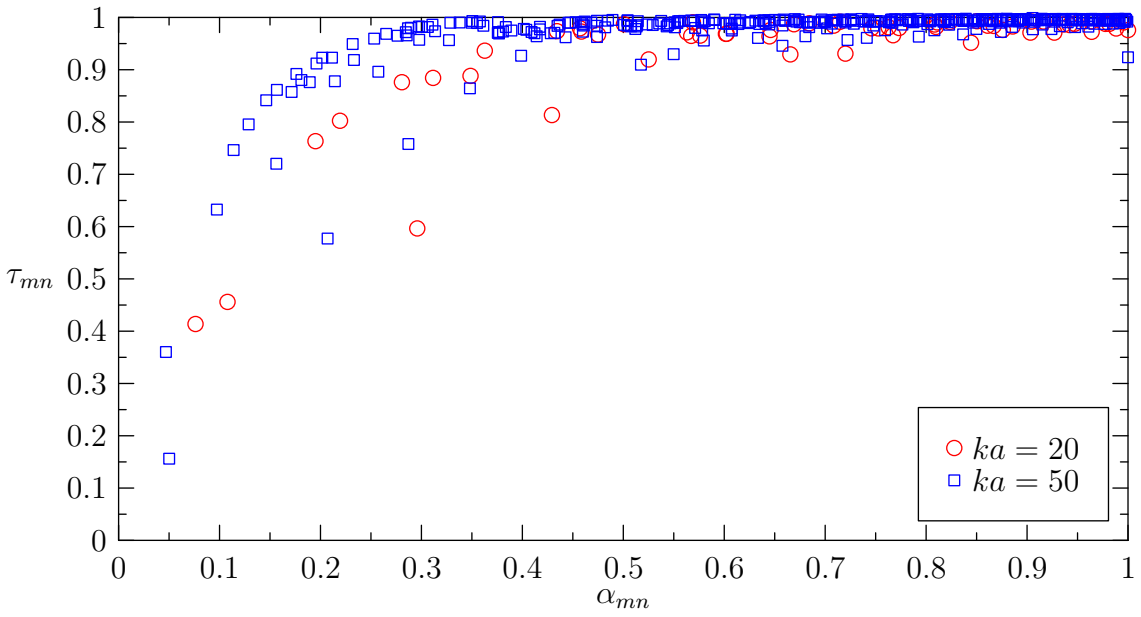

Figure 4.1 – Modal transmission coefficient as a function of cut-off ratio for zero flow at low and high frequencies.

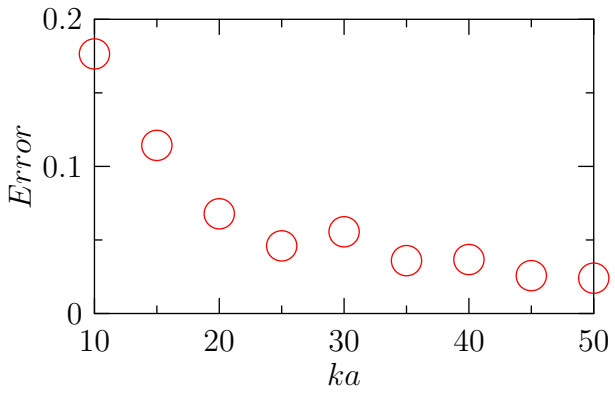

Figure 4.2 – Pourcentage of modes such that $\tau_{mn} < 0.8$.

4.3.2 Maximum angle of validity

Hence, we estimate the maximum angle below which the 1 dB accuracy condition should hold. The variation of τ_{mn} with α_{mn} is similar to that sketched in figure 4.3. The modes which are $\alpha^0_{mn} \leq \alpha_c$ all have a transmission coefficient below 0.8, which means that the model is likely to be less accurate for this particular range of modes. Besides,

$$\alpha^0_{mn} \leq \alpha_c \quad \Leftrightarrow \quad \cos\theta_{mn} \leq \alpha_c \quad \Leftrightarrow \quad \theta_{mn} \geq \cos^{-1}(\alpha_c) = \theta_c \tag{4.3.2}$$

This simple relation allows the estimation of the angle above which the present model is less accurate.

The results are shown in table 4.1. They indicate that the model should give poor result for $ka = 10$, for which θ_c is as low as $65°$, but rather good results for $ka \geq 20$,

for which $\theta_c = 80°$. However, the convergence seems to be very slow for $ka \geq 20$ which indicates that a more accurate model of the transmission coefficient should be used in order to improve the validity of the model between $80°$ and $90°$.

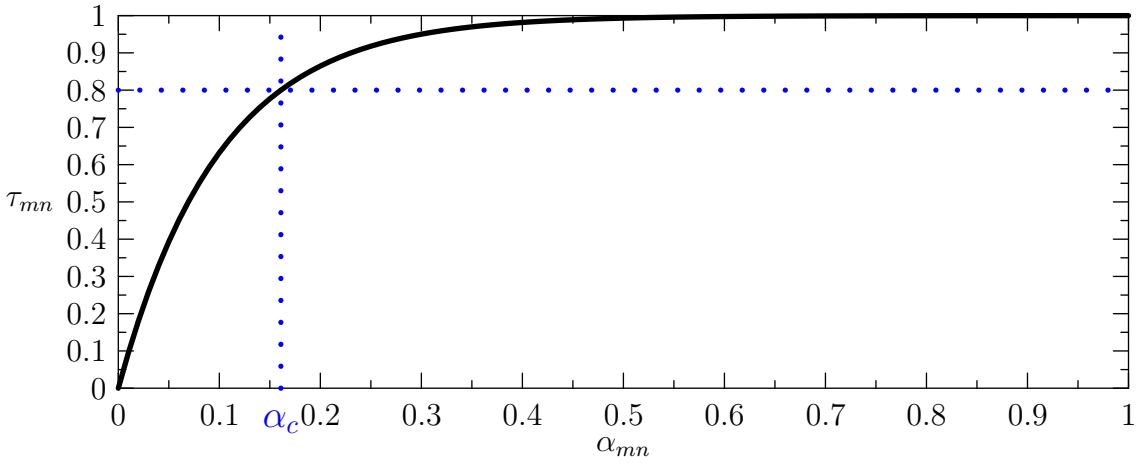

Figure 4.3 – Sketch of the variation of τ_{mn} as a function of α^0_{mn}.

ka	10	20	30	40	50
α_c	0.4	0.2	0.2	0.15	0.15
θ_c	65°	80°	80°	80°	80°

Table 4.1 – Angle above which the model is not validated.

4.4 Conclusion

The high frequency multi-mode directivity formula given in equation (3.3.26), which assumes that the transmission coefficient is equal to 1 for all angles, is valid for frequencies higher than $ka = 20$ for angles below $80°$, to a precision of approximately $1\,\text{dB}$. The quality of the model, and therefore the range of angles over which it is able to predict the multi-mode directivity factor with good accuracy, tends to increases with frequency.

Chapter 5

Results

In this chapter, the directivity factor of equation (3.4.7) is investigated. The directivity factor is plotted in figure 5.1 for $ka = 50$, for the three distribution of incoherent sources presented in this chapter. In each figure, the thick black line represents the exact result from the Wiener-Hopf Technique. The red triangles represent the solution obtained by using the flanged duct approximation. The blue circles represent the analytical solution by Joseph and Morfey [1]. The agreement is shown to be excellent for angles below about 85°.

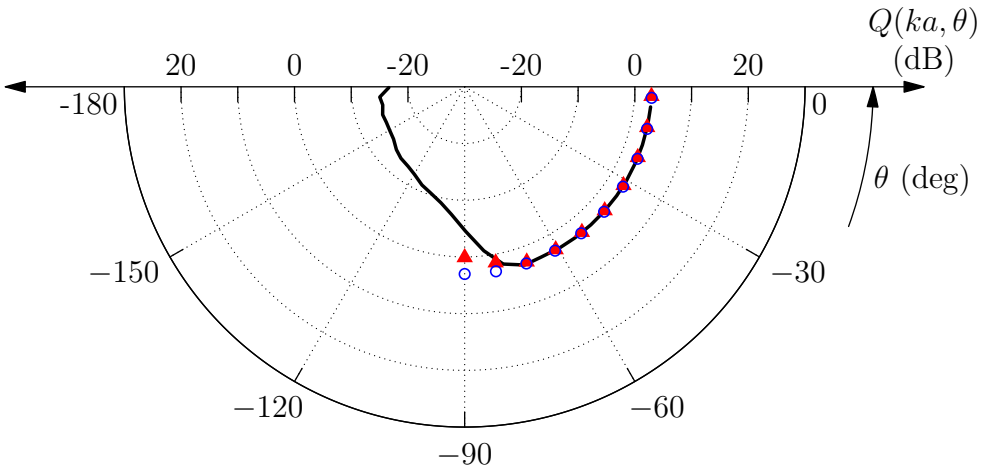

(a) Uniform distribution of incoherent monopoles

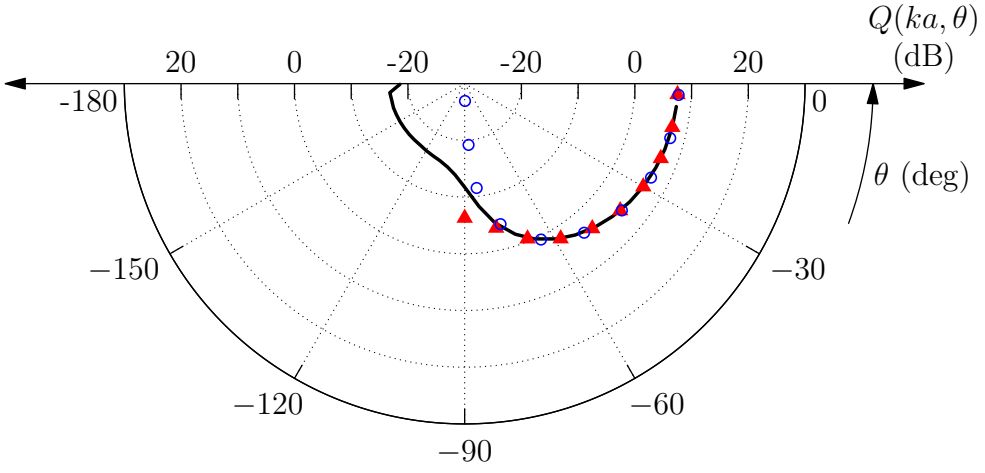

(b) Uniform distribution of incoherent dipoles

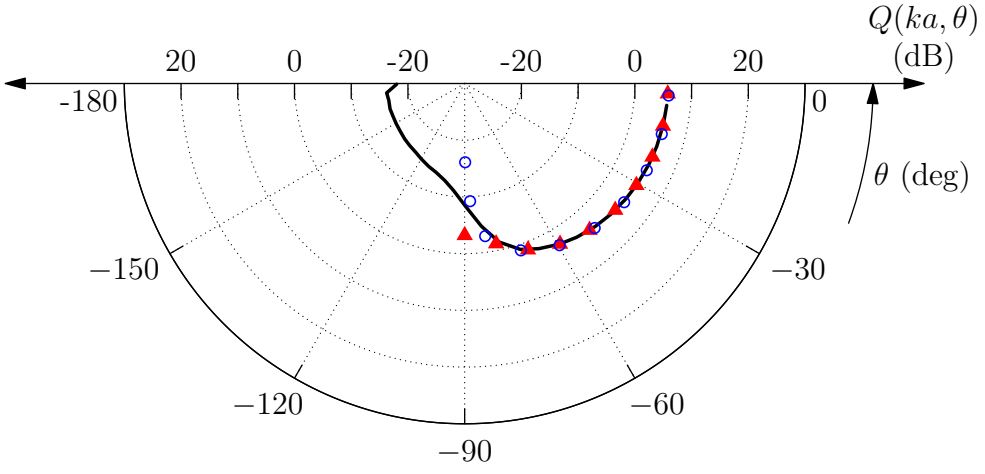

(c) Equal power per mode model

Figure 5.1 – Directivity factor of the pressure field radiating from a semi-infinite cylindrical duct without flow, for $ka = 50$ and for three different model of sound sources. In each polar plot, the black line gives the exact solution of the problem from the Wiener-Hopf Technique (from Gabard and Astley). The red crosses correspond to the flanged duct solution, and the blue circles to the analytic formula.

Part III

Multi-mode directivity with flow

Chapter 6

The Lorentz Transformation

6.1 Convected wave equation

Consider a waveguide containing a uniform flow in the z-direction. Let U be the speed of the flow. When no source is present inside the waveguide, the pressure field must satisfy the homogeneous convected wave equation:

$$\nabla^2 p(\boldsymbol{x},t) = \frac{1}{c_0^2}\left(\frac{\partial}{\partial t} + c_0 M \frac{\partial}{\partial z}\right)^2 p(\boldsymbol{x},t), \tag{6.1.1}$$

where c_0 is the speed of sound, $M = U/c_0$ the Mach number, p the pressure and $\boldsymbol{x}$ the position in the cylindrical waveguide.

If the pressure field is assumed to be harmonic,

$$p(\boldsymbol{x},\omega) = \Re\left\{p(\boldsymbol{x})e^{j\omega t}\right\},$$

then equation (6.1.1) is equivalent to the convected Helmholtz equation:

$$\boxed{\nabla^2 p(\boldsymbol{x},\omega) + \left(k - jM\frac{\partial}{\partial z}\right)^2 p(\boldsymbol{x}) = 0}, \tag{6.1.2}$$

where $k = \omega/c_0$ is the wavenumber.

6.2 Solution of the homogeneous convected wave equation

The convected equations can be solved by using the separation of variable as in the zero flow theory. However, the results can be derived more easily by using the Lorentz Transform. The Lorentz Transform gives the solution of the homogeneous convected wave equation[1] from the solution of the wave equation. Let p^0 be a regular function which satisfies

[1]The Lorentz Transform even gives the solution of the inhomogeneous convected wave equation from the solution to an inhomogeneous wave equation. See for example Chapman[20] for more details

the homogeneous wave equation, i.e.

$$\left\{\nabla^2 - \frac{1}{c_0^2}\frac{\partial^2}{\partial t^2}\right\} p^0(\boldsymbol{x}, t) = 0. \tag{6.2.1}$$

Let

$$p(\boldsymbol{x}, t) = p^0(\sigma\overline{x}, \sigma\overline{y}, \sigma\overline{\overline{z}}, \sigma t + \sigma\frac{M}{c_0}\overline{\overline{z}}), \tag{6.2.2}$$

where $\beta = \sqrt{1 - M^2}$, σ is an arbitrary constant, and where for any X equal to x, y or z,

$$\overline{X} = \frac{X}{\beta}, \quad \text{and} \quad \overline{\overline{X}} = \frac{X}{\beta^2}. \tag{6.2.3}$$

Then, according to the results obtained by Chapman [20], p is solution of the homogeneous convected wave equation

$$\left\{\nabla^2 - \frac{1}{c^2}\left(\frac{\partial}{\partial t} + c_0 M\frac{\partial}{\partial z}\right)^2\right\} p(\boldsymbol{x}, t) = 0. \tag{6.2.4}$$

6.3 Solution of the homogeneous convected Helmholtz equation

These results can be extended to obtain directly the solution to the convected Helmholtz equation. Let

$$p(\boldsymbol{x}, t) = \text{Re}\left\{p(\boldsymbol{x}, \omega)e^{j\omega t}\right\}, \tag{6.3.1}$$

$$p^0(\boldsymbol{x}, t) = \text{Re}\left\{p^0(\boldsymbol{x}, \omega)e^{j\omega t}\right\}. \tag{6.3.2}$$

$$\tag{6.3.3}$$

p^0 is solution to the wave equation if and only if it satisfies the Helmholtz equation, i.e.

$$\left(\nabla^2 + k^2\right) p^0(\boldsymbol{x}, \omega) = 0. \tag{6.3.4}$$

6.3.1 Cartesian coordinates

From equations (6.2.4) and (6.3.2),

$$p(\boldsymbol{x}, t) = \text{Re}\left\{p^0(\sigma\overline{x}, \sigma\overline{y}, \sigma\overline{\overline{z}}, \omega)e^{j\omega(\sigma t + \sigma M\overline{\overline{z}}/c_0)}\right\}$$

$$p(\boldsymbol{x}, t) = \text{Re}\left\{p^0(\sigma\overline{x}, \sigma\overline{y}, \sigma\overline{\overline{z}}, \omega)e^{j\omega\sigma M\overline{\overline{z}}/c_0}e^{j\omega\sigma t}\right\}$$

Combining this result with equation (6.3.1) gives

$$\boxed{p(\boldsymbol{x}, \omega) = p^0(\sigma\overline{x}, \sigma\overline{y}, \sigma\overline{\overline{z}}, \frac{\omega}{\sigma})e^{j\omega M\overline{\overline{z}}/c_0}.} \tag{6.3.5}$$

6.3.2 Polar coordinates

The previous results can be generalized to polar coordinates. Let $r = \sqrt{x^2 + y^2}$ and ϕ the angle defined by

$$\cos\phi = \frac{x}{r} \quad \text{and} \quad \sin\phi = \frac{y}{r}. \tag{6.3.6}$$

Equation (6.3.5) becomes

$$\boxed{p(r, \phi, z, \omega) = p^0(\sigma\overline{r}, \phi, \sigma\overline{\overline{z}}, \frac{\omega}{\sigma})e^{j\omega M\overline{\overline{z}}/c_0}.} \tag{6.3.7}$$

Figure 6.1 illustrates the effect of the Lorentz Transformation in cylindrical coordinates

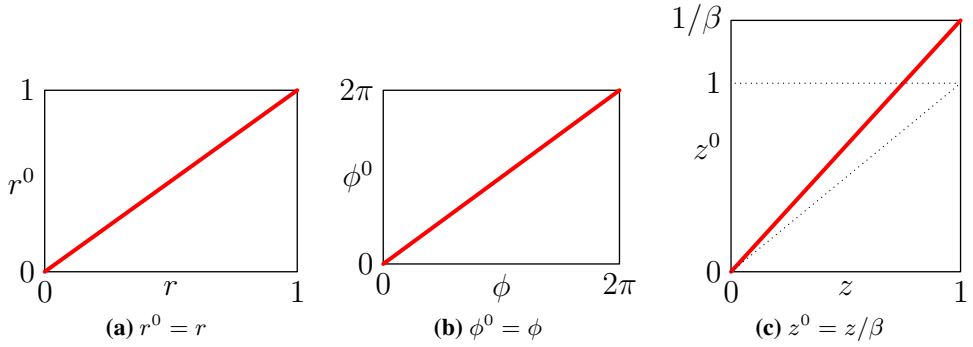

(a) $r^0 = r$ **(b)** $\phi^0 = \phi$ **(c)** $z^0 = z/\beta$

Figure 6.1 – Lorentz Transformation in cylindrical coordinates when $\sigma = \beta$. The coordinates with flow, denoted (r, ϕ, z), are converted to zero flow coordinates, (r^0, ϕ^0, z^0) which can be injected into the zero flow equations.

in the case when $\sigma = \beta$. This choice of σ will become clear at section 7.2. The radial and polar angles are unchanged by the transformation, whereas the z component increases linearly. The flow is equivalent to a stretching in the z-direction.

6.3.3 Spherical coordinates

Let $R = \sqrt{r^2 + z^2}$ and θ be the angle defined by

$$\cos\theta = \frac{z}{R} \quad \text{and} \quad \sin\theta = \frac{r}{R}. \tag{6.3.8}$$

Equation (6.3.5) becomes

$$\boxed{p(R, \phi, \theta, \omega) = p^0(\sigma\tilde{R}, \phi, \tilde{\theta}, \frac{\omega}{\sigma})e^{j\omega MR\cos\theta/(\beta^2 c_0)},} \tag{6.3.9}$$

where

$$\tilde{R} = \sqrt{\overline{r}^2 + \overline{\overline{z}}^2} = \overline{\overline{R}}\sqrt{1 - M^2\sin^2\theta}, \tag{6.3.10}$$

and $\tilde{\theta}$ is defined by

$$\cos\tilde{\theta} = \frac{\cos\theta}{\sqrt{1 - M^2\sin^2\theta}} \quad \text{and} \quad \sin\tilde{\theta} = \beta\frac{\sin\theta}{\sqrt{1 - M^2\sin^2\theta}}. \tag{6.3.11}$$

$\tilde{\theta}$ can be expressed in terms of θ by using the arctangent tan^{-1} (defined between $-\pi$ and $+\pi$), i.e.

$$\tilde{\theta} = \tan^{-1}(\beta\tan\theta). \tag{6.3.12}$$

Figure 6.3.3 illustrates the effect of the Lorentz Transformation in spherical coordinates, when $\sigma = \beta$ (see section 7.2). The angle ϕ remains the same. The radius R changes very little at low Mach numbers, but varies almost sinusoidally when the magnitude of the Mach number is close to one. The effect of the Lorentz Transformation on angle θ is more complex. At low Mach numbers, θ remains unchanged, whereas at high Mach numbers, the variation of θ depends on its value with respect to $\pi/2$:

- if $\theta \leq \pi/2$, the Lorentz Transformation tends to reduce slightly the value of θ,
- if $\theta \geq \pi/2$, the Lorentz Transformation tends to increase slightly the value of θ.

6.4 Issues regarding the application of the Lorentz Transformation

6.4.1 The frequency factor

The Lorentz Transformation involves two parameters. The first is $\beta = \sqrt{1 - M^2}$, which is fixed for a given value of the Mach number. The second is σ, which is problem-dependent. The Lorentz Transformation is not unique and one must determine the value of σ which is appropriate for the problem of interest. A possible way of determining σ is to use the boundary conditions which the solution must satisfy.

6.4.2 Singular solutions

Since the solutions to the Helmholtz equation are usually continuous everywhere, the Lorentz Transformation will only yield continuous solutions. This can be problematic when the solution is known to have a singularity. However, this problem can be overcome by using the acoustic velocity potential instead of the pressure field, since p and ϕ are not usually singular simultaneously. Since the acoustic velocity potential Φ, defined by

$$\boldsymbol{u} = \boldsymbol{\nabla}\Phi, \tag{6.4.1}$$

is also solution of the convected wave equation, it can be derived from the zero-flow velocity potential Φ^0 through a Lorentz Transformation. In all the above equations, the pressure field can be replaced by the velocity potential.

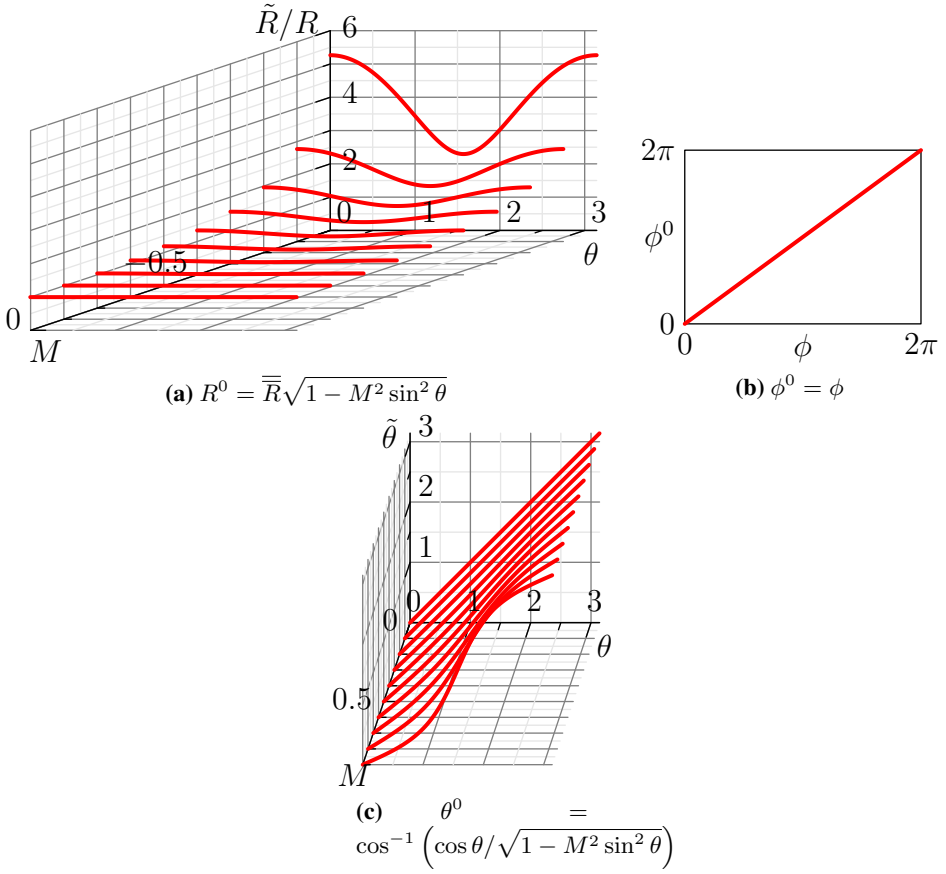

(a) $R^0 = \overline{\overline{R}}\sqrt{1 - M^2 \sin^2\theta}$

(b) $\phi^0 = \phi$

(c) $\theta^0 = \cos^{-1}\left(\cos\theta / \sqrt{1 - M^2 \sin^2\theta}\right)$

Figure 6.2 – Lorentz Transformation in spherical coordinates when $\sigma = \beta$. The coordinates with flow, denoted (R, ϕ, θ), are converted to zero flow coordinates, (R^0, ϕ^0, θ^0) which can be injected into the zero flow equations.

6.4.3 Lorentz Transformation and momentum equation

Incorrect use of the Lorentz Transformation

According to the previous paragraph, the Lorentz Transformation can *a priori* be applied to both the zero flow pressure and velocity potential, assuming that the expected solutions are continuous. However, these acoustic fields are related by the conservation momentum

$$p^0(\boldsymbol{x}, \omega) = -j\rho_0 c_0 k \Phi^0(\boldsymbol{x}, \omega). \tag{6.4.2}$$

When $M \neq 0$, the expected acoustic fields p and Φ are related through a different equation

$$p(\boldsymbol{x}, \omega) = -j\rho_0 c_0 \left(k - jM\frac{\partial}{\partial z}\right) \Phi(\boldsymbol{x}, \omega) \quad \text{when } M \neq 0, \tag{6.4.3}$$

Note that the Lorentz Transformation applied to both p^0 and Φ^0 yields expressions of p and Φ that do not satisfy equation (6.4.3) because, if LT denotes the Lorentz Transformation,

$$\text{LT}\{p^0\} = \text{LT}{-}j\rho_0 c_0 k\Phi^0 = -j\rho_0 c_0 \sigma \frac{k}{\beta}\text{LT}\{\Phi^0\},$$

so that in general

$$\text{LT}\{p^0\} \neq -j\rho_0 c_0 \left(k - jM\frac{\partial}{\partial z}\right)\text{LT}\{\Phi^0\}.$$

This shows that equation (6.4.3) is not satisfied by $\text{LT}\{p^0\}$ and $\text{LT}\{\Phi^0\}$. Thus, Lorentz Transformation breaks the link between pressure and velocity potential. This feature is illustrated in figure 6.3.

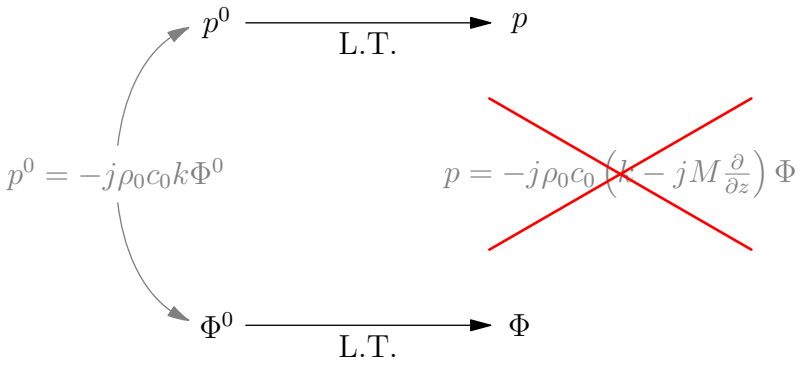

Figure 6.3 – When the Lorentz Transformation (L.T.) is applied independently to the zero-flow pressure p^0 and zero-flow velocity potential Φ^0, the relation between the two fields is not transformed correctly.

Correct use of the Lorentz Transformation

Consequently, the Lorentz Transformation can not be applied to both p^0 and Φ^0. In particular, equation (6.4.2) should not be used during the derivation. Thus, given the Lorentz Transformation p obtained from p^0, Φ should be derived using equation (6.4.3). Alternatively, given the Lorentz Transformation Φ of Φ^0, the pressure should also be derived using equation (6.4.3). In order to obtain physically acceptable solutions, the Lorentz Transformation must be applied to either p^0 or Φ^0. This principle is illustrated in figure 6.4.

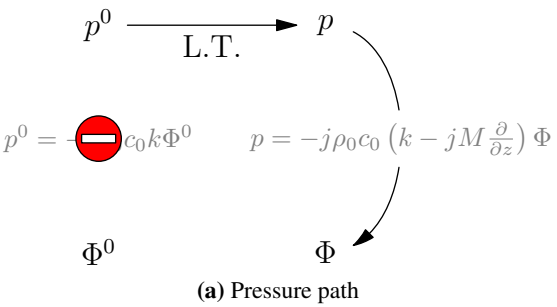

(a) Pressure path

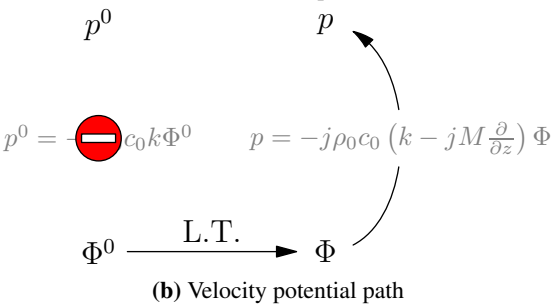

(b) Velocity potential path

Figure 6.4 – Correct application of the Lorentz Transformation (L.T.). It should be applied either to p^0 or to Φ^0 and the relation between p^0 and Φ^0 should not be used in this process.

Chapter 7

Pressure field in a cylindrical waveguide

7.1 Solution of the convected Helmholtz equation with the Lorentz Transformation

From equation (6.3.7), the solution of the homogeneous convected Helmholtz equation (6.1.2) is

$$p(r,\phi,z,\omega) = p^0(\sigma\overline{r},\phi,\sigma\overline{\overline{z}},\frac{\omega}{\sigma})e^{j\omega M\overline{\overline{z}}/c_0}, \tag{7.1.1}$$

where p^0 satisfies the homogeneous Helmholtz equation.

$$\left(\nabla^2 + k^2\right) p^0(r,\phi,z,\omega) = 0, \tag{7.1.2}$$

This equation has been solved in section 2. From equation (2.5.6), p^0 is given by

$$p^0(r,\phi,z,\omega) = \sum_{m=-\infty}^{+\infty}\sum_{n=1}^{+\infty} A_{mn}\Psi_{mn}(r,\phi)e^{-j\alpha^0_{mn}kz}$$

Expressing α^0_{mn} in terms of k, from equation (2.5.4)

$$p^0(r,\phi,z,\omega) = \sum_{m=-\infty}^{+\infty}\sum_{n=1}^{+\infty} A_{mn}\Psi_{mn}(r,\phi)e^{-j\sqrt{1-\kappa^2_{mn}/k^2}kz},$$

where $\kappa_{mn} = j_{mn}/a$. Thus, from (7.1.1),

$$p(r,\phi,z,\omega) = \sum_{m=-\infty}^{+\infty}\sum_{n=1}^{+\infty} A_{mn}\Psi_{mn}(\sigma\overline{r},\phi)e^{-j\sqrt{1-\kappa^2_{mn}/k^2\sigma^2}k\overline{\overline{z}}}e^{jkM\overline{\overline{z}}}, \tag{7.1.3}$$

or more concisely,

$$p(r,\phi,z,\omega) = \sum_{m=-\infty}^{+\infty}\sum_{n=1}^{+\infty} A_{mn}\Psi_{mn}(\sigma\overline{r},\phi)e^{-j\tilde{\alpha}_{mn}kz}, \tag{7.1.4}$$

where

$$\begin{aligned}\tilde{\alpha}_{mn} &= \frac{1}{\beta^2}\left(\underbrace{\sqrt{1-(\kappa_{mn}/k)^2\sigma^2}}_{\alpha_{mn}} - M\right), \\ \tilde{\alpha}_{mn} &= \frac{\alpha_{mn}-M}{\beta^2}.\end{aligned} \tag{7.1.5}$$

7.2 Boundary conditions

From equation (7.1.4), for any mode (m,n), the modal pressure is given by

$$p_{mn}(r,\phi,z) = A_{mn}\Psi_{mn}(\sigma\overline{r},\phi)e^{-j\tilde{\alpha}_{mn}kz}. \tag{7.2.1}$$

The modal pressure must also satisfy the rigid wall boundary condition, i.e.

$$\frac{\partial p_{mn}}{\partial r}(a,\phi,z) = 0 \quad \forall(\phi,z)$$

From the definition of Ψ_{mn} given in equation (2.5.2),

$$\begin{aligned}\left.\frac{\partial \Psi_{mn}(\sigma\overline{r},\phi)}{\partial r}\right|_{r=a} &= \left.\frac{\partial}{\partial r}\left(J_{mn}(\sigma(\kappa_{mn}/\beta)r)\frac{e^{-jm\phi}}{N_{mn}}\right)\right|_{r=a} \\ &= \frac{\sigma\kappa_{mn}}{\beta}J'_m(\sigma(\kappa_{mn}/\beta)a)\frac{e^{-jm\phi}}{N_{mn}}\end{aligned}$$

Thus, $\sigma\kappa_{mn}a/\beta$ must be a zero of J'_m for all $(m,n)\in\mathbb{Z}\times\mathbb{N}^*$. This is only possible if

$$\boxed{\sigma = \beta.} \tag{7.2.2}$$

7.3 General expression for the in-duct pressure

Combining equations (7.1.4) and (7.2.2) gives the expression for the pressure inside the duct,

$$\boxed{p(r,\phi,z,\omega) = \sum_{m=-\infty}^{+\infty}\sum_{n=1}^{+\infty} A_{mn}\Psi_{mn}(r,\phi)e^{-j\tilde{\alpha}_{mn}kz},} \tag{7.3.1}$$

where from (7.1.5),

$$\boxed{\tilde{\alpha}_{mn} = \frac{\alpha_{mn}-M}{\beta^2} \quad \text{and} \quad \alpha_{mn} = \sqrt{1-\left(\frac{\kappa_{mn}}{k}\right)^2\beta^2}.} \tag{7.3.2}$$

In the above equation, α_{mn} is the cut-off ratio with flow, and $\tilde{\alpha}_{m,n}$ the ratio between the axial wavenumber k_z and the wavenumber k. If $M = 0$, $\beta = 1$ which shows that this expression of α_{mn} is consistent with its zero flow definition given in equation (2.5.4).

7.4 Cut-on modes

As in the zero flow case, when the Mach number is non zero, only a finite number of modes are cut-on. A mode will propagate in the far field if and only if

$$\xi_{mn} < 1, \tag{7.4.1}$$

where

$$\xi_{mn} = \frac{\kappa_{mn}}{k}\beta \tag{7.4.2}$$

is the cut-on ratio with flow.

Let

$$\mathcal{O} = \Big\{(m,n) \in \mathbb{Z} \times \mathbb{N}^* \quad | \quad \xi_{mn} < 1\Big\}$$

be the set of the cut-on modes. These cut-on modes are illustrated in figure 7.1 for $ka = 20$ and for various values of the Mach number. Each square represents one cut-on modes (m,n), where m is on the x-axis and n on the y-axis. M takes 5 different values: 0 (purple), 0.4 (green), 0.6 (blue), 0.8 (red) and 0.9 (black). Note that the cut-on condition (7.4.2) varies with $\beta = \sqrt{1-M^2}$: for low Mach numbers, the number of cut-on modes varies little, whereas for higher Mach numbers, e.g. $M > 0.6$, a slight increase in the magnitude of M results in a large increase in the number of cut-on modes.

If the cut-off modes are neglected in the expression of the sound field in the duct, the pressure becomes

$$\boxed{p(r,\phi,z,\omega) = \sum_{(m,n)\in\mathcal{O}} A_{mn}\Psi_{mn}(r,\phi)e^{-j\tilde{\alpha}_{mn}kz}.} \tag{7.4.3}$$

7.5 Direction of propagation of a single mode with flow

7.5.1 Preliminary results from ray theory

Consider a ray corresponding to a single mode. The angle between the ray and the duct axis is denoted by θ. The angle between the phase velocity U_c, which is orthogonal to the wavefronts, and the duct axis is denoted by $\theta_\perp$. In general, the wave fronts are not orthogonal to the mean flow therefore $\theta \neq \theta_\perp$.

However, using the sketch presented in figure 7.2, these angles are related by,

$$\tan\theta = \left(\frac{c\sin\theta_\perp}{c\cos\theta_\perp + U}\right) \tag{7.5.1}$$

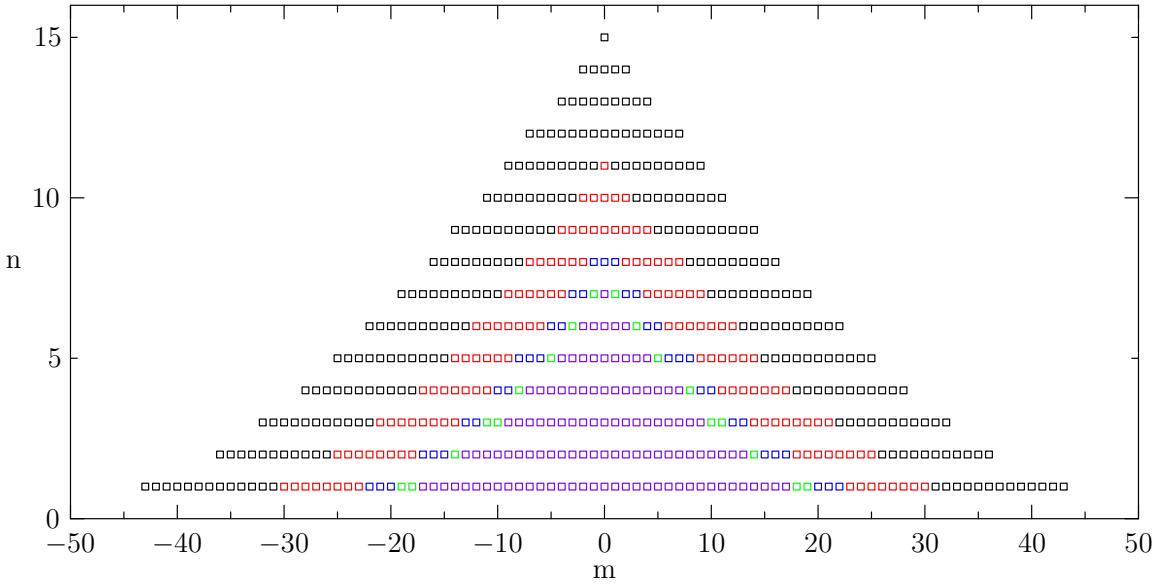

Figure 7.1 – Cut-on modes at frequency ka=20 for various values of the absolute value of the Mach number $|M|$. The purple square indicate the modes which are cut-on at $ka = 20$. Each additional layer shows the modes which become cut-on when $|M|$ increases ; $|M|$ takes the following values : 0 (purple), 0.4 (green), 0.6 (blue), 0.8 (red) and 0.9 (black).

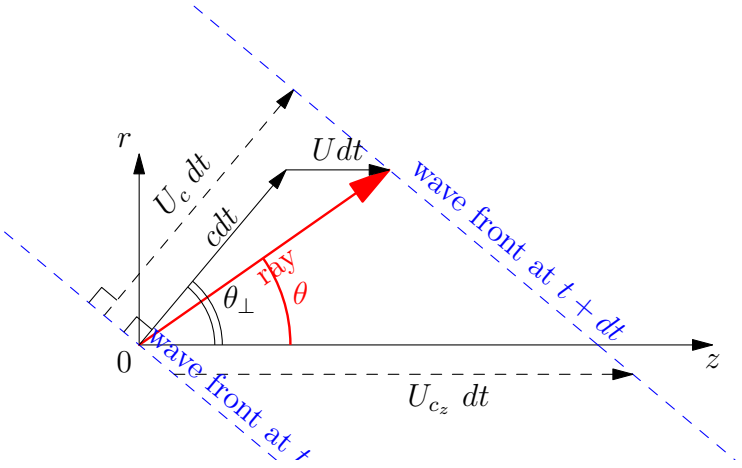

Figure 7.2 – Propagation of a ray in direction θ with respect to the z-axis. The wavefront is sketched at times t and $t + dt$. The phase velocity $U - c$, normal to the wavefronts, makes an angle ψ with the z-axis.

Besides, $\theta_\perp$ can be expressed in terms of the wavenumber k and the axial wavenumber k_z, as follows. The phase velocity is given by

$$U_c = \frac{cdt + U\cos\theta_\perp dt}{dt}, \tag{7.5.2}$$

$$U_c = c + U\cos\theta_\perp. \tag{7.5.3}$$

The phase velocity in the z-direction is defined by

$$U_c = U_{c_z} \cos\theta_\perp. \tag{7.5.4}$$

Combining equations (7.5.3) and (7.5.4), U_{c_z} can be expressed as

$$U_{c_z} = U + \frac{c}{\cos\theta_\perp}. \tag{7.5.5}$$

The wavelength in the z-direction is by definition

$$\lambda_z = \frac{U_{c_z}}{f}, \tag{7.5.6}$$

where f is the frequency of the wave. This wavelength is related to the axial wavenumber by

$$\lambda_z = \frac{2\pi}{k_z}. \tag{7.5.7}$$

Combining equations (7.5.6) and (7.5.7),

$$U_{c_z} = \frac{2\pi f}{k_z} = \frac{ck}{k_z}. \tag{7.5.8}$$

Equating equations (7.5.5) and (7.5.8), and solving for $\cos\theta_\perp$ gives

$$\cos\theta_\perp = \left(\frac{k}{k_z} - M\right)^{-1} \tag{7.5.9}$$

7.5.2 Application of ray theory to a single mode with flow

Consider a single mode (m, n) travelling towards the open end of the duct. From equations (7.5.10) and (7.5.9),

$$\tan\theta = \left(\frac{c\sin\theta_\perp}{c\cos\theta_\perp + U}\right) = \left(\frac{\sin\theta_\perp}{\cos\theta_\perp + M}\right), \tag{7.5.10}$$

where,

$$\cos\theta_\perp = \left(\frac{k}{k_z - M}\right)^{-1}. \tag{7.5.11}$$

From equations (7.4.3) and (7.3.2),

$$k_z = \frac{\alpha_{m,n} - M}{\beta^2},$$

therefore equation (7.5.11) gives

$$\cos\theta_\perp = \frac{\alpha_{m,n} - M}{1 - M\alpha_{m,n}} \tag{7.5.12}$$

Using the following trigonometric relation,

$$1 + \tan^2\theta = \frac{1}{\cos^2\theta}, \quad \sin^2\theta_\perp = 1 - \cos^2\theta_\perp,$$

it is straightforward to show from equation (7.5.10) that

$$\cos\theta = \frac{M + \cos\theta_\perp}{\sqrt{1 + M^2 + 2M\cos\theta_\perp}}.$$

Combining this result with equation (7.5.11) gives

$$\boxed{\cos\theta = \frac{\alpha_{m,n}\beta}{\sqrt{1 - M^2\alpha_{m,n}^2}}.} \tag{7.5.13}$$

$$\boxed{\sin\theta = \frac{\xi_{m,n}}{\sqrt{1 - M^2\alpha_{m,n}^2}}.} \tag{7.5.14}$$

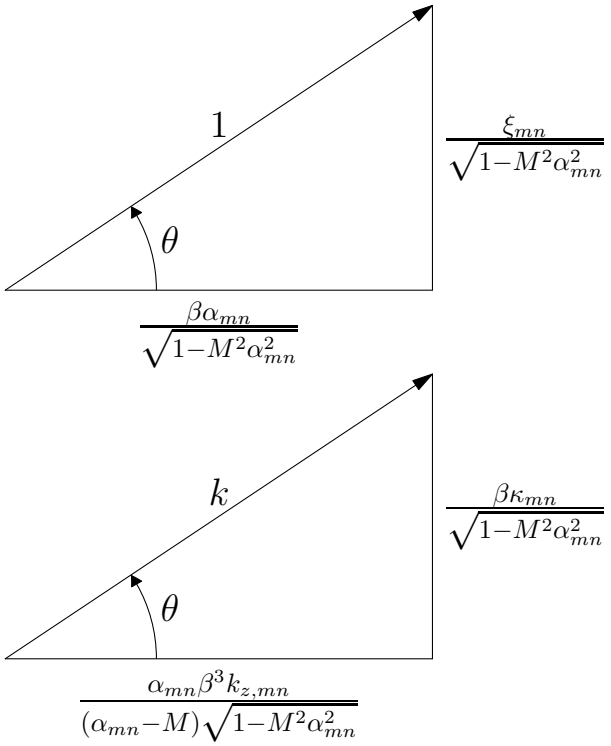

Figure 7.3 – Direction of propagation of mode (m, n) inside a cylindrical duct with flow.

These results are sketched in figure 7.3. They are more complex than the one encountered in the zero flow theory. The results are consistent with the zero flow theory, illustrated in figure 2.6.

Chapter 8

Pressure radiated to the far field

The objective of this section is to derive the expression of the pressure field in the far field when flow is taken into account. The method follows exactly that of the zero flow theory. For each cut-on mode, the mean square far field modal pressure $\overline{p}_{mn,f}(R, \theta, ka)$ is expressed in terms of

- its transfer function $|H_{mn}(ka, \theta)|$, which will be determined by using the Lorentz Transformation of the zero flow solution, or from the Wiener-Hopf solution ;
- its modal amplitude A_{mn}, which will depend on the sound sources present in the duct.

The total pressure will then be obtained by a summation of cut-on modal components, i.e.

$$|p_f(R, \phi, \theta, \omega)|^2 = \left(\frac{a}{R}\right)^2 \sum_{(m,n)\in\mathcal{O}} |H_{mn}(ka, \theta)|^2 |A_{mn}|^2 \tag{8.0.1}$$

8.1 Derivation of $|H_{mn}(ka, \theta)|$

8.1.1 Solution using the Lorentz Transformation

EXHAUST PROBLEM

Pressure with flow For an exhaust problem ($M > 0$), the velocity potential is expected to be discontinuous because of the presence of a vorticity sheet beyond the trailing edge, as illustrated by figure 8.1.

On the contrary, the pressure is assumed to be regular. The Lorentz Transformation is therefore applied to the zero flow results following the pressure path described in figure 6.4a. From equation (3.0.2), the zero flow modal pressure in the far field is given by

$$p^0_{mn,f}(R, \theta, \phi, \omega) = \frac{a}{R} A_{mn} H^0_{mn}(ka, \theta) e^{-jm\phi} e^{-jkR}, \tag{8.1.1}$$

where (m, n) is a cut-on mode. Let $p^+_{mn,f}$ be the far-field pressure radiated from an exhaust duct. Using the Lorentz Transformation in spherical coordinates, defined in equa-

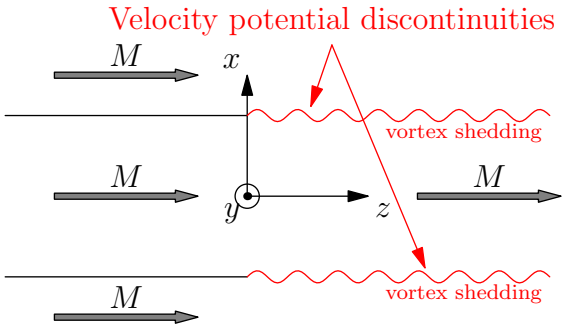

Figure 8.1 – For an exhaust problem ($M > 0$) the sheer layer creates a discontinuity of the velocity potential but the pressure field is regular.

tion (6.3.9), with a frequency factor $\sigma = \beta$, gives

$$p^+_{mn,f}(R,\theta,\phi,\omega) = \frac{\beta a}{R\sqrt{1-M^2\sin^2\theta}} A_{mn} H^0_{mn}(ka/\beta, \tan^{-1}(\beta\tan\theta)) \times e^{-jm\phi} e^{-jkR\sqrt{1-M^2\sin^2\theta}/\beta^2} e^{jkRM\cos\theta/\beta^2}, \quad (8.1.2)$$

$$\boxed{p^+_{mn,f}(R,\theta,\phi,\omega) = \frac{a}{R} A_{mn} \frac{\beta}{\sqrt{1-M^2\sin^2\theta}} H^0_{mn}(ka/\beta, \tan^{-1}(\beta\tan\theta)) e^{-jm\phi} e^{-jkRS(\theta)},} \quad (8.1.3)$$

where

$$S(\theta) = \frac{\sqrt{1-M^2\sin^2\theta} - M\cos\theta}{\beta^2}. \quad (8.1.4)$$

The function S is plotted in figure 8.2 as a function of angle θ and Mach number M. It is not an even function of M, which means that the radial wavenumber, equal to $kS(\theta)$ depends on the sign of M. The radial wavenumber varies between 0 (for $|M| = 1$) and k (for $M = 0$) upstream and increases downstream up to $10k$ for $|M| = 0.9$.

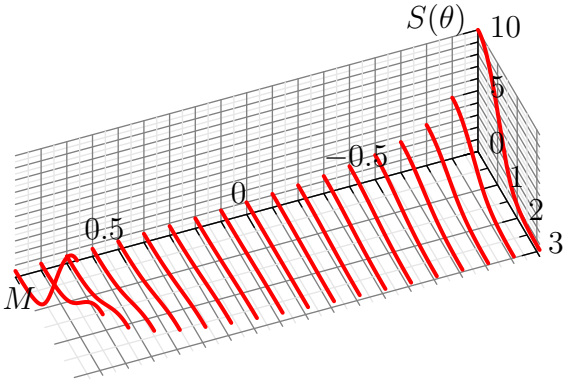

Figure 8.2 – Plot of $S(\theta)$ for $0 \leq \theta \leq \pi$ and $-0.9 \leq M \leq 0.9$.

Transfer function with flow We define the in-duct to far-field transfer function with flow for an exhaust problem, H^+_{mn}, as

$$p^+_{mn,f}(R,\theta,\phi,\omega) = \frac{a}{R} A_{mn} H^+_{mn}(ka,\theta) e^{-jm\phi} e^{-jkRS(\theta)}. \tag{8.1.5}$$

This definition is consistent with the one for the zero-flow transfer function H^0_{mn}: when $M = 0$, $S(\theta) = 1$ and H^+_{mn} reduces to H^0_{mn}. Combining equations (8.1.3) and (8.1.5) gives

$$\boxed{H^+_{mn}(ka,\theta) = \frac{\beta}{\sqrt{1 - M^2 \sin^2\theta}} H^0_{mn}(ka/\beta, \tan^{-1}(\beta \tan\theta)).} \tag{8.1.6}$$

This result is consistent with the one by Homicz and Lordi [8]. Thus, the computation of $H^+_{mn}(ka,\theta)$ from H^0_{mn} is as follows:

- ka/β is substituted for ka in $H^0_{mn}(ka,\theta)$;
- $\tan^{-1}(\beta \tan\theta)$ is substituted for θ in $H^0_{mn}(ka,\theta)$.
- the result are multiplied by $\beta/\sqrt{1 - M^2 \sin^2\theta}$.

INLET PROBLEM

For an inlet problem ($M < 0$), the pressure field is expected to be singular at the open end of the duct, as illustrated by figure 8.3. On the contrary, the velocity potential is assumed to be regular. The Lorentz Transformation must be applied to the zero flow results following the velocity potential path described in figure 6.4b. Thus, the modal velocity potential

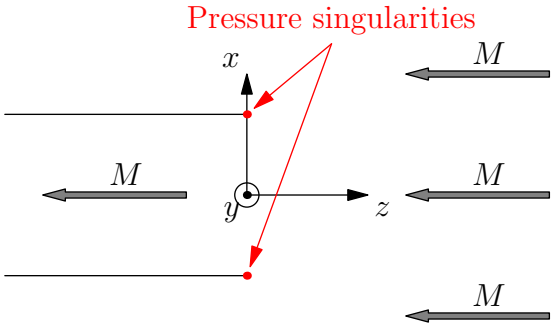

Figure 8.3 – For an inlet problem ($M < 0$) the pressure is singular at the open end of the duct but the velocity potential is regular.

without flow must first be derived.

Derivation of the velocity potential The velocity potential is a solution of the wave equation that satisfies the same boundary condition as the pressure field. This means that the expression derived for modal pressure in equation (3.0.2) also applies for modal velocity potential. However, the amplitude of the modal velocity potential is *a priori* different from

that of the modal pressure. Hence, denoting the amplitude of the modal velocity potential by B_{mn} and using equation (3.0.2), yields

$$\Phi^0_{mn,f}(R,\theta,\phi,\omega) = \frac{a}{R} B_{mn} H^0_{mn}(ka,\theta) e^{-jm\phi} e^{-jkR}. \tag{8.1.7}$$

The modal far field velocity potential with flow can then be derived by applying the Lorentz Transformation to $\Phi^0_{mn,f}$. The result can be obtained directly by using the results obtained for an exhaust problem. Substituting B_{mn} for A_{mn} and p^+_{mn} for $\Phi^-_{mn,f}$ in equation (8.1.3) gives

$$\Phi^-_{mn,f}(R,\theta,\phi,\omega) = \frac{a}{R} B_{mn} \frac{\beta}{\sqrt{1-M^2\sin^2\theta}} H^0_{mn}(ka/\beta, \tan^{-1}(\beta\tan\theta)) e^{-jm\phi} e^{-jkRS(\theta)}, \tag{8.1.8}$$

where H^0_{mn} is the in-duct to far field transfer function without flow and $S(\theta)$ the function defined in equation (8.1.4).

Derivation of the pressure The modal far field pressure can then be derived by substituting equation (8.1.8) into equation (6.4.3), i.e.

$$p^-_{mn,f}(R,\phi,\theta,\omega) = -j\rho_0 c_0 \left(k - jM\frac{\partial}{\partial z}\right) \Phi^-_{mn,f}(R,\phi,\theta,\omega). \tag{8.1.9}$$

The partial derivative on the right hand side can be evaluated by using the chain rule, i.e.

$$\frac{\partial \Phi^-_{mn,f}}{\partial z} \Phi^-_{mn,f} R \frac{\partial R}{\partial z} + \frac{\partial \Phi^-_{mn,f}}{\partial \theta} \frac{\partial \theta}{\partial z}, \tag{8.1.10}$$

where

$$\begin{aligned} &\text{since} \quad R = \sqrt{r^2+z^2}, \quad \frac{\partial R}{\partial z} = \frac{z}{R} = \cos\theta; \\ &\text{since} \quad z = R\cos\theta, \quad 1 = \frac{\partial R}{\partial z}\cos\theta - R\sin\theta\frac{\partial\theta}{\partial z} \quad \text{and} \quad \frac{\partial\theta}{\partial z} = -\frac{\sin\theta}{R}. \end{aligned}$$

Applying the above formulas to equation (8.1.10) and retaining only the first order terms (far field approximation), gives

$$\frac{\partial \Phi^-_{mn,f}}{\partial z}(R,\theta,\Phi,\omega) = -jk(\cos(\theta)S(\theta) - \sin\theta S'(\theta))\Phi^-_{mn,f}(R,\theta,\Phi,\omega). \tag{8.1.11}$$

Since

$$S'(\theta) = \frac{M\sin\theta}{\sqrt{1-M^2\sin^2\theta}} S(\theta), \tag{8.1.12}$$

Equation (8.1.11) is equivalent to

$$\frac{\partial \Phi^{-}_{mn,f}}{\partial z} = -jk\left(\cos(\theta) - \frac{M\sin^2\theta}{\sqrt{1-M^2\sin^2\theta}}\right) S(\theta)\Phi^{-}_{mn,f}(R,\theta,\Phi,\omega). \tag{8.1.13}$$

Combining equations (8.1.9) and (8.1.13) gives

$$p^{-}_{mn,f}(R,\phi,\theta,\omega) = -j\rho_0 c_0 k \times \left[1 - M\left(\cos\theta - \frac{M\sin^2\theta}{\sqrt{1-M^2\sin^2\theta}}\right) S(\theta)\right] \Phi^{-}_{mn,f}(R,\phi,\theta,\omega) \tag{8.1.14}$$

Simplification of the relation between pressure and velocity potential The above equation may be simplified as follows. Let

$$Y(\theta) = \sqrt{1-M^2\sin^2\theta}. \tag{8.1.15}$$

The first term under the brackets in equation (8.1.14) is given by

$$\begin{aligned} 1 - (M\cos\theta)S(\theta) &= 1 - (M\cos\theta)\frac{(Y(\theta) - M\cos\theta)}{\beta^2} \\ &= \frac{\beta^2 - MY(\theta)\cos\theta + M^2\cos^2\theta}{\beta^2} \\ &= \frac{Y(\theta)(1 - M\cos\theta)}{\beta^2} \end{aligned}$$

Thus,

$$1 - (M\cos\theta)S(\theta) = Y(\theta)S(\theta) \tag{8.1.16}$$

The second term under the brackets in equation (8.1.14) can also be expressed in terms of $Y(\theta)$, i.e.

$$\frac{M^2\sin^2\theta}{\sqrt{1-M^2\sin^2\theta}}S(\theta) = \frac{1-Y^2(\theta)}{Y(\theta)}S(\theta) \tag{8.1.17}$$

Combining equations (8.1.16) and (8.1.17),

$$\left(1 - M\cos\theta + \frac{M^2\sin^2\theta}{\sqrt{1-M^2\sin^2\theta}}\right) S(\theta) = \left(Y(\theta) + \frac{1-Y(\theta)^2}{Y(\theta)}\right) S(\theta) = \frac{S(\theta)}{Y(\theta)}. \tag{8.1.18}$$

Substituting equations (8.1.18) and (8.1.15) into equation (8.1.14) gives

$$p^{-}_{mn,f}(R,\phi,\theta,\omega) = -j\rho_0 c_0 k \frac{S(\theta)}{\sqrt{1-M^2\sin^2\theta}} \Phi^{-}_{mn,f}(R,\phi,\theta,\omega). \tag{8.1.19}$$

This equation relates the modal pressure with the modal velocity potential. Since the modal velocity potential has been derived in paragraph (a), it is now possible to obtain an explicit analytical expression for the modal pressure. This will give an expression for the in-duct to far field transfer function.

Calculation of the in-duct to far field transfer function Combining equations (8.1.8) and (8.1.19) gives

$$p^-_{mn,f}(R,\phi,\theta,\omega) = -j\rho_0 c_0 k \frac{S(\theta)}{1-M^2\sin^2\theta}\frac{a}{R}B_{mn}\beta H^0_{mn}(ka/\beta, \tan^{-1}(\beta\tan\theta)) \times e^{-jm\phi}e^{-jkRS(\theta)} \quad (8.1.20)$$

Let H^-_{mn} be the in-duct to far field transfer function for an inlet duct. H^-_{mn} is defined by

$$p^-_{mn,f}(R,\theta,\phi,\omega) = \frac{a}{R}A_{mn}H^-_{mn}(ka,\theta)e^{-jm\phi}e^{-jkRS(\theta)}. \quad (8.1.21)$$

In order to obtain the inlet transfer function H^-_{mn} from equations (8.1.20) and (8.1.21), B_{mn} must be expressed in terms of A_{mn}. These two coefficients are respectively the modal amplitude of the incident velocity potential wave and the modal amplitude of the incident pressure wave, for a given cut-on mode (m,n). According to equation (7.3.1), for an inlet duct,

$$\begin{cases} p^-_{mn}(\boldsymbol{x},\omega) = A_{mn}\Psi_{mn}(r,\phi)e^{-j\tilde{\alpha}_{mn}kz} \\ \Phi^-_{mn}(\boldsymbol{x},\omega) = B_{mn}\Psi_{mn}(r,\phi)e^{-j\tilde{\alpha}_{mn}kz}, \end{cases} \quad (8.1.22)$$

where $\boldsymbol{x} = (R,\phi,\omega)$. Applying the relation between pressure and velocity potential, i.e. equation (6.4.3), to p^-_{mn} and Φ^-_{mn} gives

$$\begin{aligned} p^-_{mn}(\boldsymbol{x},\omega) &= -j\rho_0 c_0 \left(k - jM\frac{\partial}{\partial z}\right)\Phi^-_{mn}(\boldsymbol{x},\omega), \\ &= -j\rho_0 c_0 k(1-M\tilde{\alpha}_{mn})\Phi^-_{mn}(\boldsymbol{x},\omega), \\ &= -j\rho_0 c_0 k\frac{1-M\alpha_{mn}}{\beta^2}\Phi^-_{mn}(\boldsymbol{x},\omega), \\ &= -j\rho_0 c_0 k\frac{1-M\alpha_{mn}}{\beta^2}B_{mn}\Psi_{mn}(r,\phi)e^{-j\tilde{\alpha}_{mn}kz}. \end{aligned}$$

Comparing this result with the expression of p^-_{mn} in equation (8.1.22) gives

$$A_{mn} = -j\rho_0 c_0 k\frac{1-M\alpha_{mn}}{\beta^2}B_{mn}, \quad (8.1.23)$$

so that

$$B_{mn} = \frac{\beta^2}{-j\rho_0 c_0 k(1-M\alpha_{mn})}A_{mn}. \quad (8.1.24)$$

Substituting equation (8.1.24) into equation (8.1.21) gives

$$p^-_{mn,f}(R,\phi,\theta,\omega) = \frac{a}{R}\frac{\beta^3}{1-M\alpha_{mn}}\frac{S(\theta)}{1-M^2\sin^2\theta} A_{mn}H^0_{mn}(ka/\beta, \tan^{-1}(\beta\tan\theta))e^{-jm\phi}e^{-jkRS(\theta)}. \quad (8.1.25)$$

Comparing this result with the definition of H^-_{mn} given in equation (8.1.21),

$$H^-_{mn}(ka,\theta) = \frac{\beta^3}{1-M\alpha_{mn}}\frac{S(\theta)}{1-M^2\sin^2\theta}H^0_{mn}(ka/\beta, \tan^{-1}(\beta\tan\theta)). \quad (8.1.26)$$

Substituting $S(\theta)$ with its definition, i.e. equation (8.1.4), gives

$$\boxed{H^-_{mn}(ka,\theta) = \frac{\beta}{1-M\alpha_{mn}}\frac{\sqrt{1-M^2\sin^2\theta}-M\cos\theta}{1-M^2\sin^2\theta}H^0_{mn}(ka/\beta, \tan^{-1}(\beta\tan\theta))}. \quad (8.1.27)$$

Note that this result differs from the one suggested by Homicz and Lordi [8]. In that paper, it is thought that $\cos\psi$ should be replaced by $\cos\tilde{\psi}$ in the equation following equation (10c); in that case, Homicz and Lordi's results would be consistent with our expression of H_{mn} for $M < 0$.

GEOMETRICAL INTERPRETATION OF THE RADIATED WAVE

The expressions of the transfer functions for an exhaust and an inlet problem, given in equations (8.1.6) and (8.1.27), can be used to derive the direction of the main radiation lobe for mode (m,n). From the zero flow theory, $H^0_{mn}(ka,\theta)$ is maximum when

$$\cos\theta = \alpha^0_{mn}$$

Thus, $H^0_{mn}(ka/\beta, \tan^{-1}(\beta\tan\theta))$ is maximum when

$$\cos(\tan^{-1}(\beta\tan\theta)) = \alpha^0_{mn}(ka/\beta) = \alpha_{mn},$$

, i.e. when

$$\frac{\cos\theta}{\sqrt{1-M^2\sin^2\theta}} = \alpha_{mn}. \quad (8.1.28)$$

Solving for $\cos\theta$ gives

$$\cos\theta = \frac{\alpha\beta}{\sqrt{1-\alpha^2M^2}} \quad (8.1.29)$$

This shows that, whatever the sign of M, the direction of the main radiation lobe, denoted by θ_{mn}, is given by

$$\cos\theta_{mn} = \frac{\alpha_{mn}\beta}{\sqrt{1-\alpha^2_{mn}M^2}}. \quad (8.1.30)$$

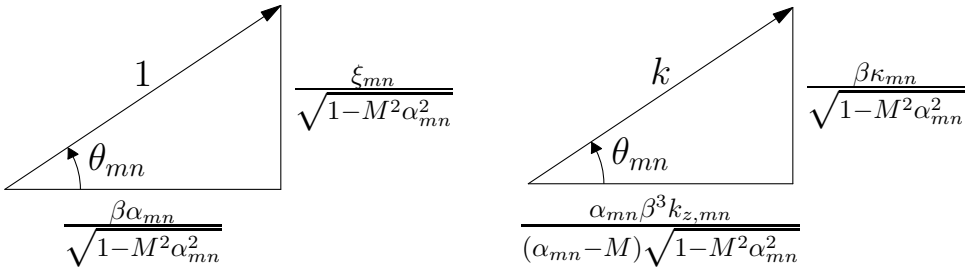

Figure 8.4 – Direction of the main lobe of radiation in the far field for mode (m, n) with flow.

Note that θ_{mn} corresponds to the direction of propagation of mode (m, n) inside the duct when it is seen as a ray, as illustrated in figure 7.3. Thus, for a single mode, the direction of maximum radiation in the far field corresponds to the direction of propagation of the mode inside the duct. The direction of the main radiation lobe for mode (m, n) is illustrated in figure 8.4.

8.1.2 Solution using the Wiener-Hopf Technique

The sound radiated from a duct with flow has also been derived by Gabard and Astley by using the Wiener Hopf Technique [14]. Their results are reproduced below using the above notation. The modal pressure $p_{mn}^{\pm}$ for both positive and negative Mach numbers is given by

$$p_{mn}^{\pm}(R, \theta, \omega) = \frac{a}{R} A_{mn} \frac{V(u_s, ka)}{\pi\sqrt{1 - M^2 \sin^2\theta}} e^{j(m+1)\pi/2} e^{-jkRS(\theta)}, \tag{8.1.31}$$

where

$$u_s = \frac{\cos\alpha_{mn} - M}{\beta^2}, \tag{8.1.32}$$

$$V(u_s, ka) = ka \frac{(1 - u_s M)^2}{\sqrt{(1 - u_s M)^2 - u_s^2}} \frac{F_+(u_s)}{H_m^{(1)'}(\lambda(u_s)ka)}, \tag{8.1.33}$$

$$\text{with} \quad F_+(u_s) = B_{mn} e^{jm\phi} \frac{(1 - \tilde{\alpha}_{mn} M)\lambda(\tilde{\alpha}_{mn})^2 \lambda(u_s)^2}{ka(u_s - M^{-1})^2(\tilde{\alpha}_{mn} - M^{-1})} \frac{\tilde{K}_-(\tilde{\alpha}_{mn})}{\tilde{K}_+(u_s)} \left(\frac{u - M^{-1}}{u - \tilde{\alpha}_{mn}} - \gamma \right), \tag{8.1.34}$$

$$\text{and} \quad \lambda(u) = \sqrt{(1 - uM)^2 - u^2}. \tag{8.1.35}$$

In the definition of F_+, γ represents the amount of vortex shedding. If $\gamma = 1$, the maximum amount of vorticity is shed from the duct trailing edge (Kutta condition). This occurs for an exhaust problem. For an inlet duct, there is no vortex shedding and $\gamma = 0$. The functions $\tilde{K}_+$ and $\tilde{K}_-$ are obtained by factorizing the Wiener-Hopf kernel $K(u)$ as follows

$$K(u) = \frac{\tilde{K}_-(u)}{\tilde{K}_+(u)} (u - M^{-1})^2, \tag{8.1.36}$$

where $\tilde{K}_+$ and $\tilde{K}_-$ are non zero and regular and

$$K(u) = (1 - uM)^2 \lambda(u) \left(\frac{J_m(ka\lambda(u)}{J'_m(ka\lambda(u)} - \frac{H_m^{(1)}(ka\lambda(u))}{H_m^{(1)'}(ka\lambda(u))} \right). \tag{8.1.37}$$

Note that the factorization of $K(u)$ is a difficult task. The interested reader can refer to Gabard and Astley [14] for more details.

8.1.3 Validation of the Lorentz Transformation

In section 8.1.1, the modal transfer function H_{mn} is derived by applying the Lorentz Transformation to the zero flow solution. In that case, H_{mn} is expressed in terms of the zero flow transfer function H^0_{mn}, as illustrated by equations (8.1.6) and (8.1.27). This gives a first method to calculate H_{mn}. A second method consists in using the Wiener-Hopf Technique, as presented in section 8.1.2, which gives an exact result.

Figure 8.5 shows a comparison of the transfer functions H_{mn} obtained from each method, for $ka = 20$. In each figure, the thick black line represents the modal directivity obtained from the Wiener-Hopf Technique, while the thin white line represents the modal directivity obtained from the Lorentz Transformation. Two modes are considered, i.e mode $(1, 1)$ and mode $(8, 5)$, as well as two different values for the Mach number, which are $M = -0.6$ (inlet duct) and $M = 0.6$ (exhaust duct). Note that for $ka = 20$ and $|M| = 0.6$, mode $(1, 1)$ is well cut-on whereas mode $(8, 5)$ is nearly cut-off. Thus, each sub-figure represents the directivity, obtained by two different methods, for one mode and one value of the Mach number.

In all figures, the white line lies exactly on top of the thick black line, which shows that the Lorentz Transformation gives exactly the same result than the Wiener-Hopf Technique. This is true in all cases: for an inlet duct or an exhaust duct, and for a well cut-on mode or a nearly cut-off mode. These results validate the methodology allowing the calculation of the far field transfer functions with flow from the Lorentz Transformation.

Another important result is that the directivity is almost independent of the sign of M. The directivities for $M = -0.6$ are almost identical to that for $M = 0.6$. Actually, the angular position of the main lobe, zeros and secondary lobes are the same. Moreover, the magnitude is nearly identical for $\theta < \pi/2$. Therefore, in the following figures, the directivities will only be plotted for positive values of M.

8.1.4 Validation of the flanged duct transfer functions

The flanged duct transfer functions, obtained by applying the Lorentz Transformation method and using the flanged duct approximation of the zero flow transfer functions, are compared to Wiener-Hopf solution in figure 8.7. The Wiener-Hopf directivities are plotted in black, and the flanged duct directivities in dotted red. Two modes are considered at

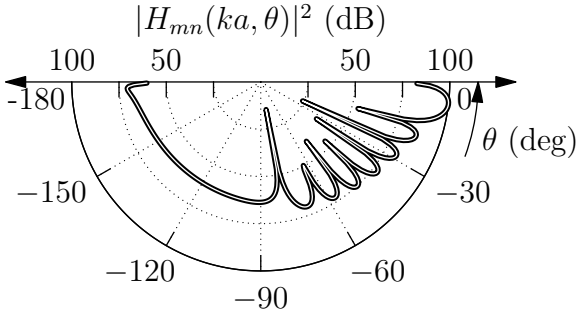

(a) ka=20, (m,n)=(1,1), M=0.6, mode well cut-on

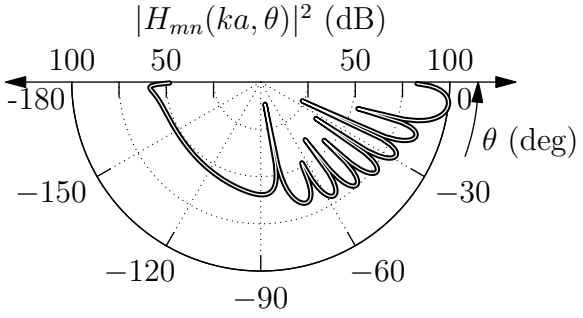

(b) ka=20, (m,n)=(1,1), M=-0.6, mode well cut-on

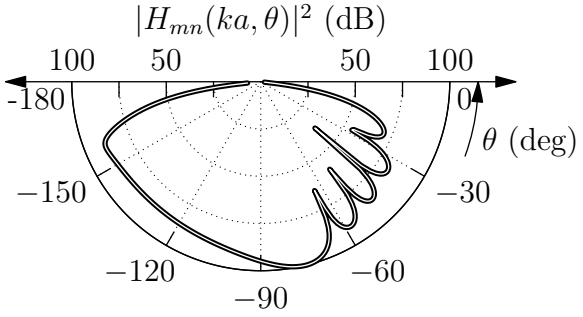

(c) ka=20, (m,n)=(8,5), M=0.6, mode nearly cut-off

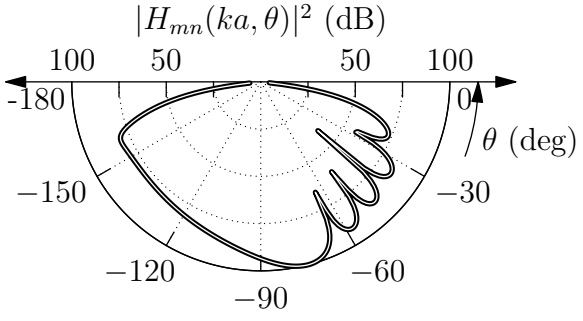

(d) ka=20, (m,n)=(8,5), M=-0.6, mode well cut-on

Figure 8.5 – Comparison of the modal transfer functions with flow from the zero flow solution given by the Wiener Hopf Technique followed by a Lorentz Transformation (thin white line), or the direct solution with flow from the Wiener Hopf Technique (thick black line). The results are given at ka=20, M=-0.6 and 0.6, for two different modes. Mode (1,1) is well cut-on ($\alpha_{1,1} = 0.99$) and mode (8,5) is close to cut-off ($\alpha_{8,5} = 0.18$).

frequency $ka = 20$ and Mach number $M = 0.6$; mode (1,2) is a well cut-on mode (figure 8.7a), and mode (8,5) is close to cut-off (figure 8.7b).

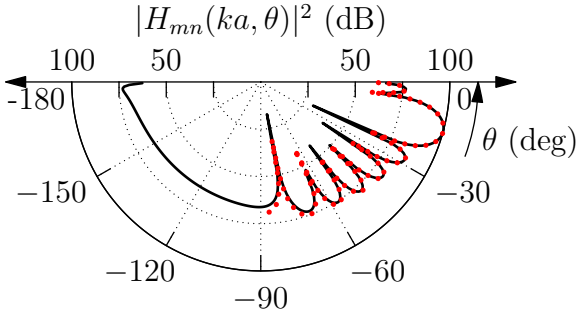

(a) ka=20, (m,n)=(1,2), M=0.6, mode well cut-on

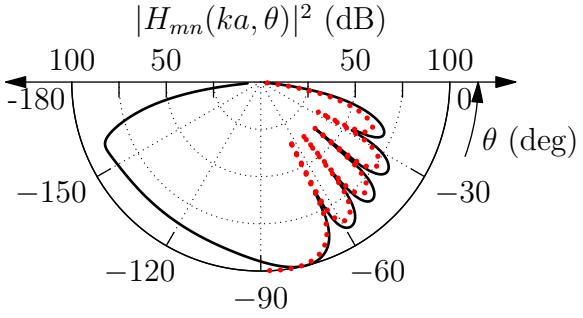

(b) ka=20, (m,n)=(8,5), M=0.6, mode nearly cut-off

Figure 8.6 – Comparison of the modal transfer functions obtained by using a flanged duct model together with a Lorentz Transformation, or the exact direct Wiener Hopf Technique. The frequency is ka=20 and two modes are considered. A well cut-on mode, (1,2), and a nearly cut-off mode, (8,5). The results are given for M=-0.6.

In both cases, the flanged duct transfer function with flow is in good agreement with the exact Wiener-Hopf Technique. However, the level of agreement varies with the cut-off ratio. On the one hand, the agreement is very good for modes which are well cut-on. For these modes, the position and magnitude of almost all the secondary lobes is estimated correctly, the accuracy reducing only above $85°$. On the other hand, for modes which are close to cut-off, the flanged duct solution predicts correctly the position and magnitude of the main lobe but is less accurate for the secondary lobes: though the position is estimated precisely, the magnitude is slightly under estimated. In conclusion, the flanged duct model is very accurate for well cut-on modes, and slightly less so for almost cut-off modes. In all cases, it predicts exactly the position of the main lobe. The flanged duct transfer functions should therefore give a good approximation of the multi-mode directivity.

8.1.5 Variation of the modal directivity with Mach number

Figure 8.7 shows the variation of the single mode directivity with Mach number. The Mach number is successively equal to 0, 0.6 and 0.9. The frequency is $ka = 20$. Two modes are considered, a mode which is well cut-on when $M = 0$, i.e mode (8,1) (top sub-figures), and a mode which is close to cut-off, i.e mode (7,4) (bottom sub-figures).

In all cases, increasing the Mach number results in an increase in the number the number of secondary lobes. However, the effect on the direction of the main radiation lobe depends

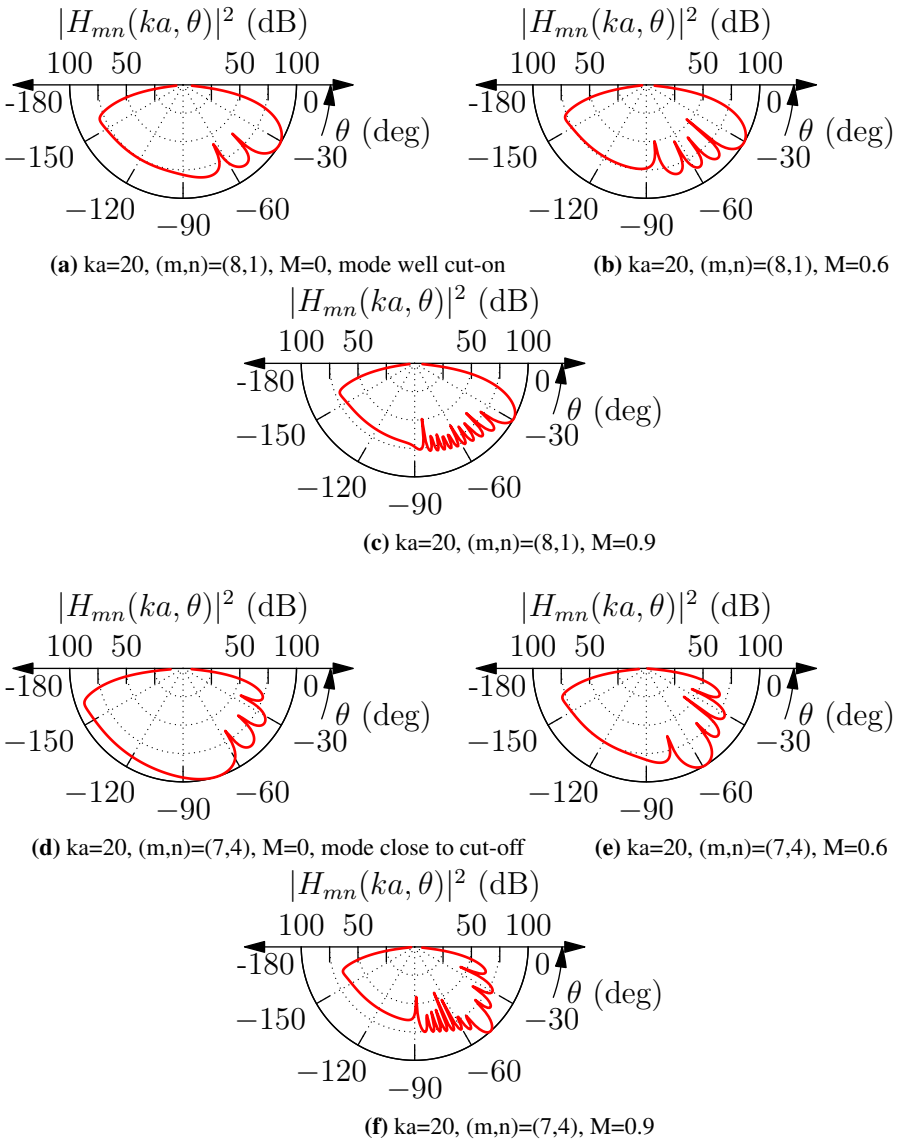

(a) ka=20, (m,n)=(8,1), M=0, mode well cut-on

(b) ka=20, (m,n)=(8,1), M=0.6

(c) ka=20, (m,n)=(8,1), M=0.9

(d) ka=20, (m,n)=(7,4), M=0, mode close to cut-off

(e) ka=20, (m,n)=(7,4), M=0.6

(f) ka=20, (m,n)=(7,4), M=0.9

Figure 8.7 – Variation of the modal transfer function with Mach number for mode $(8,1)$ which is well cut-on at zero Mach number (top), and mode $(7,4)$ which is almost cut-off at zero Mach number (bottom). The direction of the main lobe varies little for mode $(8,1)$ and significantly for mode $(7,4)$. The frequency is ka=20.

on the cut-off ratio of the mode at $M = 0$. Thus, if the mode is well cut-on for zero flow, then the direction of the main radiation lobe remains the same, as illustrated by mode $(8,1)$. On the contrary, if the mode is close to cut-off for zero flow, then the main radiation lobe tends to move towards the duct axis, as illustrated by mode $(7,4)$. This can be explained as follows. From equation (8.1.30), the direction of the main radiation lobe is given by

$$\theta_{mn} = \cos^{-1}\left(\frac{\alpha_{mn}\beta}{\sqrt{1-\alpha_{mn}^2 M^2}}\right). \tag{8.1.38}$$

The cut-off ratio is related to the zero flow cut-off ratio by

$$\alpha_{mn} = \sqrt{(\alpha^0_{mn})^2\beta^2 + M^2}. \tag{8.1.39}$$

Combining equations (8.1.38) and (8.1.39) gives

$$\theta_{mn}(\alpha^0_{mn}) = \cos^{-1}\left(\frac{\sqrt{(\alpha^0_{mn})^2\beta^2 + M^2}\beta}{\sqrt{1-((\alpha^0_{mn})^2\beta^2 + M^2)M^2}}\right). \tag{8.1.40}$$

Figure 8.8 shows the variation of the main radiation lobe θ_{mn} as a function of the zero flow cut-off ratio $\alpha^0_{m,n}$, for various values of the Mach number. For well cut-on modes, $\alpha^0_{m,n}$ is close to one, and θ_{mn} varies little with the Mach number. On the contrary, for modes close to cut-off, $\alpha^0_{m,n}$ is close to zero, and θ_{mn} varies significantly with Mach number.

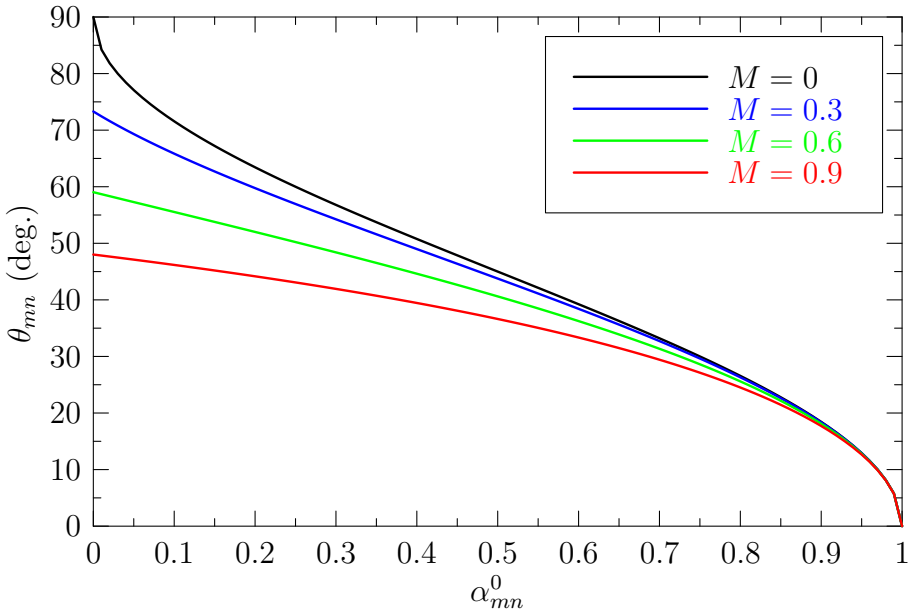

Figure 8.8 – Direction of the main radiation lobe θ_{mn} as a function of the zero flow cut-off ratio for Mach numbers of 0, 0.3, 0.6 and 0.9. The angle θ_{mn} varies significantly for modes which are close to cut-off when $M = 0$, and little for modes which are well cut-on when $M = 0$.

8.2 Mode weighting models

8.2.1 Green's function in a rigid wall infinite cylinder with flow

Let $G(\boldsymbol{x}|\boldsymbol{y}, \omega)$ be the harmonic Green's function in a rigid wall infinite duct with flow. The Green function G satisfies

$$\nabla^2 G(\boldsymbol{x}|\boldsymbol{y}, \omega) + \left(k - jM\frac{\partial}{\partial z}\right)^2 G(\boldsymbol{x}|\boldsymbol{y}, \omega) = -\delta(\boldsymbol{x} - \boldsymbol{y}). \tag{8.2.1}$$

The Laplacian can be projected in the plane xy, i.e

$$\nabla^2 = \nabla_\perp^2 + \frac{\partial^2}{\partial z^2},$$

so that (8.2.1) is equivalent to

$$\nabla_\perp^2 G(\boldsymbol{x}|\boldsymbol{y},\omega) + \frac{\partial^2}{\partial z^2} G(\boldsymbol{x}|\boldsymbol{y},\omega) + \left(k - jM\frac{\partial}{\partial z}\right)^2 G(\boldsymbol{x}|\boldsymbol{y},\omega) = -\delta(\boldsymbol{x}-\boldsymbol{y}). \quad (8.2.2)$$

In the following derivation, the coordinates of $\boldsymbol{x}$ and $\boldsymbol{y}$ will be denoted by (x_1, x_2, x_3) and (y_1, y_2, y_3). The projection of $\boldsymbol{x}$ and $\boldsymbol{y}$ on the xy-plane will be denoted by $\boldsymbol{x}_s$ and $\boldsymbol{y_s}$. Assume that G is of the form

$$G(\boldsymbol{x}|\boldsymbol{y},\omega) = \sum_{(m,n)\in\mathcal{O}} \Psi_{mn}(\boldsymbol{x}_s) F_{mn}(x_3). \quad (8.2.3)$$

Then, equation (8.2.2) implies that

$$\sum_{(m,n)\in\mathcal{O}} \left[\nabla_\perp^2 \Psi_{mn}(\boldsymbol{x}_s)\right] F_{mn}(x_3) + \Psi_{mn}(\boldsymbol{x}_s)\left(\beta^2\frac{\partial^2}{\partial z^2} - 2j\frac{\partial}{\partial z} + k^2\right) F_{mn}(x_3) = -\delta(\boldsymbol{x}-\boldsymbol{y}) \quad (8.2.4)$$

Using the properties (2.4.3) and (2.4.5) of the mode shape functions, multiplying (8.2.4) by $\Psi_{ql}^*(\boldsymbol{x}_s)$, and integrating over a duct cross section $\mathcal{A}$ gives

$$\forall (m,n) \in \mathcal{O}, \quad \left(\beta^2\frac{\partial^2}{\partial z^2} - 2j\frac{\partial}{\partial z} + k^2\right) F_{mn}(x_3) = -\frac{1}{\mathcal{A}}\Psi_{ql}^*(\boldsymbol{y_s})\delta(x_3 - y_3). \quad (8.2.5)$$

This inhomogeneous differential equation can be solved by using the mode matching method on the left and right sides of the cross section $x_3 = y_3$. The main results are presented below. The solutions of the homogeneous differential equation are as follows:

$$\text{if} \quad x_3 < y_3, \quad F_{ql}(x_3) = Ce^{jK^- x_3}, \quad \text{where} \quad K^- = \frac{\alpha_{ql} + M}{1 - M^2}k$$

$$\text{if} \quad x_3 > y_3, \quad F_{ql}(x_3) = De^{jK^+ x_3}, \quad \text{where} \quad K^+ = \frac{\alpha_{ql} - M}{1 - M^2}k$$

The two solutions are matched by integrating equation (8.2.5) in the region

$$y_3 - \epsilon \leq x_3 \leq y_3 + \epsilon,$$

and letting ϵ tend towards 0. This gives

$$C = -\frac{j}{2\mathcal{A}\alpha_{ql}k}\Psi^*_{ql}(\boldsymbol{y_s})e^{jK^-(x_3-y_3)}; D = -\frac{j}{2\mathcal{A}\alpha_{ql}k}\Psi^*_{ql}(\boldsymbol{y_s})e^{-jK^+(x_3-y_3)}.$$

F_{mn} can be expressed in a compact form for all values of x_3, i.e.

$$F_{ql}(x_3) = -\frac{j}{2\mathcal{A}\alpha_{ql}k}\Psi^*_{ql}(\boldsymbol{y_s})e^{-jk(\alpha_{ql}|x_3-y_3|-M(x_3-y_3))/\beta^2}. \tag{8.2.6}$$

Substituting equation (8.2.6) into equation (8.2.3)y gives the

$$G(\boldsymbol{x}|\boldsymbol{y},\omega) = \sum_{(m,n)\in\mathcal{O}} -\frac{j}{2\mathcal{A}\alpha_{mn}k}\Psi_{mn}(\boldsymbol{x}_s)\Psi^*_{mn}(\boldsymbol{y}_s)e^{-jk(\alpha_{mn}|x_3-y_3|-M(x_3-y_3))/\beta^2}. \tag{8.2.7}$$

When $x_3 > y_3$, the parameter $\tilde{\alpha}_{mn}$, which has been defined in equation (7.3.2), can be used to simplify the above expression, i.e.

$$\boxed{G(\boldsymbol{x}|\boldsymbol{y},\omega) = \sum_{(m,n)\in\mathcal{O}} -\frac{j}{2\mathcal{A}\alpha_{mn}k}\Psi_{mn}(\boldsymbol{x}_s)\Psi^*_{mn}(\boldsymbol{y}_s)e^{-jk\tilde{\alpha}_{mn}(x_3-y_3)}.} \tag{8.2.8}$$

8.2.2 Generalization of the Kirchhoff-Helmholtz equation with flow

An equation similar to the Kirchhoff-Helmholtz equation can be derived when the mean flow is irrotational, which is the case in this study. Let $G(\boldsymbol{x}|\boldsymbol{y},\omega)$ be a Green's function satisfying equation (3.2.2). Let $Q_{vol}(\boldsymbol{y})$ be a volume distribution of acoustic sources in a volume V surrounded by a surface S. Following the results presented by Howe [21], the pressure field is given by

$$p(\boldsymbol{x},\omega) = \int_V Q_{vol}(\boldsymbol{y},\omega)G(\boldsymbol{x}|\boldsymbol{y},\omega)\ d^3\boldsymbol{y} + \int_S \left\{ \left(G(\boldsymbol{x}|\boldsymbol{y},\omega)\frac{\partial p}{\partial y_i}(\boldsymbol{y},\omega) - p(\boldsymbol{y},\omega)\frac{\partial G}{\partial y_i}(\boldsymbol{x}|\boldsymbol{y},\omega) \right) \times(\delta_{ij} - M_iM_j) + \frac{2j\omega Mj}{c_0}p(\boldsymbol{y},\omega)G(\boldsymbol{x}|\boldsymbol{y},\omega) \right\} n_j\ d^2S(\boldsymbol{y}). \tag{8.2.9}$$

If the Green's function is the one derived in section 8.2.1, the surface integral vanishes everywhere except at the open end of the duct. This means that the pressure field generated by a volume distribution $Q(\boldsymbol{y},\omega)$ is of the form

$$p(\boldsymbol{x},\omega) = \int_V Q_{vol}(\boldsymbol{y},\omega)G(\boldsymbol{x}|\boldsymbol{y},\omega)\ d^3\boldsymbol{y} + p'(\boldsymbol{x},\omega), \tag{8.2.10}$$

where $p'(\boldsymbol{x},\omega)$ is a wave reflected from the open end of the duct. At high frequency, the reflected wave can be expected to be negligible in comparison with the incident wave so

that the following approximation can be made,

$$p(\boldsymbol{x},\omega) = \int_V Q_{vol}(\boldsymbol{y},\omega) G(\boldsymbol{x}|\boldsymbol{y},\omega)\ d^3\boldsymbol{y}, \tag{8.2.11}$$

which is identical to the zero-flow Kirchhoff-Helmholtz equation.

In the following sections, this formula will be applied with different models of volume source distributions. To simplify the notation, each point $\boldsymbol{y}$ will be decomposed as $(\boldsymbol{y_s}, y_3)$.

8.2.3 Uniform distribution of incoherent monopoles

Let $Q_{vol}(\boldsymbol{y},\omega)$ be a distribution of incoherent monopoles located at $y_3 = z_0$. The term Q_{vol} can be expressed as

$$Q_{vol}(\boldsymbol{y},\omega) = \rho_0 c_0 j q_s(\boldsymbol{y_s},\omega) \left(k - jM\frac{\partial}{\partial y_3}\right) \delta(y_3 - z_0), \tag{8.2.12}$$

$$Q_{vol}(\boldsymbol{y},\omega) = \rho_0 c_0 j q_s(\boldsymbol{y_s},\omega) \left(k\delta(y_3 - z_0) - jM\delta'(y_3 - z_0)\right), \tag{8.2.13}$$

where $q_s(\boldsymbol{y_s},\omega)$ is a volume velocity source per unit surface. Since the monopoles are incoherent, q_s has the following property

$$E\left\{q_s(\boldsymbol{y_s},\omega) q_s(\boldsymbol{y'_s},\omega)\right\} = \overline{2\overline{Q_s^2}}\mathcal{A}\delta(\boldsymbol{y_s} - \boldsymbol{y'_s}), \tag{8.2.14}$$

where $\overline{Q_s^2}$ is the mean square volume velocity per unit surface of the monopoles. In equation (8.2.13), the derivative of the Dirac delta function is taken in the sense of the derivative of a distribution, which is defined by the following property

$$\int_{-\infty}^{+\infty} f(y_3)\delta'(y_3 - z_0)\ dy_3 = -\int_{-\infty}^{+\infty} f'(y_3)\delta(y_3 - z_0)\ dy_3 = -f'(z_0). \tag{8.2.15}$$

From equation (8.2.11),

$$p(\boldsymbol{x},\omega) = \int_V Q_{vol}(\boldsymbol{y},\omega) G(\boldsymbol{x}|\boldsymbol{y},\omega)\ d^3\boldsymbol{y} = \int_{\mathcal{A}}\int_{-\infty}^{0} l(\boldsymbol{y_s},\omega)\ \mathrm{d}y_3\, \mathrm{d}\boldsymbol{y_s}, \tag{8.2.16}$$

where

$$l(\boldsymbol{y_s},\omega) = \int_{-\infty}^{0} Q_{vol}(\boldsymbol{y},\omega) G(\boldsymbol{x}|\boldsymbol{y},\omega)\ dy_3. \tag{8.2.17}$$

Combining equations (8.2.13) and (8.2.17) gives

$$\begin{aligned} l(\boldsymbol{y_s},\omega) = &\int_{-\infty}^{0} \rho_0 c_0 j q_s(\boldsymbol{y_s},\omega) k G(\boldsymbol{x}|\boldsymbol{y},\omega)\delta(y_3 - z_0)\ dy_3 \\ &- \int_{-\infty}^{0} \rho_0 c_0 q_s(\boldsymbol{y_s},\omega) M \frac{\partial G}{\partial y_3}(\boldsymbol{x}|\boldsymbol{y},\omega)\ dy_3 \end{aligned} \tag{8.2.18}$$

From equations (8.2.15) and (8.2.18),

$$l(\boldsymbol{y_s},\omega) = \rho_0 c_0 j q_s(\boldsymbol{y_s},\omega) kG(\boldsymbol{x}|\boldsymbol{y},\omega)\Big|_{y_3=z_0} - \rho_0 c_0 q(\boldsymbol{y_s},\omega) M \frac{\partial G}{\partial y_3}(\boldsymbol{x}|\boldsymbol{y},\omega)\Big|_{y_3=z_0}. \quad (8.2.19)$$

Substituting (8.2.19) into (8.2.16) gives

$$p(\boldsymbol{x},\omega) = \rho_0 c_0 j \int_{\mathcal{A}} q_s(\boldsymbol{y_s},\omega) kG(\boldsymbol{x}|\boldsymbol{y},\omega)\Big|_{y_3=z_0} - \rho_0 c_0 q_s(\boldsymbol{y_s},\omega) M \frac{\partial G}{\partial y_3}(\boldsymbol{x}|\boldsymbol{y},\omega)\Big|_{y_3=z_0} d^2\boldsymbol{y_s}. \quad (8.2.20)$$

If $x_3 > z_0$, then $y_3 = z_0 \rightarrow x_3 > y_3$, and from equation (8.2.8),

$$G(\boldsymbol{x}|\boldsymbol{y},\omega) = \sum_{(m,n)\in\mathcal{O}} -\frac{j}{2\mathcal{A}\alpha_{mn}k} \Psi^*_{mn}(\boldsymbol{y_s}) \Psi_{mn}(\boldsymbol{x}_s) e^{-j\tilde{\alpha}_{mn}k(x_3-y_3)} \quad (8.2.21)$$

$$\frac{\partial G}{\partial z}(\boldsymbol{x}|\boldsymbol{y},\omega) = \sum_{(m,n)\in\mathcal{O}} -\frac{\tilde{\alpha}_{mn}}{2\mathcal{A}\alpha_{mn}} \Psi^*_{mn}(\boldsymbol{y_s}) \Psi_{mn}(\boldsymbol{x}_s) e^{-j\tilde{\alpha}_{mn}k(x_3-y_3)} \quad (8.2.22)$$

Substituting (8.2.21) and (8.2.22) into equation (8.2.20) gives

$$p(\boldsymbol{x},\omega) = \rho_0 c_0 \sum_{(m,n)\in\mathcal{O}} \frac{1-M\tilde{\alpha}_{mn}}{2\mathcal{A}\alpha_{mn}} e^{j\tilde{\alpha}_{mn}ky_3} \left(\int_{\mathcal{A}} q(\boldsymbol{y_s},\omega) \Psi^*(\boldsymbol{y_s}) \; d^2\boldsymbol{y_s} \right) \Psi_{mn}(\boldsymbol{x}_s) e^{-j\tilde{\alpha}_{mn}kx_3}. \quad (8.2.23)$$

From the general expression of p given in equation (2.5.1), the modal amplitude coefficient A_{mn} is given by

$$A_{mn} = \rho_0 c_0 \frac{1-M\tilde{\alpha}_{mn}}{2\mathcal{A}\alpha_{mn}} e^{j\tilde{\alpha}_{mn}ky_3} \int_{\mathcal{A}} q_s(\boldsymbol{y_s},\omega) \Psi^*(\boldsymbol{y_s}) \; d^2\boldsymbol{y_s}. \quad (8.2.24)$$

Thus,

$$E\{|A_{mn}|^2\} = \rho_0^2 c_0^2 \left(\frac{1-M\tilde{\alpha}_{mn}}{2\mathcal{A}\alpha_{mn}} \right)^2 \times \int_{\mathcal{A}'} \int_{\mathcal{A}} \Psi^*_{mn}(\boldsymbol{y_s}) \Psi_{mn}(\boldsymbol{y'_s}) E\{q_s(\boldsymbol{y_s},\omega) q_s^2(\boldsymbol{y'_s},\omega)\} \; \mathrm{d}^2\boldsymbol{y_s} \, \mathrm{d}^2\boldsymbol{y'_s} \quad (8.2.25)$$

Since the monopoles are assumed to be incoherent, from equation (8.2.14),

$$E\{|A_{mn}|^2\} = \rho_0^2 c_0^2 \overline{Q_s^2} \mathcal{A} \left(\frac{1-M\tilde{\alpha}_{mn}}{2\mathcal{A}\alpha_{mn}} \right)^2 \int_{\mathcal{A}} |\Psi_{mn}(\boldsymbol{y'_s})|^2 \; d^2\boldsymbol{y_s},$$

$$E\{|A_{mn}|^2\} = \frac{\rho_0^2 c_0^2}{4} \overline{Q_s^2} \left(\frac{1-M\tilde{\alpha}_{mn}}{\alpha_{mn}} \right)^2.$$

Expressing $\tilde{\alpha}_{mn}$ in terms of α_{mn} gives the modal amplitude for a uniform distribution of incoherent monopoles, i.e.

$$\boxed{E\{|A_{mn}|^2\} = \frac{\rho_0^2 c_0^2}{2}\overline{Q_s^2}\frac{(1-M\alpha_{mn})^2}{\beta^2}\alpha_{mn}^{-2},} \tag{8.2.26}$$

which is the result derived by Joseph *et al.* [15], although they did not use the Green's function but a mode matching method. If $M = 0$, the above formula gives the result for zero flow (see section 3.2.1).

8.2.4 Uniform distribution of incoherent axial dipoles

In the case of a uniform distribution of incoherent axial dipoles, the derivation follows closely the one for zero flow presented in section 3.2.2. The volume distribution of sources Q_{vol} is again given by

$$Q_{vol}(\boldsymbol{y}) = -\boldsymbol{\nabla}_{\boldsymbol{y}} \cdot \boldsymbol{f_{vol}}(\boldsymbol{y}), \tag{8.2.27}$$

where

$$\boldsymbol{f_{vol}}(\boldsymbol{y}) = f_s(\boldsymbol{y_s})\delta(y_3 - z_0)\boldsymbol{e_z}. \tag{8.2.28}$$

$f_s(\boldsymbol{y_s})$ is a force per unit surface and $\boldsymbol{e_z}$ is the unit vector in the z-direction. At high frequency, the pressure wave generated in the duct is given by equation (8.2.11) which is the one used in the zero flow. Consequently, the part of the derivation presented at section 3.2.2 for which the Green's function is not replaced by its value remains applicable. Thus, from equation (3.2.9),

$$p(\boldsymbol{x},\omega) = -\int_{\mathcal{A}} \frac{\partial G(\boldsymbol{x}|\boldsymbol{y},\omega)}{\partial y_3}\Big|_{y_3=z_0} f_s(\boldsymbol{y_s},\omega)\ d^2\boldsymbol{y_s}. \tag{8.2.29}$$

Substituting (8.2.22) in equation (8.2.29), and assuming $x_3 > y_3$,

$$p(\boldsymbol{x},\omega) = \sum_{(m,n)\in\mathcal{O}} \frac{\tilde{\alpha}_{mn}}{2\mathcal{A}\alpha_{mn}}\Psi_{mn}(\boldsymbol{x_s})e^{-j\tilde{\alpha}_{mn}k(x_3-z_0)}\int_{\mathcal{A}} \Psi^*_{mn}(\boldsymbol{y_s})f_s(\boldsymbol{y_s},\omega)\ d^2\boldsymbol{y_s}. \tag{8.2.30}$$

Comparing (8.2.30) with the general expression for $p(\boldsymbol{x},\omega)$ gives

$$A_{mn} = \frac{\tilde{\alpha}_{mn}}{2\mathcal{A}\alpha_{mn}}e^{j\tilde{\alpha}_{mn}kz_0}\int_{\mathcal{A}} \Psi^*_{mn}(\boldsymbol{y_s})f_s(\boldsymbol{y_s},\omega)\ d^2\boldsymbol{y_s} \tag{8.2.31}$$

A comparison of this result with that obtained in the zero- case in equation (3.2.10) shows that the absolute value of A_{mn} is related to A^0_{mn} by

$$|A_{mn}| = \frac{\tilde{\alpha}_{mn}}{\alpha_{mn}}|A^0_{mn}|$$

Thus,

$$E\{|A_{mn}|^2\} = \left(\frac{\tilde{\alpha}_{mn}}{\alpha_{mn}}\right)^2 E\{|A^0_{mn}|^2\}$$

Combining this result with equation (3.2.11) gives

$$E\{|A_{mn}|^2\} = \left(\frac{\tilde{\alpha}_{mn}}{\alpha_{mn}}\right)^2 \frac{\overline{F_s^2}}{2},$$

where $\overline{F_s^2}$ is the mean square force per unit surface of the axial dipole distribution. From the definition of $\tilde{\alpha}_{mn}$ given in equation (7.3.2), the weighting model for a uniform distribution of dipoles is given by

$$\boxed{E\{|A_{mn}|^2\} = \frac{\overline{F_s^2}}{2}\left(\frac{\alpha_{mn} - M}{\beta\alpha_{mn}}\right)^2.} \tag{8.2.32}$$

This result is again equivalent to the one obtained by Joseph *et al.* [15]. If $M = 0$, this expression reduces to (7.3.2).

8.2.5 Equal power per mode

The power transmitted along the duct through section z is given by

$$W(z) = \int_{\mathcal{A}} I_z(\boldsymbol{y_s}, z)\ d^2\boldsymbol{y_s}, \tag{8.2.33}$$

where $I_z(\boldsymbol{y_s}, z)$ is the axial acoustic intensity.

Acoustic intensity in an isentropic and irrotational flow

From [22, 23], a generalized definition of the time averaged intensity $\boldsymbol{I}$, valid for an isentropic and irrotational mean flow, is given by

$$\boldsymbol{I} = < p\boldsymbol{u} > + \frac{\boldsymbol{M}}{\rho_0 c_0} < p^2 > + \boldsymbol{M} < p(\boldsymbol{u}\cdot\boldsymbol{M}) > + \rho_0 c_0 < \boldsymbol{u}(\boldsymbol{u}\cdot\boldsymbol{M}) >, \tag{8.2.34}$$

where $\boldsymbol{M} = \boldsymbol{U}/c_0$ is the velocity of the mean flow divided by c_0, and $\boldsymbol{u}$ is the acoustic velocity.

Acoustic intensity in the duct and transmitted power

Let I_z be the acoustic intensity transmitted along the duct. In this problem, $\boldsymbol{M} = (0, 0, M)$, so that equation (8.2.34) becomes

$$I_z(\boldsymbol{y_s}, z) = \frac{1}{2}\left(\frac{M}{\rho_0 c_0}|p(\boldsymbol{y}, \omega)|^2 + \rho_0 c_0 M|u_z(\boldsymbol{y}, \omega)|^2 + (1 + M^2)\text{Re}\left\{p(\boldsymbol{y}, \omega)u_z^*(\boldsymbol{y}, \omega)\right\}\right). \tag{8.2.35}$$

Thus, from equations (8.2.33) and (8.2.35), $W(z)$ can be expressed as

$$W(z) = \int_{\mathcal{A}} \frac{M}{2\rho_0 c_0}|p|^2 \; d^2\boldsymbol{y_s} + \int_{\mathcal{A}} \frac{1}{2}\rho_0 c_0 M|u_z|^2 \; d^2\boldsymbol{y_s} + \text{Re}\left\{\int_{\mathcal{A}} \frac{1}{2}(1+M^2)pu_z^* \; d^2\boldsymbol{y_s}\right\}, \tag{8.2.36}$$

where the coordinates $(\boldsymbol{y_s}, z, \omega)$ have been omitted for simplicity. The acoustic velocity in the z-direction, u_z can be derived from the acoustic velocity potential, i.e.

$$u_z(\boldsymbol{y}, \omega) = \frac{\partial \Phi}{\partial z}(\boldsymbol{y}, \omega). \tag{8.2.37}$$

The acoustic velocity potential in the duct has been discussed in section 8.1.1 for the inlet duct, where $M \leq 0$, but equations (8.1.22) and (8.1.24) are also applicable when $M > 0$. Thus, the velocity potential in the duct is given by

$$\Phi(\boldsymbol{y}, \omega) = \frac{\beta^2}{-j\rho_0 c_0 k} \sum_{(m,n)\in\mathcal{O}} \frac{A_{mn}}{1 - M\alpha_{mn}} \Psi_{mn}(\boldsymbol{y_s}) e^{-j\tilde{\alpha}_{mn} kz}. \tag{8.2.38}$$

Substituting (8.2.38) in (8.2.37) gives

$$u_z(\boldsymbol{y}, \omega) = \frac{1}{\rho_0 c_0} \sum_{(m,n)\in\mathcal{O}} \frac{\alpha_{mn} - M}{1 - M\alpha_{mn}} A_{mn} \Psi_{mn}(\boldsymbol{y_s}) e^{-j\tilde{\alpha}_{mn} kz}. \tag{8.2.39}$$

The general expression for p has been given in equation (7.3.1), which is reproduced below:

$$p(\boldsymbol{y}, \omega) = \sum_{(m,n)\in\mathcal{O}} A_{mn} \Psi_{mn}(\boldsymbol{y_s}) e^{-j\tilde{\alpha}_{mn} kz}. \tag{8.2.40}$$

Using the property (2.4.5) of the mode shape functions, it is straightforward to show from (8.2.39) and (8.2.40) that

$$\begin{aligned}
\int_{\mathcal{A}} |p_f(\boldsymbol{y_s}, z, \omega)|^2 \; d^2\boldsymbol{y_s} &= \sum_{(m,n)\in\mathcal{O}} |A_{mn}|^2 \mathcal{A} \\
\int_{\mathcal{A}} |u_z(\boldsymbol{y_s}, z, \omega)|^2 \; d^2\boldsymbol{y_s} &= \frac{1}{\rho_0 c_0} \sum_{(m,n)\in\mathcal{O}} \left(\frac{\alpha_{mn} - M}{1 - M\alpha_{mn}}\right)^2 |A_{mn}|^2 \mathcal{A} \\
\int_{\mathcal{A}} p(\boldsymbol{y_s}, z, \omega) u_z^*(\boldsymbol{y_s}, z, \omega) \; d^2\boldsymbol{y_s} &= \frac{1}{\rho_0 c_0} \sum_{(m,n)\in\mathcal{O}} \left(\frac{\alpha_{mn} - M}{1 - M\alpha_{mn}}\right) \mathcal{A}
\end{aligned} \tag{8.2.41}$$

Substituting (8.2.41) into (8.2.36) gives

$$W(z) = \frac{1}{2} \sum_{(m,n)\in\mathcal{O}} \frac{\mathcal{A}}{\rho_0 c_0} |A_{mn}|^2 \left[M + M\left(\frac{\alpha_{mn} - M}{1 - M\alpha_{mn}}\right) + (1+M^2)\left(\frac{\alpha_{mn} - M}{1 - M\alpha_{mn}}\right)\right].$$

After some algebra,

$$\boxed{W = \frac{\mathcal{A}}{2\rho_0 c_0} \sum_{(m,n)\in\mathcal{O}} \left(\frac{1-M^2}{1-\alpha_{mn}M}\right)^2 \alpha_{mn}|A_{mn}|^2}. \tag{8.2.42}$$

Equal power per mode model

Thus, the expected value of the modal power is

$$E\{W_{mn}\} = \frac{\mathcal{A}}{2\rho_0 c_0} \left(\frac{1-M^2}{1-\alpha_{mn}M}\right)^2 \alpha_{mn} E\{|A_{mn}|^2\}. \tag{8.2.43}$$

If the power is equally shared between all the propagating modes, the modal power is constant, say

$$W_{mn} = W_0,$$

and from equation (8.2.43)

$$\boxed{E\{|A_{mn}|^2\} = 2\rho_0 c_0 \frac{W_0}{\mathcal{A}} \left(\frac{1-\alpha_{mn}M}{1-M^2}\right)^2 \alpha_{mn}^{-1}.} \tag{8.2.44}$$

If $M = 0$, this expression is identical to the one found in the zero flow theory.

8.2.6 General expression of the modal amplitude

The modal amplitude distribution for the above models can be written in general form. From equations (8.2.26), (8.2.32) and (8.2.42),

$$\boxed{E\{|A_{mn}|^2\} = F_{\mu,\nu,\gamma}(\alpha_{mn}) = P^2_{\mu,\nu,\gamma} \left(\frac{M-\alpha_{mn}}{1-M^2}\right)^{2\mu} \left(\frac{1-\alpha_{mn}M}{1-M^2}\right)^{2\nu} \frac{1}{\alpha_{mn}^{\gamma}}}, \tag{8.2.45}$$

where the values taken by $P_{\mu,\nu,\gamma}$ and (μ,ν,γ) depend on the source model, as illustrated in table 8.1. Note that the expressions for $P_{\mu,\nu,\gamma}$ are identical to the ones found in the zero flow case (see table 3.2.4). Besides, the formula given in equation (8.2.45) differs slightly from previous results by Joseph *et al.* [15]. The above formula is more general and contains an additional parameter, γ, which allows to include to take into account the equal power per mode model.

	Monopole	Dipole	Equal Power
$P_{\mu,\nu,\gamma}$	$\rho_0 c_0 (\overline{Q_s^2}/2)^{1/2}$	$(\overline{F_s^2}/2)^{1/2}$	$(2\rho_0 c_0 W_0/\mathcal{A})^{1/2}$
(μ,ν,γ)	(0,1,2)	(1,0,2)	(0,1,1)

Table 8.1 – modal amplitudes for three model of sources in a semi-infinite cylindrical duct with flow

Figure 8.9 shows the variation of function $F_{\mu,\nu,\gamma}$ for the above source models, for M

varying between -0.9 and 0.9, and $\alpha_{m,n}$ varying between 0 and 1. The modal amplitude $F_{\mu,\nu,\gamma}$ follows the same trend for a uniform distribution of incoherent monopoles, and an equal power per mode model. The modal amplitude for a uniform distribution of axial dipoles is different. For this type of source, the modal amplitude goes to zero along the line $\alpha_{m,n} = M$ (for $M > 0$). This is consistent with the fact that dipole sources usually generate destructive interferences: in free field the sound field generated by a dipole is zero in the direction orthogonal to the dipole's direction. However, this phenomenon does not occur for negative values of the Mach number. This is due to the fact that we are studying the wave travelling from the source to the open end of the duct. Symmetrically, the modal amplitude distribution for the wave travelling between the source and the infinite side of the duct, would have zeros for negative Mach numbers.

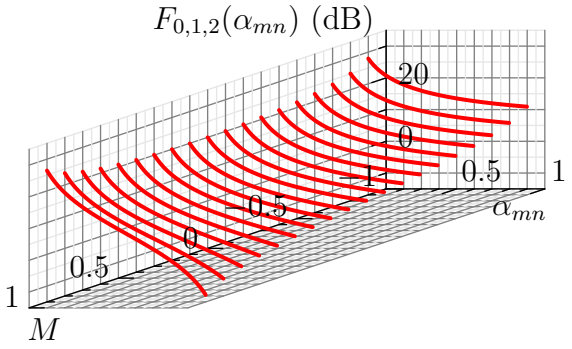

(a) Uniforms distribution of incoherent monopoles: (μ, ν, γ)=(0,1,2)

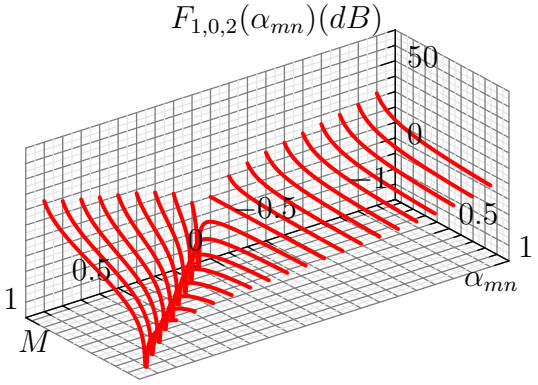

(b) Uniforms distribution of incoherent axial dipoles: (μ, ν, γ)=(1,0,2)

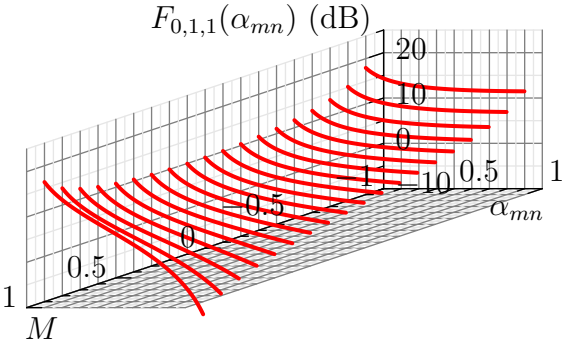

(c) Equal power per mode model: (μ, ν, γ)=(0,1,1)

Figure 8.9 – Logarithmic plots of the weighting model $F_{\mu,\nu,\gamma}$ as a function of cut-off ratio α_{mn} and Mach number M for various source models. The cut-off ratio varies between 0.1 and 1 and the Mach number between -0.9 and 0.9.

8.3 High frequency approximation for the multi-mode far field directivity

8.3.1 Introduction

The aim in this section is to derive a simple analytic formula for the multi-mode directivity function with flow for a general source distributions such as those presented in section 8.2. The proof relies in observing that the power radiated from the duct in a particular direction is approximately equal to that travelling along the duct in that same direction (neglecting the reflected wave). Since for a given source, the power travelling in the duct in any direction can be obtained easily, this allows the estimation of the far field power in an any direction. Moreover, the far field power radiated in a particular direction is related to the directivity of the pressure field through the radial intensity. Thus, these energy considerations give one method the estimate analytically the pressure directivity in the far field.

8.3.2 Far field intensity with flow

The time averaged intensity in the radial direction, denoted by I_R, is derived from equation (8.2.34), which gives

$$I_R(R,\phi,\theta,\omega) = \frac{1}{2} \times \mathrm{Re}\left\{ p_f u_{R,f}^* + \rho_0 c_0 M u_{z,f} u_{R,f}^* + \frac{M\cos\theta}{\rho_0 c_0} p_f p_f^* + M^2 \cos\theta p u_{z,f}^* \right\}, \quad (8.3.1)$$

where the coordinates (R,ϕ,θ,ω) have been omitted on the right hand side for simplicity. The velocities $u_{R,f}$ and $u_{z,f}$ can be derived from the velocity potential, which can be expressed in terms of the acoustic pressure.

Expression of the velocity potential as a function of pressure

Equation (8.1.20) gives the relation between pressure and velocity potential. It has been derived for an inlet duct but is equally valid in the case of an exhaust duct. In addition, the relation is identical for all cut-on modes so p_f can be substituted for $p_{mn,f}$. Thus, for positive and negative Mach numbers,

$$p_f(R,\phi,\theta,\omega) = -j\rho_0 c_0 k \frac{S(\theta)}{\sqrt{1-M^2\sin^2\theta}} \Phi_f(R,\phi,\theta,\omega),$$

or equivalently,

$$\Phi_f(R,\phi,\theta,\omega) = \frac{1}{-j\rho_0 c_0 k} \frac{Y(\theta)}{S(\theta)} p_f(R,\phi,\theta,\omega), \quad (8.3.2)$$

where $Y(\theta) = \sqrt{1-M^2\sin\theta}$.

Derivation of $u_{R,f}$ and $u_{z,f}$

The velocities $u_{R,f}$ and $u_{z,f}$ can be derived from the velocity potential. By definition of Φ_{mn},

$$u_{R,f} = \frac{\partial \Phi_{mn}}{\partial R}, \tag{8.3.3}$$

$$u_{\theta} = \frac{1}{R}\frac{\partial \Phi_{mn}}{\partial \theta}. \tag{8.3.4}$$

In addition,

$$u_{z,f} = u_{R,f}\cos\theta - u_{\theta}\sin\theta. \tag{8.3.5}$$

Combining equations (8.3.3), (8.3.4), and (8.3.5) with equation (8.3.2) gives

$$u_{R,f} = \frac{Y(\theta)}{\rho_0 c_0} p \tag{8.3.6}$$

$$u_{z,f} = \left(\frac{Y(\theta)}{\rho_0 c_0}\cos\theta - \frac{M\sin^2\theta}{\rho_0 c_0}\right) p_f \tag{8.3.7}$$

Note that only the first order terms have been retained in these two equations and that the following properties of p_f have been used

$$\frac{\partial p_f}{\partial R} = -jkS(\theta)p_f + O(1/R);$$
$$\frac{1}{R}\frac{\partial p_f}{\partial \theta} = -jkS'(\theta)p_f + O(1/R).$$

Far field intensity

Substituting equations (8.3.6) and (8.3.7) into (8.3.1) gives

$$I_R(R,\phi,\theta,\omega) = \frac{|p_f|^2}{2\rho_0 c_0} \times \left[Y + (MY\cos\theta - M^2\sin^2\theta)Y + M\cos\theta + M^2\cos\theta(Y\cos\theta - M\sin^2\theta)\right]$$

This expression can be simplified by substituting $1 - Y^2$ for the $M^2\sin^2\theta$ terms, and by gathering the remaining $M\cos\theta$ terms. After some algebra,

$$I_R(R,\phi,\theta,\omega) = \frac{|p_f|^2}{2\rho_0 c_0}\left[Y(\theta)(Y(\theta) + M\cos\theta)^2\right] = \frac{|p_f|^2}{2\rho_0 c_0}F(\theta). \tag{8.3.8}$$

Multiplying $F(\theta)$ by $(Y(\theta) - M\cos\theta)^2$,

$$(Y(\theta) - M\cos\theta)^2 F(\theta) = Y(\theta)(Y^2(\theta) - M^2\cos^2\theta)^2 = Y(\theta)(1 - M^2)^2 = \beta^4 Y(\theta),$$

so that

$$F(\theta) = \frac{\beta^4}{(Y(\theta) - M\cos\theta)^2} Y(\theta), \tag{8.3.9}$$

or

$$\boxed{F(\theta) = \frac{\sqrt{1 - M^2 \sin^2\theta}}{S(\theta)^2}.} \tag{8.3.10}$$

Substituting equation (8.3.9) into (8.3.8) gives

$$\boxed{I_R(R, \phi, \theta, \omega) = \frac{|p_f|^2}{2\rho_0 c_0} F(\theta).} \tag{8.3.11}$$

Thus, I_R is equal to the mean intensity of a plane wave multiplied by a directivity function $F(\theta)$, which is plotted in figure 8.10. The figure shows that, if $M > 0$, the intensity is maximum along the axis of the duct, that is for $\theta = 0$, and it tends to zero for $\theta = \pi$. In particular, if the Mach number tends to 1, the intensity travelling upstream tends to 0. Similarly, if $M < 0$, the intensity is maximum for $\theta = \pi$ and tends to zero for $\theta = 0$. If the Mach number tends to -1, the intensity travelling upstream tends to 0. As could be expected, if the mean flow is significantly large in comparison with the speed of sound, it prevents the radiation of sound in the upstream direction.

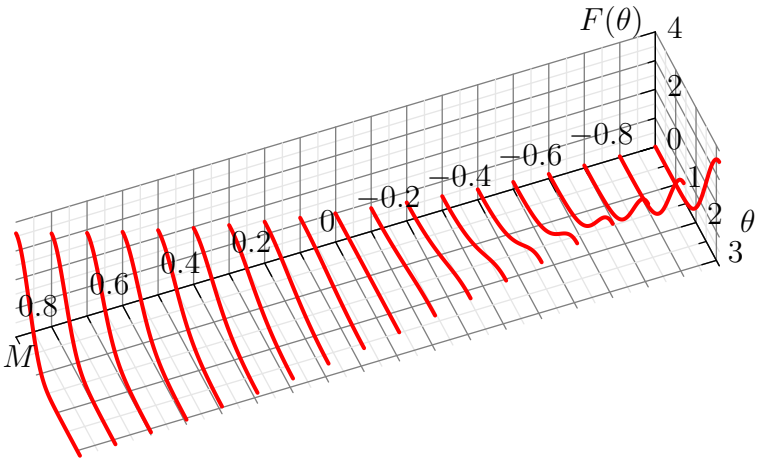

Figure 8.10 – $F(\theta)$ as a function of θ and M, for θ between 0 and π and M between -0.9 and 0.9.

8.3.3 Far field power with flow radiated in direction θ

Consider the surface $\mathcal{S}$ defined, in the spherical coordinate system (R', ϕ', θ') by

$$\begin{cases} R' = R, \\ 0 \leq \phi' \leq 2\pi, \\ \theta \leq \theta' \leq \theta + d\theta. \end{cases}$$

By definition of the time average acoustic intensity, the mean power radiated to the far field through surface $\mathcal{S}$, denoted by $E\{dW_f(\theta)\}$, is given by

$$dW_f(\theta) = \int_{\mathcal{S}} I_R(R, \phi, \theta', \omega)\ d^2\boldsymbol{y_s},$$
$$dW_f(\theta) = \int_0^{2\pi} \int_{\theta}^{\theta+d\theta} I_R(R, \phi, \theta, \omega) R^2 \sin\theta'\ \mathrm{d}\theta'\,\mathrm{d}\phi'.$$

From equation (8.3.11),

$$dW_f(\theta) = \frac{\pi R^2}{\rho_0 c_0} |p_f|^2 F(\theta) \sin\theta d\theta. \tag{8.3.12}$$

Taking the expected value of the above equation,

$$\boxed{E\{dW_f(\theta)\} = \frac{\pi R^2}{\rho_0 c_0} E\{|p_f|^2\} F(\theta) \sin\theta d\theta.} \tag{8.3.13}$$

8.3.4 Relation between far field power and in-duct power

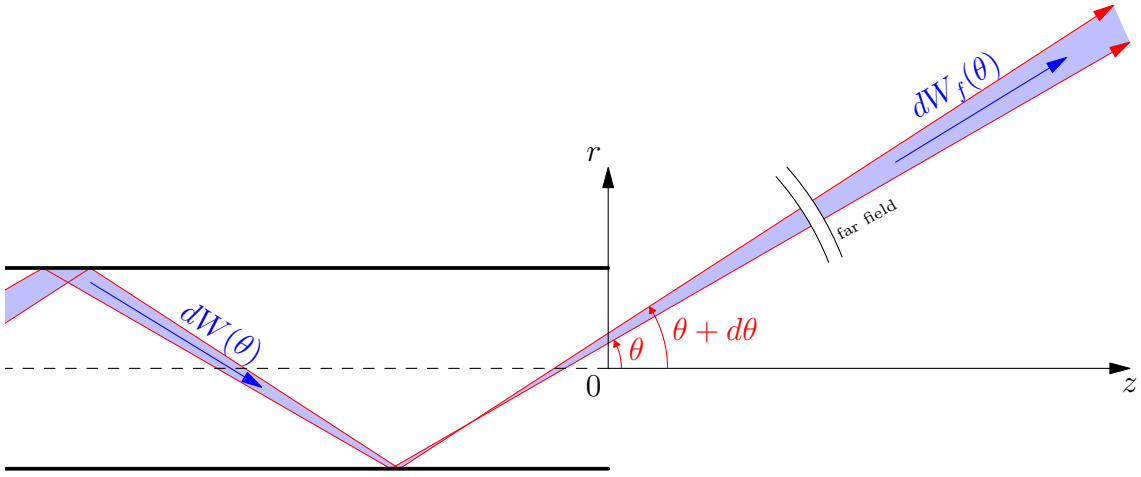

Figure 8.11 – Relation between power transmitted along the duct between angles θ and $\theta + d\theta$, denoted by $dW(\theta)$, and power radiated to the far field between angles θ and $\theta + d\theta$, denoted by $dW_f(\theta)$. If the open-end of the duct is acoustically transparent, $dW(\theta) = dW_f(\theta)$.

Consider the sound power $dW_f(\theta)$ radiated to the far field between angles θ and $\theta + d\theta$. Interpreting the acoustic waves in terms of rays, $dW_f(\theta)$ is given by the sum of the powers carried along by the rays travelling between angles θ and $\theta + d\theta$. Assuming that no energy is lost at the open-end of the duct, the power transported by one ray into the far field is equal to the power transported by that same ray inside the duct. This is illustrated in figure 8.11. Thus, $dW_f(\theta)$ is equal to the power transported inside the duct by rays travelling

between angles θ and $\theta + d\theta$, which is denoted by $dW(\theta)$, i.e

$$\boxed{dW_f(\theta) = dW(\theta)} \tag{8.3.14}$$

8.3.5 In duct power transmitted in direction θ

Interpreting the modes in terms of rays, the in-duct power transmitted along the duct between θ and $\theta + d\theta$ is the sum of the modal power transmitted by each mode travelling in a direction contained between θ and $\theta + d\theta$. From figure 8.4, the direction of propagation of mode (m, n) with flow is given by

$$\cos\theta_{mn} = \frac{\alpha_{mn}\beta}{\sqrt{1 - \alpha_{mn}^2 M^2}},$$

therefore

$$dW(\theta) = \sum_{(m,n)\in\mathcal{O}_\theta} W_{mn}, \tag{8.3.15}$$

where

$$\mathcal{O}_\theta = \{(m, n) \in \mathcal{O} \text{ such that } \theta \leq \theta_{mn} \leq \theta + d\theta\}. \tag{8.3.16}$$

Combining equations (8.2.43) and (8.2.45), the expected value of the modal power for the idealized source distributions studied previously can be expressed as,

$$\boxed{E\{W_{mn}\} = \frac{\mathcal{A}}{2\rho_0 c_0} L_{\mu,\nu,\gamma}(\alpha_{mn}),} \tag{8.3.17}$$

where

$$\boxed{L_{\mu,\nu,\gamma}(\alpha_{mn}) = P^2_{\mu,\nu,\gamma}(1 - M^2)^{2(1-\mu-\nu)}(M - \alpha_{mn})^{2\mu}(1 - \alpha_{mn}M)^{2(\nu-1)}\alpha_{mn}^{1-\gamma}.} \tag{8.3.18}$$

The function $L_{\mu,\nu,\gamma}$ is plotted in figure 8.12 for a distribution of incoherent monopoles and a distribution of incoherent axial dipoles. The case of an equal power per mode distribution has not been plotted since, in that case, $L_{\mu,\nu,\gamma}$ is constant. Thus, by definition of $dW(\theta)$ and $\mathcal{O}_\theta$,

$$\boxed{E\{dW(\theta)\} = \frac{\mathcal{A}}{2\rho_0 c_0} \sum_{(m,n)\in\mathcal{O}_\theta} L_{\mu,\nu,\gamma}(\alpha_{mn})}, \tag{8.3.19}$$

For all $(m, n) \in \mathcal{O}_\theta$, $\theta_{mn} \approx \theta$ because $d\theta \ll \theta$, therefore

$$\alpha_{mn} = \frac{\cos\theta_{mn}}{\sqrt{1 - M^2\sin^2\theta_{mn}}} \approx \frac{\cos\theta}{\sqrt{1 - M^2\sin^2\theta}} = \alpha(\theta). \tag{8.3.20}$$

Substituting this result into equation (8.3.19), the in-duct power travelling in direction θ

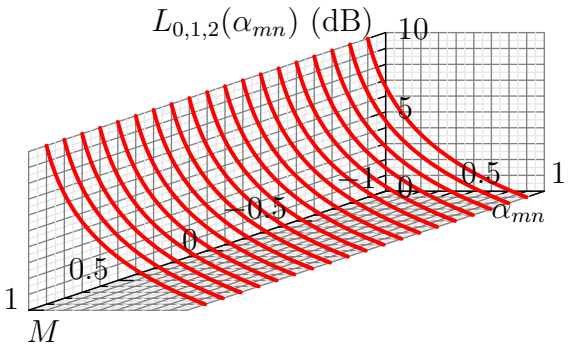

(a) Uniform distribution of incoherent monopoles, (μ, ν, γ)=(0,1,2).

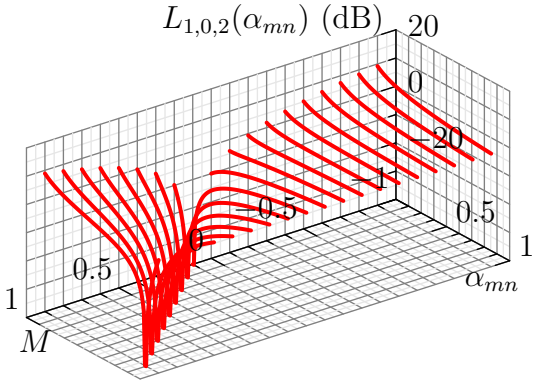

(b) Uniform distribution of incoherent dipoles, (μ, ν, γ)=(1,0,2).

Figure 8.12 – Modal power function $L_{\mu,\nu,\gamma}$ plotted as a function of Mach number M and cut-off ratio α_{mn}. The cut-off ratio varies between 0 and 1 and the Mach number between -0.9 and 0.9.

can be expressed as

$$E\{dW(\theta)\} = \frac{\mathcal{A}}{2\rho_0 c_0} \sum_{(m,n)\in\mathcal{O}_\theta} G_{\mu,\nu,\gamma}(\theta), \tag{8.3.21}$$

where

$$G_{\mu,\nu,\gamma}(\theta) = L_{\mu,\nu,\gamma}(\alpha(\theta)). \tag{8.3.22}$$

Thus,

$$E\{dW(\theta)\} = \frac{\mathcal{A}}{2\rho_0 c_0} \text{Card}\Big(\mathcal{O}_\theta\Big) G_{\mu,\nu,\gamma}(\theta), \tag{8.3.23}$$

where $\text{Card}\Big(\mathcal{O}_\theta\Big)$ is the number of modes in $\mathcal{O}_\theta$.

Derivation of $\mathcal{O}_\theta$. To estimate $\text{Card}\Big(\mathcal{O}_\theta\Big)$, we introduce the function $N(\theta)$ defined as the number of modes (m, n) such that $\theta_{mn} \leq \theta$, i.e.

$$N(\theta) = \text{Card}\Big(\{(m,n) \in \mathcal{O} \quad \text{such that} \quad \theta_{mn} \leq \theta\} \Big) \tag{8.3.24}$$

By definition of $N(\theta)$,

$$\text{Card}\Big(\mathcal{O}_\theta\Big) = N(\theta + d\theta) - N(\theta). \tag{8.3.25}$$

Since $d\theta \ll \theta$, the above expression can be expressed in terms of the derivative of $N(\theta)$, denoted by $N'(\theta)$,

$$\text{Card}\Big(\mathcal{O}_\theta\Big) = N'(\theta)d\theta \tag{8.3.26}$$

In the above expression, $N'(\theta)$ can be interpreted as a modal density.

The function $N(\theta)$ can be estimated as follows. First observe that

$$0 \leq \theta_{mn} \leq \theta \leq \frac{\pi}{2} \quad \Leftrightarrow \quad k\sin\theta_{mn} \leq k\sin\theta. \tag{8.3.27}$$

From figure 7.3,

$$\begin{cases} k\sin\theta_{mn} = \dfrac{\kappa_{mn}}{\sqrt{1-M^2\alpha_{mn}}}, \\ k\sin\theta = \dfrac{\kappa(\theta)}{\sqrt{1-M^2\alpha(\theta)}}, \end{cases} \tag{8.3.28}$$

where $\kappa(\theta)$ is defined by

$$\kappa(\theta) = k\sin\theta\sqrt{1-M^2\alpha(\theta)}. \tag{8.3.29}$$

Substituting the expression for $\alpha(\theta)$, given in equation (8.3.20), $\kappa(\theta)$ can be expressed as

$$\kappa(\theta) = \frac{\beta k\sin(\theta)}{\sqrt{1-M^2\sin^2\theta}}. \tag{8.3.30}$$

For $0 \leq \theta \leq \pi/2$, the cosine and sine functions are respectively decreasing and increasing, therefore it is straightforward to show that $\alpha(\theta)$ is decreasing with θ. Thus,

$$0 \leq \theta_{mn} \leq \theta \leq \frac{\pi}{2} \quad \Leftrightarrow \quad \alpha_{mn} \geq \alpha(\theta) \quad \Leftrightarrow \quad \sqrt{1-M^2\alpha_{mn}^2} \leq \sqrt{1-M^2\alpha^2(\theta)}. \tag{8.3.31}$$

Combining equations (8.3.27) and (8.3.31),

$$0 \leq \theta_{mn} \leq \theta \leq \frac{\pi}{2} \quad \Leftrightarrow \quad \kappa_{mn} \leq \kappa(\theta). \tag{8.3.32}$$

Then, let $M(\kappa)$ denote the number of cut-on modes (m,n) such that $\kappa_{mn} \leq \kappa$, i.e

$$M(\kappa) = \text{Card}\Big(\ \{(m,n) \in \mathcal{O} \quad \text{such that} \quad \kappa_{mn} \leq \kappa\}\ \Big). \tag{8.3.33}$$

Equation (8.3.32) shows that

$$N(\theta) = M(\kappa(\theta)). \tag{8.3.34}$$

Good analytical approximations for $M(\kappa)$ have been derived. For example, following Roe [19] and Rice [16],

$$M(\kappa) = \frac{(\kappa a)^2}{4} + \frac{\kappa a}{2} \approx \frac{(\kappa a)^2}{4} \tag{8.3.35}$$

if the second order term is neglected, which is a good approximation when $\kappa a \gg 1$ (well cut-on modes). Combining equations (8.3.33), (8.3.34) and (8.3.35), $N(\theta)$ can be

expressed as

$$N(\theta) = \frac{(ka)^2}{4}\beta^2 \frac{\sin^2\theta}{1 - M^2\sin^2\theta}. \tag{8.3.36}$$

Differentiating the above expression gives

$$N'(\theta) = \frac{(ka)^2}{2} \frac{\sin\theta\cos\theta}{(1 - M^2\sin^2\theta)^2}. \tag{8.3.37}$$

Thus, substituting equation (8.3.37) into equation (8.3.26), the number of cut-on modes which radiate between angle θ and $\theta + d\theta$ is given by

$$\text{Card}\Big(\mathcal{O}_\theta\Big) = \frac{(ka)^2}{2} \frac{\sin\theta\cos\theta}{(1 - M^2\sin^2\theta)^2 d\theta}. \tag{8.3.38}$$

In duct power in direction θ. The in-duct power transmitted between propagation angles θ and $\theta + d\theta$ is obtained by combining equations (8.3.38) and (8.3.23), i.e.

$$\boxed{E\big\{dW(\theta)\big\} = \frac{(ka)^2\mathcal{A}}{4\rho_0 c_0} \frac{\sin\theta\cos\theta}{(1 - M^2\sin^2\theta)^2} G_{\mu,\nu,\gamma}(\theta) d\theta.} \tag{8.3.39}$$

8.3.6 Multi-Mode far field directivity

Substituting the in-duct power, from equation (8.3.39), and the far field power, given by equation (8.3.13), into equation (8.3.14), gives

$$\frac{\pi R^2}{\rho_0 c_0} E\big\{|p_f|^2\big\} F(\theta)\sin\theta d\theta = \frac{(ka)^2\mathcal{A}}{4\rho_0 c_0} \frac{\sin\theta\cos\theta}{(1 - M^2\sin^2\theta)^2} G_{\mu,\nu,\gamma}(\theta) d\theta. \tag{8.3.40}$$

Solving the above equation for $E\big\{|p_f|^2\big\}$, and substituting $\mathcal{A}$ by πa^2 gives

$$\boxed{E\big\{|p_f(R,\phi,\theta)|^2\big\} = \Big(\frac{a}{R}\Big)^2 \frac{(ka)^2}{4} G_{\mu,\nu,\gamma}(\theta) T(\theta)}, \tag{8.3.41}$$

where

$$\boxed{\begin{aligned} G_{\mu,\nu,\gamma}(\theta) &= P^2_{\mu,\nu,\gamma}(1 - M^2)^{2(1-\mu-\nu)}(M - \alpha(\theta))^{2\mu}(1 - \alpha(\theta)M)^{2(\nu-1)}\alpha(\theta)^{1-\gamma}, \\ T(\theta) &= \frac{\cos\theta}{F(\theta)(1 - M^2\sin^2\theta)} = \frac{S(\theta)^2\cos\theta}{(1 - M^2\sin^2\theta)^{5/2}}. \end{aligned}} \tag{8.3.42}$$

Equation (8.3.42) is the main result of this dissertation. The expressions of $G_{\mu,\nu,\gamma}$ for a uniform distribution of incoherent monopoles (a), a uniform distribution of incoherent

axial dipoles (b), or an equal power per mode model (c), are given below:

$$\begin{aligned}
&\text{(a)} \quad G_{0,1,2} = \rho_0 c_0 \frac{\overline{Q_s^2}}{2} \frac{1}{\alpha(\theta)}, \\
&\text{(b)} \quad G_{1,0,2} = \frac{\overline{F_s^2}}{2} \left(\frac{M - \alpha(\theta)}{1 - \alpha(\theta) M} \right)^2 \frac{1}{\alpha(\theta)}, \\
&\text{(a)} \quad G_{0,1,1} = 2\rho_0 c_0 \frac{W_0}{\mathcal{A}}.
\end{aligned}$$

An immediate consequence of equation (b) is that the far field pressure goes to zero for a uniform distribution of incoherent axial dipoles when

$$\alpha(\theta) = M$$

Substituting equation (8.3.20) into the above relation and solving for θ yields the angle for which the pressure field goes to zero, denoted by θ_0,

$$\theta_0 = \cos^{-1} \left(\frac{M}{\sqrt{1 + M^2}} \right). \tag{8.3.43}$$

Equation (8.3.41) gives the far field directivity of mean square pressure in the high fre-

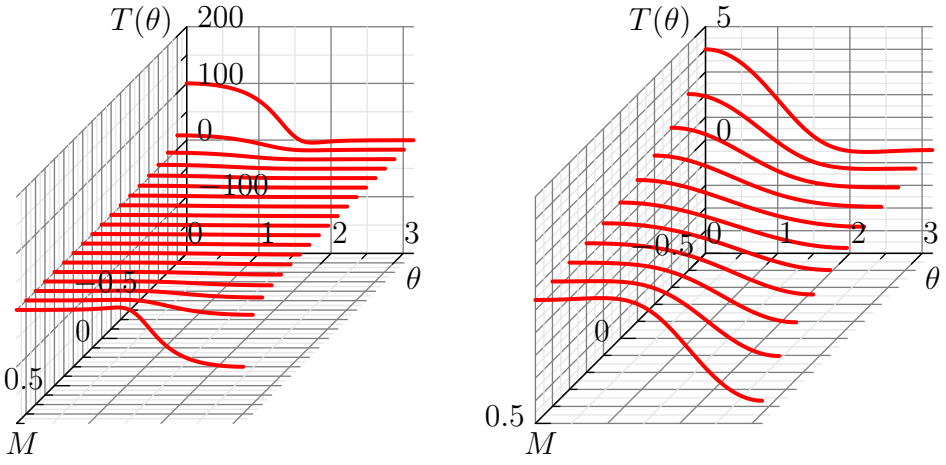

(a) Full plot, M varies between -0.9 and 0.9

(b) Zoomed plot, M varies between -0.5 and 0.5

Figure 8.13 – Function T plotted as a function of θ and M. T represents a directivity factor in the multi-mode broadband directivity factor.

quency limit. It is a product of two functions: the first, $G_{\mu,\nu,\gamma}$ describes the directivity of a particular source distribution; the second T, represents a directivity factor which depends on the Mach number only. These functions are plotted respectively in figure 8.14 and 8.13.

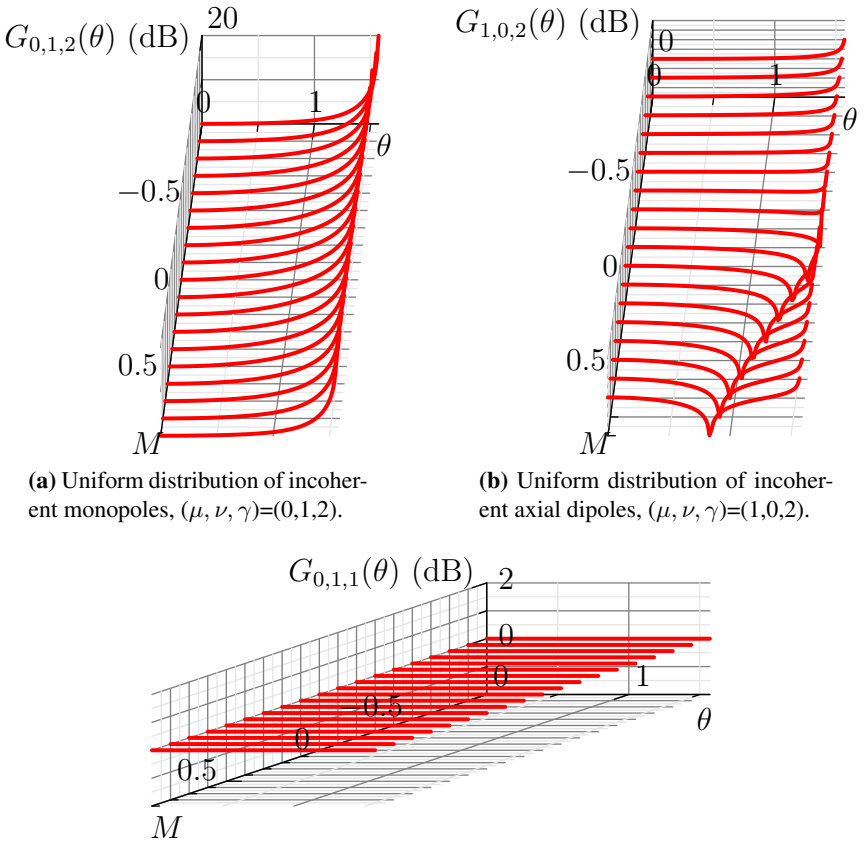

(a) Uniform distribution of incoherent monopoles, (μ, ν, γ)=(0,1,2).

(b) Uniform distribution of incoherent axial dipoles, (μ, ν, γ)=(1,0,2).

(c) Equal power per mode model, (μ, ν, γ)=(0,1,1).

Figure 8.14 – Function $G_{\mu,\nu,\gamma}$ plotted as a function of θ and M. It represents the weighting coeficient for modes whose cut-off ratio is close to $\alpha(\theta)$.

8.4 Directivity factor

The non-dimensional directivity factor can be defined as

$$Q(ka,\theta) = \frac{2\pi R^2}{\rho_0 c_0 E\{W\}} E\{|p_f(R,\phi,\theta,\omega)|^2\}. \tag{8.4.1}$$

Note that for a spherical source, $Q(ka,\theta) = 1$. The terms $E\{p_f^2(R,\phi,\theta,\omega)\}$ and $E\{W\}$ can be computed by using a discrete modal summation or by applying a continuous analytic formula.

8.4.1 Modal expression of the directivity factor with flow

The modal expression for $E\{p_f^2(R,\phi,\theta,\omega)\}$ is obtained from equations (8.0.1) and (8.2.45),

$$E\{p_f^2(R,\phi,\theta,\omega)\} = \left(\frac{a}{R}\right)^2 \sum_{(m,n)\in\mathcal{O}} |H_{mn}(ka,\theta)|^2 F_{\mu,\nu,\gamma}(\alpha_{mn}), \tag{8.4.2}$$

The expected value of the source power, $E\{W\}$, can be expressed by summing the modal powers, given by equation equation (8.3.17), over all the cut-on modes:

$$E\{W\} = \frac{\pi a^2}{2\rho_0 c_0} \sum_{(m,n)\in\mathcal{O}} L_{\mu,\nu,\gamma}(\alpha_{mn}). \tag{8.4.3}$$

The directivity factor is then obtained by substituting equations (8.4.2) and (8.4.3) into equation (8.4.1).

$$\boxed{Q(ka,\theta) = \frac{4\sum_{(m,n)\in\mathcal{O}} |H_{mn}(ka,\theta)|^2 F_{\mu,\nu,\gamma}(\alpha_{mn})}{\sum_{(m,n)\in\mathcal{O}} L_{\mu,\nu,\gamma}(\alpha_{mn})}.} \tag{8.4.4}$$

8.4.2 Analytic estimation of the directivity factor with flow in the high frequency limit

Alternatively, when studying the forward arc ($\theta \leq \pi/2$), the directivity factor can be estimated directly by using the analytical expressions derived in in this chapter. Thus, the mean square pressure can be expressed from equation (8.3.41) as

$$E\{|p_f(R,\phi,\theta)|^2\} = \left(\frac{a}{R}\right)^2 \frac{(ka)^2}{4} G_{\mu,\nu,\gamma}(\theta) T(\theta). \tag{8.4.5}$$

The expected value of the source power can be obtained by integrating the elementary contributions $E\{dW(\theta)\}$ between 0 and $\pi/2$. Thus, from equation (8.3.39),

$$E\{W\} = \int_0^{\pi/2} E\{dW(\theta)\} = \frac{\pi a^2}{\rho_0 c_0} \frac{(ka)^2}{4} \int_0^{\pi/2} (G_{\mu,\nu,\gamma}(\theta)\sin\theta\cos\theta)/[(1-M^2\sin^2\theta)^2]\ d\theta. \tag{8.4.6}$$

Substituting equations (8.4.5) and (8.4.6) into equation (8.4.1) gives

$$\boxed{Q(ka,\theta) = \frac{2G_{\mu,\nu,\gamma}(\theta)T(\theta)}{\int_0^{\pi/2} (G_{\mu,\nu,\gamma}(\theta)\sin\theta\cos\theta)/[(1-M^2\sin^2\theta)^2]\ d\theta}.}. \tag{8.4.7}$$

Chapter 9

Validation

The model is validated by using the same arguments as those presented for the zero flow theory. For a given value of the Mach number, we study

- the variation of the modal transmission coefficients as a function of frequency,
- the angle above which the accuracy of the analytic model deteriorates.

9.1 Variation with frequency

Figures 9.1a and 9.1b represent the modal transmission coefficient as a function of cut-off ratio for all cut-on modes for $ka = 20$ and $ka = 50$. The former assumes $M = -0.3$, and the latter $M = 0.6$. Both figures show that the modal transmission coefficient tend to converge towards 1 as frequency increases. This is similar to that observed in the zero flow case. We plot the percentage of modes such that $\tau_{mn} \leq 0.8$ as a function of frequency, for $M - -0.3$ (figure 9.2a) and $M = 0.6$ (figure 9.2b). This percentage clearly converges towards 0.

9.2 Maximum angle of validity

Using the same arguments as the one presented in the zero flow theory, we can estimate the angle above which the model's accuracy starts to deteriorates. Note however that the underlying simplified shape of the transmission coefficient which is assumed is less applicable when flow is present (compare figures 4.3 and 9.1b).

ka	20	50
α_c	0.2	0.1
θ_c	80°	85°

(a) M=-0.3

ka	20	50
α_c	0.2	0.15
θ_c	80°	85°

(b) M=0.6

Table 9.1 – Angle θ_c above which the accuracy of the model deteriorates for different values of the Mach number.

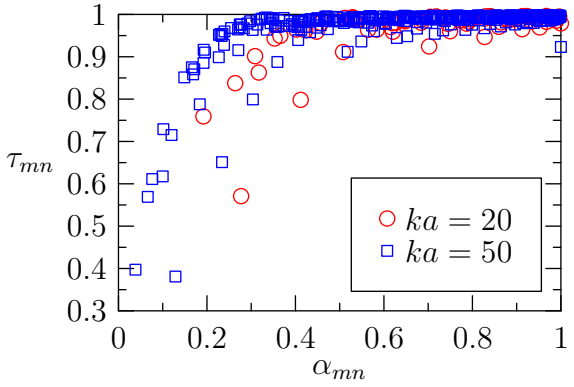

(a) M=-0.3

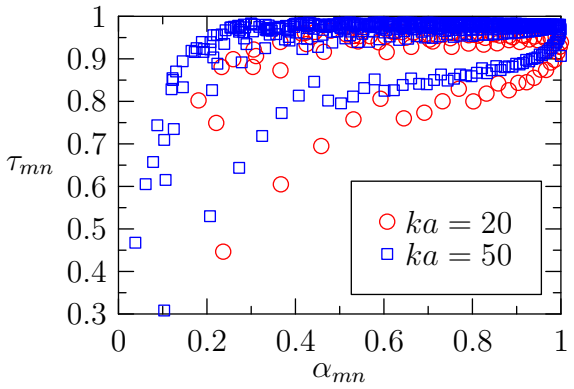

(b) M=-0.6

Figure 9.1 – Variation of the transmission coefficients as a function of cut-off ratio for $ka = 20$ and $ka = 50$. The Mach number is constant

9.3 Sound power variation with Mach number

To validate the analytic formula for the in-duct power, given in equation (8.4.6), we plot the variation of the in-duct power with flow normalized by the zero flow in-duct power, denoted by $W_M/W_{M=0}$, with Mach number, for the three model of idealized sources. The results from this thesis are compared to the analytic solution obtained by Joseph *et. al* [15], which are reproduced below:

$$\text{Monopole} \qquad \frac{W_M}{W_{M=0}} = \frac{1}{1-M^2} \tag{9.3.1}$$

$$\text{Dipole} \qquad \frac{W_M}{W_{M=0}} = -\frac{M^4 + M^3 - M^2 - 2M - 2(1-M^2)\log(1-M)}{3M^3(1-M^2)} \tag{9.3.2}$$

$$\text{Equal Power} \qquad \frac{W_M}{W_{M=0}} = \frac{1}{1-M^2} \tag{9.3.3}$$

Note however, that the equation for the dipole distribution has been modified in comparison to the one presented in the original paper: M has been changed to $-M$. This is due to an error in the paper. In figure 9.3, the circles, squares and crosses represent respectively the convective amplification, obtained from equation (8.4.6), for a uniform distribution of

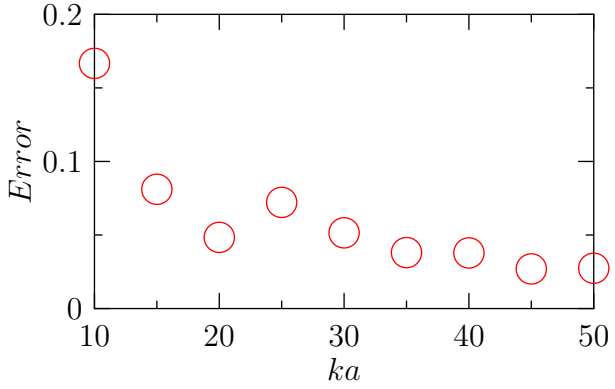

(a) M = -0.3

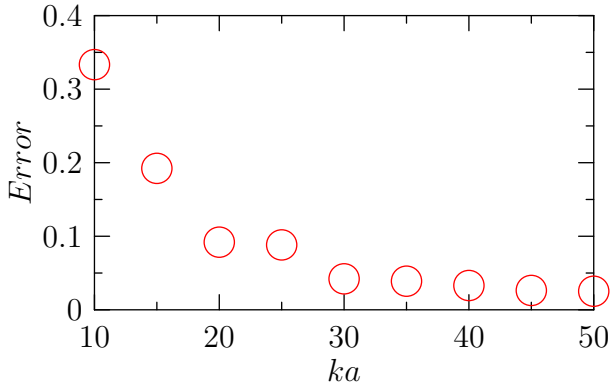

(b) M = 0.6

Figure 9.2 – Percentage of modes such that $\tau_{mn} < 0.8$.

monopoles, a uniform distribution of axial dipoles, and an equal power per mode model. These results fit perfectly the results obtained from the above analytic formulae by Joseph *et al.*. This validates our integral expression of the in-duct power.

The figure shows that, for a distribution of incoherent monopoles or an equal power per mode model, the presence of flow generates the same amplification of the sound power due to convection, which increases with Mach number. The case of an incoherent distribution of axial dipoles is more complex. There is a range of values of the Mach number, between $M = 0$ and $M = 0.6$, in which the flow decreases the sound power in comparison with the zero flow case. This decrease in sound power is maximum for about $M = 0.4$.

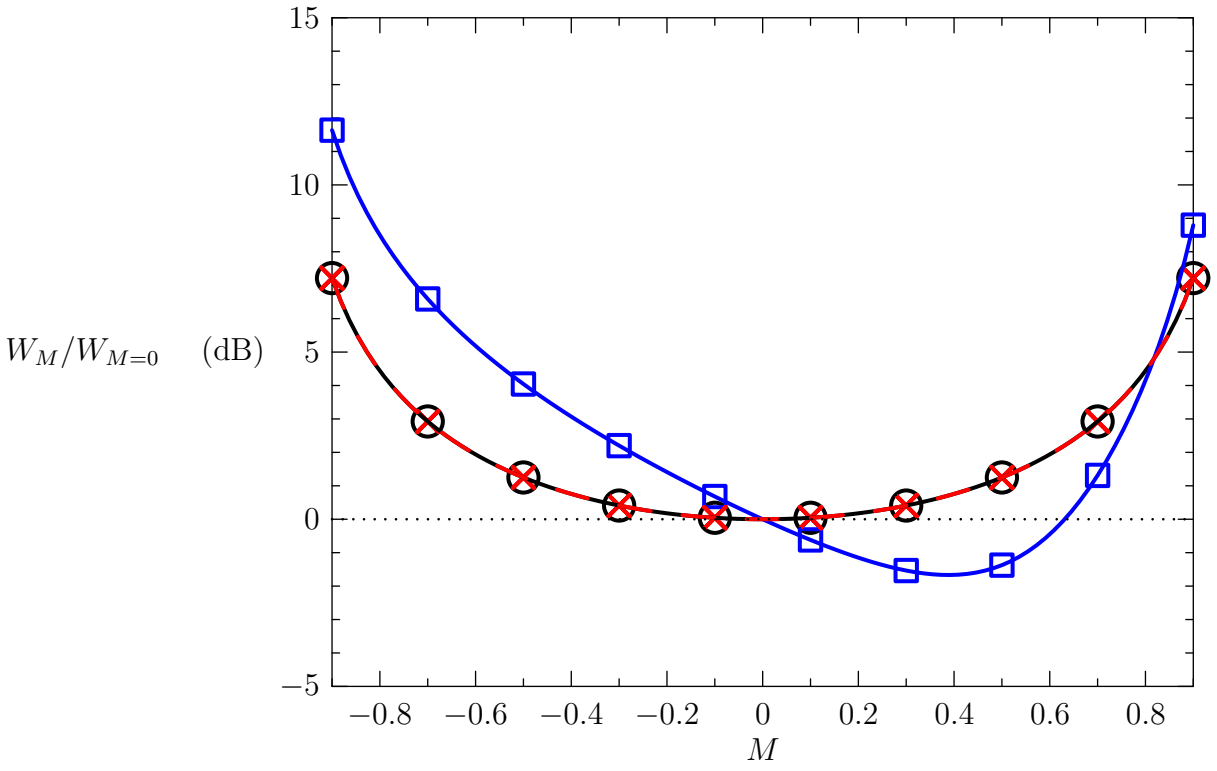

Figure 9.3 – In duct power with flow normalized by the zero flow in-duct power, as a function of Mach number, for the source distributions of incoherent distribution of monopoles, incoherent distribution of axial dipoles, and equal power per mode.

Chapter 10

Results

The directivity factor corresponding to the multi-mode directivity with flow, is plotted for $ka = 50$ and M between -0.9 and 0.9, for a uniform distribution of incoherent monopoles (figures 10.1 and 10.2), a uniform distribution of axial dipoles (figures 10.3 and 10.4), and an equal power per model model (figures 10.5 and 10.6). For each source distribution, the results are presented in the first page for negative Mach numbers, and on the second page for positive Mach numbers. Each sub-figure shows a polar plot of the directivity factor for a particular source distribution and a given Mach number. The thick black line represents the exact result, obtained from the Wiener-Hopf Technique formulation of Gabard and Astley[14], the red triangles represent the directivity obtained by applying the Lorentz Transformation to the flanged duct solution for zero flow, and the blue circles represent the directivity factor obtained by using the analytic formula derived in this thesis (equation (8.4.7)).

The agreement between the exact multi-mode directivity with flow, the approximate flanged duct directivity, and the high frequency analytic formula, is shown to be excellent for the three source distributions over the full range of subsonic Mach numbers. The flanged duct and analytic formulation give exact predictions up to more than 80°, as predicted in the previous chapter. It is interesting to see that the analytic formula is able to describe the correct variation of the multi-mode directivity for the three different source distributions, despite the fact that the corresponding behaviour of the directivity factor is very different. In particular, the complex behaviour resulting from the presence of interference in the case of a uniform distributions of incoherent axial dipoles is well predicted.

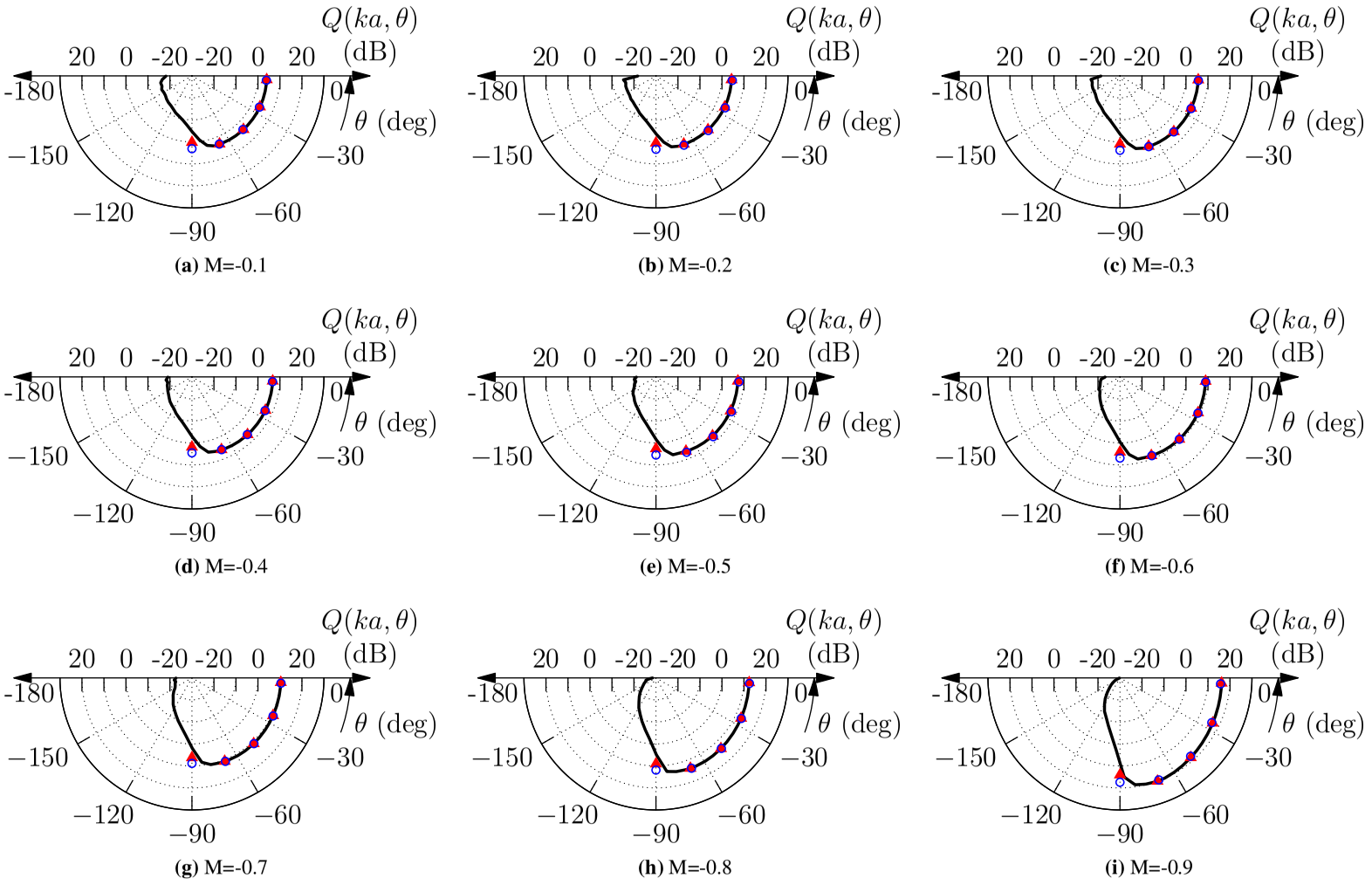

(a) M=-0.1 **(b)** M=-0.2 **(c)** M=-0.3

(d) M=-0.4 **(e)** M=-0.5 **(f)** M=-0.6

(g) M=-0.7 **(h)** M=-0.8 **(i)** M=-0.9

Figure 10.1 – $M < 0$, Uniform distribution of incoherent monopoles

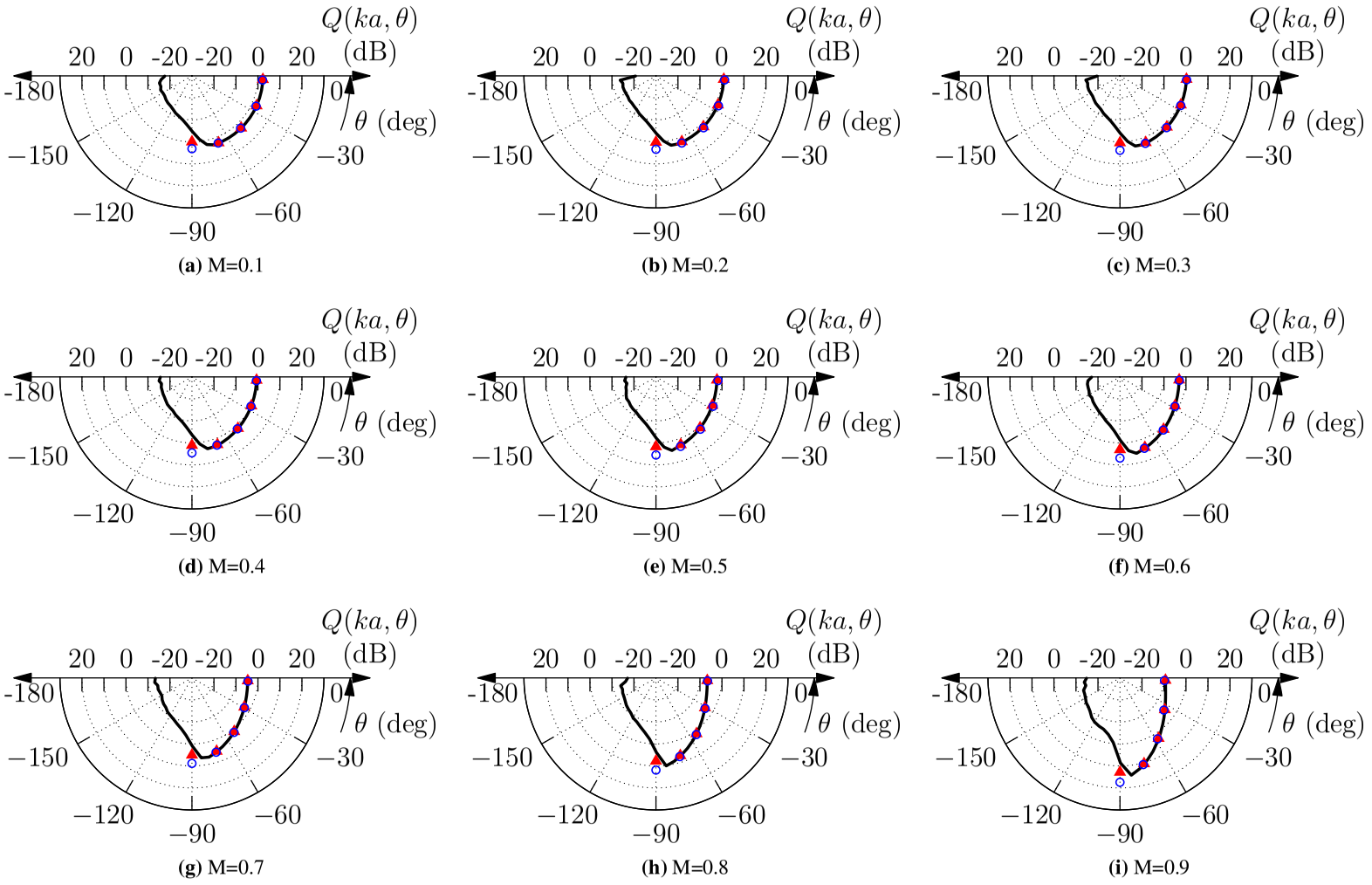

(a) M=0.1 **(b)** M=0.2 **(c)** M=0.3

(d) M=0.4 **(e)** M=0.5 **(f)** M=0.6

(g) M=0.7 **(h)** M=0.8 **(i)** M=0.9

Figure 10.2 – $M > 0$, Uniform distribution of incoherent monopoles

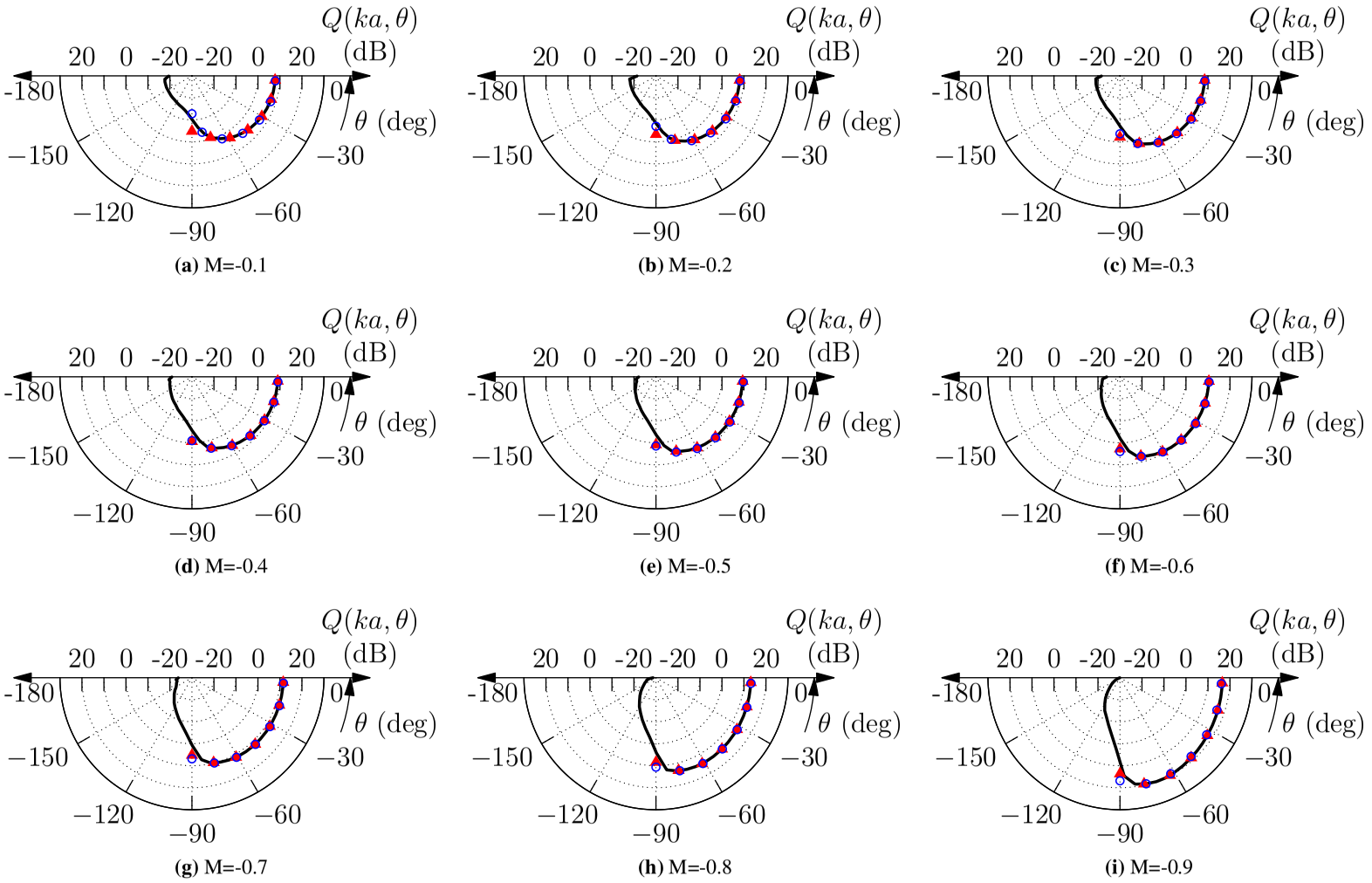

(a) M=-0.1 **(b)** M=-0.2 **(c)** M=-0.3

(d) M=-0.4 **(e)** M=-0.5 **(f)** M=-0.6

(g) M=-0.7 **(h)** M=-0.8 **(i)** M=-0.9

Figure 10.3 – $M < 0$, Uniform distribution of incoherent dipoles

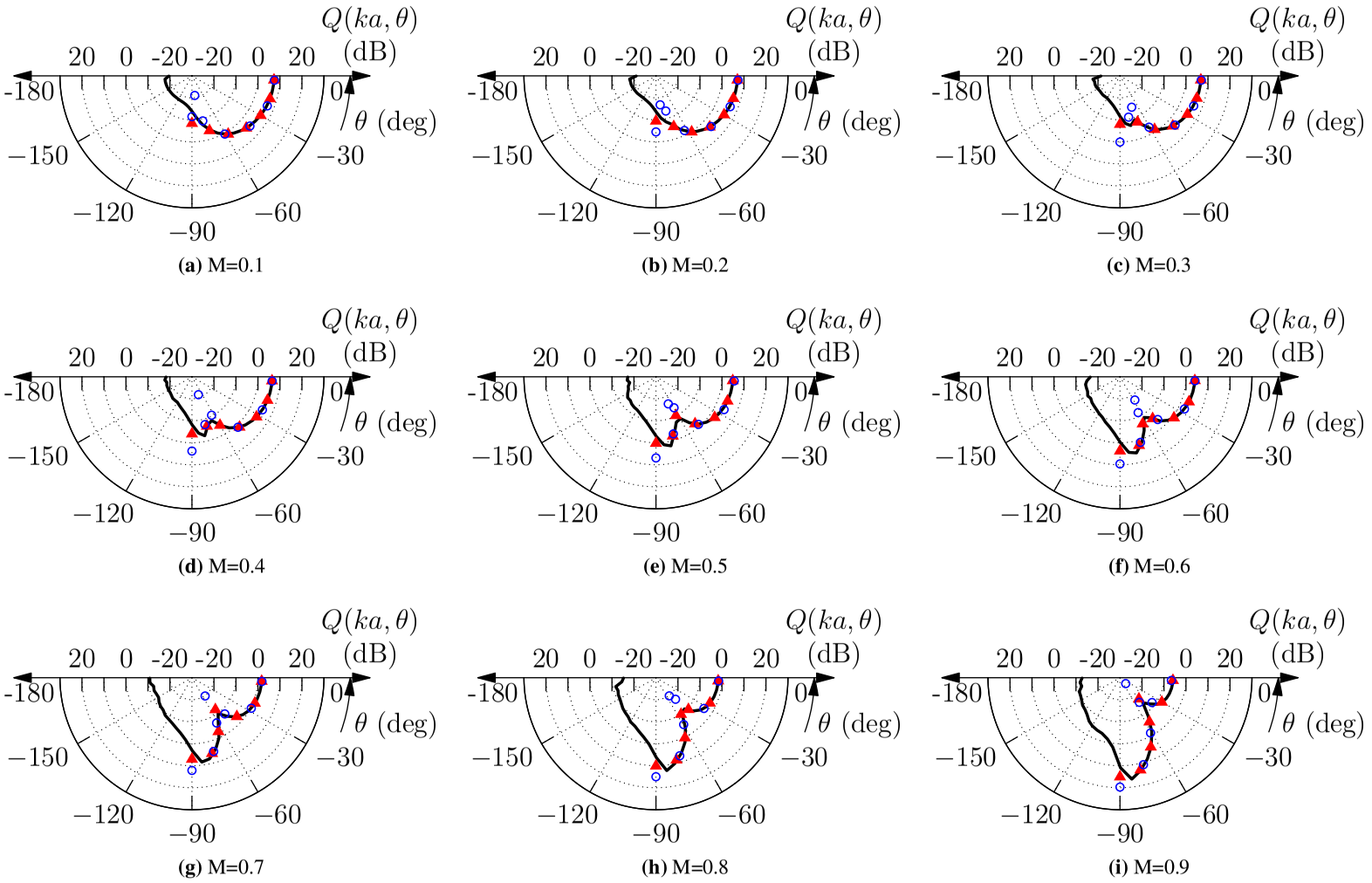

(a) M=0.1 **(b)** M=0.2 **(c)** M=0.3

(d) M=0.4 **(e)** M=0.5 **(f)** M=0.6

(g) M=0.7 **(h)** M=0.8 **(i)** M=0.9

Figure 10.4 – $M > 0$, Uniform distribution of incoherent dipoles

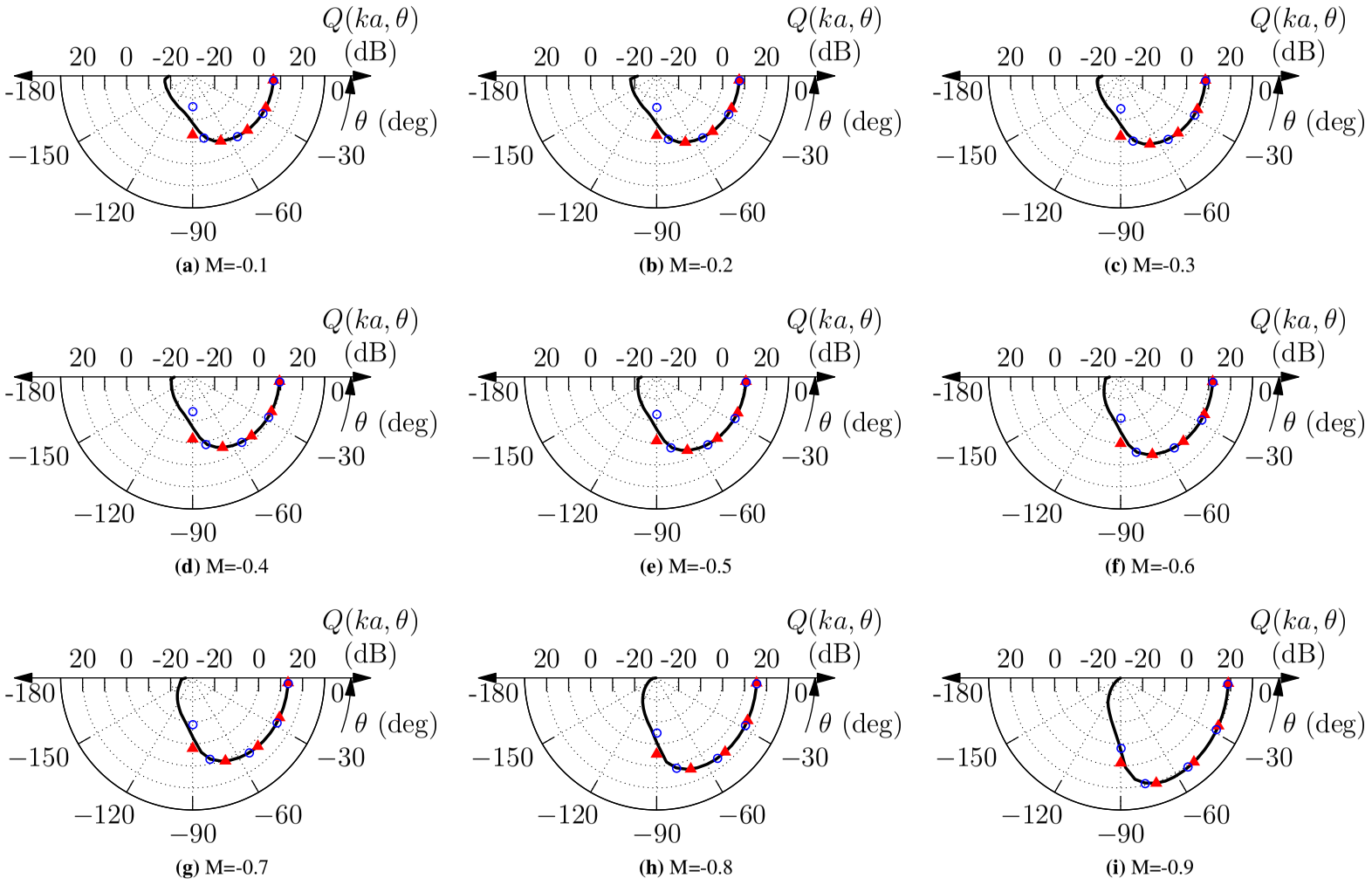

(a) M=-0.1 **(b)** M=-0.2 **(c)** M=-0.3

(d) M=-0.4 **(e)** M=-0.5 **(f)** M=-0.6

(g) M=-0.7 **(h)** M=-0.8 **(i)** M=-0.9

Figure 10.5 – $M < 0$, Equal power per mode model

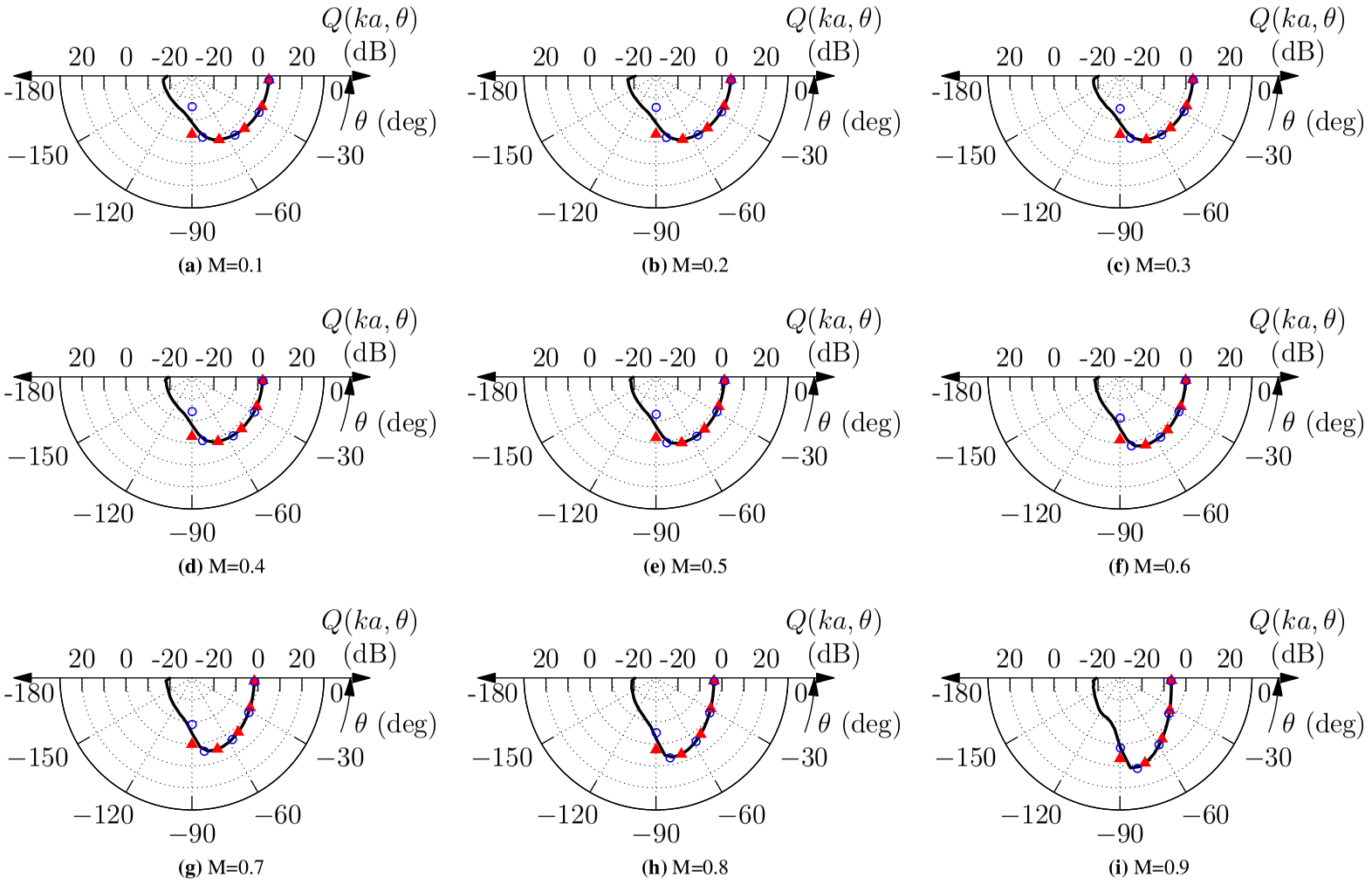

(a) M=0.1 **(b)** M=0.2 **(c)** M=0.3

(d) M=0.4 **(e)** M=0.5 **(f)** M=0.6

(g) M=0.7 **(h)** M=0.8 **(i)** M=0.9

Figure 10.6 – $M > 0$, Equal power per mode model

Conclusion

In part II, the derivation leading to the high frequency analytic formula for the multi-mode directivity from a semi-infinite cylindrical duct without flow, first obtained by Joseph and Morfey [1], has been outlined. This derivation is then generalized to an inlet duct with flow, or an exhaust duct with flow in part III. The main results of this analysis are as follows.

- A high frequency approximation of the multi-mode directivity with constant mean flow, valid for a general family of incoherent source distributions in the forward arc, has been derived. It is in excellent agreement with exact numerical results up to approximately $80°$.
- The in-duct to far field transfer functions with flow can be obtained by careful application of the Lorentz Transformation to the zero flow solution.
- The in-duct to far field transfer function with flow for an inlet duct is approximately equal to that for an exhaust duct in the forward arc.
- The relation between the direction of propagation of a mode propagating inside a duct and the mode cut-off ratio has been derived.
- The direction of maximum radiation from the duct is equal to the direction of propagation of the mode inside the duct. The variation of this angle of maximum radiation with Mach number depends on the value of the cut-off ratio for zero flow. In particular, if the cut-off ratio for zero flow is close to one, the direction of maximum radiation changes little when the Mach number is increased.
- The average far field radial intensity with flow has been derived. It is related to the mean square pressure by a directivity function which depends on the Mach number.

Future work

Future work would consists in improving the multi-mode directivity formula by deriving an analytical expression for the transmission coefficient of the open end of the duct. The formula would also need to be extended to the case when the mean flow outside the duct is different from that inside the duct.

Bibliography

[1] P. Joseph and C. L. Morfey. Multimodal radiation from an unflanged, semi-infinite circular duct. *J. Acoust. Soc. Am.*, 105 (5):2590–2600, 1999.

[2] P. M. Morse. *Vibration and Sound*. American Institute of Physics for the Acoustical Society of America, 1948.

[3] JM Tyler and TG Sofrin. Axial Flow Compressor Noise Studies. *SAE Transactions*, 70:309–332, 1962.

[4] C. L. Morfey. Rotating pressure patterns in ducts: their generation and transmission. *J. Sound Vib.*, 1:60–87, 1964.

[5] C. L. Morfey. A note on the radiation efficiency of acoustic duct modes. *J. Sound Vib.*, 9 (3):367–372, 1968.

[6] H. Levine and J. Schwinger. On the radiation of sound from an unflanged circular pipe. *Physical Review*, 73 (4):383–406, 1948.

[7] L. A. Weinstein. *The Theory of Diffraction and the Factorization Method*. Golem, Boulder, CO, 1969.

[8] G. F. Homicz and J. A. Lordi. A note on the radiative directivity patterns of duct acoustic modes. *J. Sound Vib.*, 41 (3):283–290, 1975.

[9] A. V. Saule. Modal structure inferred from static far-field noise directivity. In *American Institute of Aeronautics and Astronautics, Aero-Acoustics Conference, 3 rd, Palo Alto, Calif*, 1976.

[10] E. J. Rice. Multimodal far-field acoustic radiation pattern. *AIAA Journal*, 16:906–911, 1978.

[11] R. M. Munt. The interaction of sound with a subsonic juet issuing from a semi-infinite cylindrical pipe. *J. Sound. Vib.*, 83:609–640, 1977.

[12] R. M. Munt. Acoustic transmission properties of a jet pipe with subsonic jet flow: I. the cold jet reflection coefficient. *J. Sound. Vib.*, 142:413–436, 1990.

[13] S. W. Rienstra. Sound radiated from annular duct in flow. *J. Sound. Vib.*, 94:267–288, 1984.

[14] G. Gabard and R. J. Astley. Theoretical model for sound radiation from annular jet pipes: far- and near-field solutions. *J. Fluid. Mech.*, 549:315–341, 2006.

[15] P. Joseph, Morfey C. L., and C. R. Lowis. Multi-mode sound transmission in ducts with flow. *Journal of Sound and Vibration*, 264(3):523–544, 2003.

[16] EJ Rice. Modal density function and number of propagating modes in ducts. *The Journal of the Acoustical Society of America*, 60:S112, 1976.

[17] ME Goldstein. *Aeroacoustics*. McGraw-Hill, New York, 1976.

[18] F.O. Castres and P.F. Joseph. Experimental investigation of an inversion technique for the determination of broadband duct mode amplitudes by the use of near-field sensor arrays. *The Journal of the Acoustical Society of America*, 122:848, 2007.

[19] G.M. Roe. Frequency Distribution of Normal Modes. *The Journal of the Acoustical Society of America*, 13:1, 1941.

[20] C. J. Chapman. Similarity variables for sound radiation in a uniform flow. *Journal of Sound and Vibration*, 233(1):157–164, 2000.

[21] M. S. Howe. *Acoustics of Fluid-Structure Interactions*. Cambridge University Press, 1998.

[22] RH Cantrell and RW Hart. Interaction between Sound and Flow in Acoustic Cavities: Mass, Momentum, and Energy Considerations. *The Journal of the Acoustical Society of America*, 36:697, 1964.

[23] C. L. Morfey. Sound transmission and generation in ducts with flow. *J. Sound. Vib.*, 14:37–55, 1971.